Multiple-site damage crack growth behaviour in Fibre Metal Laminate structures

Wang, Wandong

DOI
10.4233/uuid:e786ee1f-8fea-4ef2-a67b-08fad87ae0f1

Publication date
2017

Document Version
Final published version

Citation (APA)
Wang, W. (2017). *Multiple-site damage crack growth behaviour in Fibre Metal Laminate structures*. [Dissertation (TU Delft), Delft University of Technology]. https://doi.org/10.4233/uuid:e786ee1f-8fea-4ef2-a67b-08fad87ae0f1

MULTIPLE-SITE DAMAGE CRACK GROWTH BEHAVIOUR IN FIBRE METAL LAMINATE STRUCTURES

MULTIPLE-SITE DAMAGE CRACK GROWTH BEHAVIOUR IN FIBRE METAL LAMINATE STRUCTURES

Proefschrift

ter verkrijging van de graad van doctor
aan de Technische Universiteit Delft,
op gezag van de Rector Magnificus prof. ir. K.C.A.M. Luyben,
voorzitter van het College voor Promoties,
in het openbaar te verdedigen op woensday 12 april 2017 om 12:30 uur

door

Wandong WANG

Master of Science in Aeronautical Engineering,
Beihang University, Beijing, China,
geboren te Xingren, Ningxia, China

Dit proefschrift is goedgekeurd door de

promotor: prof. dr. ir. R. Bededictus
copromotor: dr. C. D. Rans

Samenstelling promotiecommissie:

Rector Magnificus,	voorzitter
Prof. dr. ir. R. Benedictus,	Technische Universiteit Delft
Dr. C. D. Rans,	Technische Universiteit Delft
Onafhankelijke leden:	
Dr. ir. H. J. K. Lemmen,	Airbus Operations GmbH, Germany
Prof. dr. S. Wu	Beihang University, China
Prof. dr. V. Kostopoulos	University of Patras, Greece
Prof. dr. ir. L. J. Sluys	Technische Universiteit Delft
Prof. dr. I. M. Richardson	Technische Universiteit Delft

Keywords: Fatigue Crack Growth, Fibre Metal Laminate, MSD, Load Redistribution

Printed by: BOXPress

Front & Back: A test set-up picture and three crack configurations studied in this research on the front cover, and the structure of this thesis on the back cover.

ISBN 978-94-6295-642-1

An electronic version of this dissertation is available at
http://repository.tudelft.nl/.

To my family

Wandong Wang

SUMMARY

Fibre metal laminates (FMLs) were developed and refined for their superior crack growth resistance and critical damage size that complimented the damage tolerance design philosophy utilized in the aerospace sector. Robust damage tolerance tools have been developed for FMLs. However, they tend to focus on the evolution of an isolated crack. There is also a risk that they will be invalidated overtime as a result of the occurrence of multiple cracks within one structure (one form of widespread fatigue damage). To combat another failure due to widespread fatigue damage, the airworthiness regulations were revised to include the concept of a Limit of Validity (LOV) of the damage tolerance analyses. Consequently, it is crucial to examine fatigue crack growth (FCG) in FMLs containing Multiple-site Damage (MSD) cracks despite their superior damage tolerance merits.

The focus of this thesis therefore is to analyse MSD crack growth in FML structures. Mechanically fastened FML joints are potentially weak structural designs that are susceptible to MSD due to the stress rising contributors such as secondary bending, pin loading and open holes subjected to bypass loading. In this thesis, predictive models were developed to address several key mechanisms that affect FCG in FML joints containing MSD, and validated with corresponding experimental work. Then the predictive models were systematically integrated and implemented for FML joints.

It was identified that the nature of fatigue in FMLs led to the load redistribution mechanism as the key factor to be modelled in predicting MSD growth in FMLs. The structural stiffness reductions caused by the presence of multiple cracks resulted in load redistribution from the other cracks to the single crack to be analysed, exacerbating the total stress intensity factor (SIF) experienced at the tips of the single crack, increasing the crack growth rate (CGR). The load redistribution mechanism was first substantiated by investigating FCG in FMLs containing discretely notched layers. The prediction model fairly captured the load redistribution mechanism by idealizing the notches in the metal layers as removals of metal strips. The crack acceleration over a major portion of the crack propagation was well predicted with the model; however, the surge in CGR over roughly 3 mm crack length prior to the link-up was underestimated since the plasticity interaction was not accounted for.

The capability of modelling the load redistribution mechanism allows the states of multiple cracks to be analysed one by one. It was found that the load redistribution could not be symmetric for every crack and non-symmetric crack configurations therefore developed in FMLs with finite width. Hence, non-symmetric crack growth in FMLs was also investigated in this work. It was also found that both crack tip non-symmetry and delamination shape non-symmetry affected the crack growth in the metal layers. The model for non-symmetric crack growth in FMLs was validated with experimental data. Good correlation was observed.

The model for MSD growth in FML panels sequentially analyses each crack state.

The other cracks are idealized as removals of metal strips when analyzing the state of a single crack. This non-physical idealization of the cracks led to consistently conservative prediction results in comparison with the test data. Nevertheless, the prediction model provided good predictions of the evolution of MSD configurations. Additionally, it was proven that a very non-conservative predicted fatigue life could be obtained if the load redistribution mechanism was not considered.

The effects of pin loading on FCG in FMLs were also investigated. The test data showed very rapid growth of the crack in the vicinity of the pin loading. The CGR decreased with increasing crack length. The model applied the principle of superposition to split the non-symmetric tension-pin loading into simpler tensile loading and a pair of point loads acting on the crack flanks. The SIFs for the simpler loading cases were derived and superposed to obtain the total SIF as a result of the tension-pin loading. The predicted CGR and equivalent delamination shape correlated with the measurements very well, but the model failed to predict the crack path and the measured delamination shape which were trivial issues for this work.

The relevance and applicability of the developed models in this thesis for predicting the MSD behaviour in mechanically fastened FML joints was examined. The predicted results captured the trends of the measured CGR in FML joints containing MSD cracks, although there were some discrepancies. The discrepancies are mainly due to the two major shortcomings of the model which are neglecting the load redistribution over multiple fastener rows and neglecting the effects of secondary bending stresses.

SAMENVATTING

Vezelmetaallaminaten (fibre metal laminates, FMLs) zijn ontwikkeld en verfijnd vanwege de superieure scheurgroeiweerstand en kritische scheurlengte, die de schade tolerantie filosofie die in de luchtvaart sector gebruikt wordt complementeren. Er zijn robuuste schade tolerantie modellen ontwikkeld voor FMLs; echter, deze modellen richten zich op de evolutie van een geïsoleerde scheur. Het risico bestaat dat deze modellen ongeldig worden door het bestaan van meerdere scheuren in een constructie (één van de vormen van verspreide vermoeiingsschade). Om nog een ongeval als resultaat van verspreide vermoeiingsschade te voorkomen zijn de luchtwaardigheidsregelementen aangepast om een geldigheidslimiet (limit of validity, LOV) op te nemen voor schade tolerantie analyses. Als gevolg hiervan is het essentieel dat vermoeiingsscheurgroei (fatigue crack growth, FCG) in FMLs met meerdere schade locaties (muliple-site damage, MSD) wordt onderzocht, ondanks hun superieure schade tolerantie eigenschappen.

Dit proefschrift richt zich op de analyse van MSD scheurgroei in FML constructies. Mechanische verbindingen in FML constructies zijn potentiele zwakke punten in het ontwerp, die vatbaar zijn voor MSD door de spannings-verhogende bijdragen zoals secundaire buiging, penbelasting en open gaten belast met omloopbelasting. In dit proefschrift zijn voorspellende modellen ontwikkeld die een aantal sleutelmechanismen behandelen die invloed hebben op FCG in FML verbindingen met MSD. Deze modellen zijn ook gevalideerd met experimenteel werk. De voorspellende modellen zijn hierna systematisch geïntegreerd en toegepast op FML verbindingen.

Er werd geïdentificeerd dat de aard van vermoeiing in FMLs er toe leidde dat het krachtherverdelingsmechanisme de beslissende factor bleek te zijn voor het modeleren van MSD groei in FMLs. De constructieve stijfheidsvermindering als gevolg van meerdere scheuren zorgde ervoor dat de spanningsintensiteitsfactor (stress intensity factor, SIF) aan de scheurtip van een enkele scheur werd overschat, omdat de krachtherverdeling van de andere scheuren naar de geanalyseerde scheur niet werd meegenomen. Dit resulteerde in een hogere scheursnelheid (crack growth rate, CGR). Het krachtherverdelingsmechanisme werd voor het eerst onderbouwd door onderzoek naar FCG in FMLs met discreet gekerfde lagen. Het voorspellingsmodel benaderde het krachtherverdelingsmechanisme redelijk door de kerven in de metaallagen te idealiseren als verwijderde stroken metaal. De scheurversnelling van een groot deel van de scheurpropagatie werd goed voorspeld door het model. Echter, de abrupte versnelling in CGR tijdens ongeveer 3 mm scheurlengte vlak voor de scheurhereniging werd onderschat omdat er geen rekening werd gehouden met plasticiteitsinteractie.

Door het modeleren van het krachtherverdelingsmechanisme kan de situatie van meerdere scheuren één voor één geanalyseerd worden. De krachtherverdeling kon niet symmetrisch zijn voor iedere scheur en in FMLs met eindige breedte kwamen daardoor asymmetrische scheurconfiguraties voor. Als gevolg is asymmetrische scheurgroei in FMLs ook onderzocht in dit werk. Zowel scheur tip asymmetrie als delaminatievorm

asymmetrie hebben invloed op de scheurgroei in de metaallagen. Het model voor asymmetrische scheurgroei in FMLs is gevalideerd met experimentele data. Er werd een goede correlatie geobserveerd.

Het model voor MSD groei in FML panelen analyseert iedere scheurstaat opeenvolgend. De andere scheuren worden tijdens de analyse geïdealiseerd als verwijderde metaalstrips. Deze niet-fysische idealisatie van de scheuren leidt consequent tot conservatieve voorspellingsresultaten in vergelijking met de testdata. Desondanks laat het voorspellingsmodel goede voorspellingen van de evolutie van de MSD configuraties zien. Daarnaast is bewezen dat een zeer onconservatieve voorspelling van het vermoeiingsleven verkregen wordt als het krachtherverdelingsmechanisme niet mee wordt genomen in de analyse.

De effecten van penbelastingen op FCG in FMLs zijn ook onderzocht. De testdata laten een zeer snelle scheurgroei zien in nabijheid van penbelasting. De CGR vertraagt naarmate de scheurlengte langer wordt. Het model past het superpositieprincipe toe bij het opsplitsen van asymmetrische trek-penbelasting in een eenvoudigere trekbelasting en een paar puntbelastingen die aangrijpen op de scheurflank. De SIFs voor de eenvoudigere belastingscenario's zijn afgeleid en gesuperpositioneerd om de totale SIF te herleiden als resultaat van de trek-penbelasting. De voorspelde CGR en equivalente delaminatievorm laten een uitstekende overeenkomst zien met de metingen. Echter, het model voorspelde niet het scheurpad en de gemeten delaminatievorm, maar dit waren onbelangrijke factoren voor dit werk.

De relevantie en toepasbaarheid van de ontwikkelde modellen in dit proefschrift voor het voorspellen van MSD gedrag in mechanisch verbonden FMLs is ook onderzocht. De voorspelde resultaten toonden de trend van gemeten CGR in FML verbindingen met MSD scheuren, hoewel er enige discrepanties waren. De verschillen zijn voornamelijk toe te schrijven aan de twee grotere vereenvoudigingen van het model. Deze zijn het verwaarlozen van de krachtherverdeling over meerdere bevestigingsrijen en het negeren van spanningen als gevolg van secundaire buiging.

CONTENTS

NOMENCLATURE

LATIN SYMBOLS

a	Half Crack or delamination length	mm
Δa	Crack increment	mm
a_0, a_s	Initial crack length	mm
$a1_*$, $a2_*$	Crack length measured from saw-cut tip	mm
$b(x)$	Delamination shape	mm
Δb	Delamination increment	mm
C_{cg}, C_d	Paris constants	–
d	Distance between crack center and the center of a panel	mm
d_{ff}	Distance between the equivalent load of the far-field load after decomposition and the center of a panel	mm
e	eccentricity	–
E	Young's modulus	MPa
E_x, E_y	Young's modulus	GPa
E_{FML}, E_{lam}	Young's modulus of an FML panel	MPa
E_m	Young's modulus of a metal layer	MPa
E_f, E_{fibre}	Young's modulus of a fibre layer	MPa
E_{notch}	Young's modulus of the remaining material at the discretely notched area	MPa
f	Frencequency	Hz
$f_{fastener}$	Fastener flexibility	???
f_{fplate}	Plate flexibility	???
$F_{transfer}$	Load transfer due to discretely notched layers	N
F_{pin}	Pin load	N
F_{bypass}	Bypass load	N
F_{app}	Applied load	N
G	Strain energy release rate	KJ/m^2
G_{xy}	Shear modulus	GPa
G_{max}	Maximum strain energy release rate	KJ/m^2
G_{min}	Minimum strain energy release rate	KJ/m^2
ΔG	Strain energy release rate range	KJ/m^2
i	imaginary unit	–
i	i^{th} Bar element	–
i	i^{th} crack	–
j	Number of interfaces	–
K	Stress intensity factor	$MPa\sqrt{mm}$
K_∞, K_{ff}	Stress intensity factor due to far-field applied load	$MPa\sqrt{mm}$
K_{br}	Stress intensity factor due to bridging load	$MPa\sqrt{mm}$

K_{eff}	Effective stress intensity factor	$MPa\sqrt{mm}$
K_{total}	Total stress intensity factor at the crack tip	$MPa\sqrt{mm}$
$K_{redistribution}$	Stress intensity factor due to far-field load and load redistribution	$MPa\sqrt{mm}$
K_{joint}	Stress intensity factor at a crack tip in a joint	$MPa\sqrt{mm}$
ΔK	Stress intensity factor range	$MPa\sqrt{mm}$
L	Distance from a crack tip to the free edge ahead	mm
L_{row}	Row pitch	mm
$L_{fastener}$	Fastener pitch	mm
n_f	Number of fibre layers	–
n_m	Number of metal layers	–
N	Fatigue life	$cycle$
ΔN	Fatigue life reduction	$cycle$
ΔN	Fatigue life interval	$cycle$
N_{FML_single}	Fatigue life of a single crack in an FML	$cycle$
N_{FML}	Fatigue life of MSD cracks in an FML	$cycle$
N_{metal}	Fatigue life of MSD cracks in a metal panel	$cycle$
n_{cg}, n_d	Paris constants	–
P	Point load	N/mm
P_1	Equivalent load of the stress distribution in front of crack tip 1	N
P_2	Equivalent load of the stress distribution in front of crack tip 2	N
$P_{applied}$, P_{app}	Total applied load	N
$P_{applied,notch}$	Total applied load on a laminate containing notches	N
$P_{applied,M(T)}$	Total applied load on an M(T) laminate	N
$P_{f,1}$	Far-field load in bridging fibres	N
$P_{f,2}$	Far-field load in the fibre layers except for bridging fibres	N
$P_{ff,i}$	Equivalent load of the far-field applied load after decomposition for crack i	mm
P_m	Far-field load in the metal layers	N
R	Stress ratio	–
r_p	Plastic zone size	mm
S	Stress	MPa
s_f	Stress in the fibre layers	MPa
s_{br}	Brdging stresses	MPa
S_{hc}	Distance between hole centre to specimen centre	mm
t	Thickness	mm
t_f	Thickness of a fibre layer	mm
t_m	Thickness a metal layer	mm
t_{FML}, t_{lam}	Thickness of FML laminate	mm
$T1$, $T2$, $T3$	Load transferred by the 1^{st}, 2^{nd}, 3^{rd} fastener rows	mm
v, v_∞, v_{ff}	Crack opening displacement due to far-field load	mm

v_{x,x_i}	Crack opening displacement at location x due to a brdging load at x_i	mm
v_f	Crack opening displacement of a central crack in a panel with finite width	mm
v_{br}	Crack opening displacement due to briding load	mm
v_{xy}, v_{yx}	Poisson's ratio	–
W, w	Width	mm
w_i	Width of a bar element of delamination	mm
x	Position from the centre of a specimen	mm
x, y	Coordinates	mm
x_c	Centroid of a stress distribution	mm
x_l	Position of left notch edge	mm
x_r	Position of right notch edge	mm
Z_I	Westergaard stress function	–
z	Complex number	–

GREEK SYMBOLS

δ_f	Elongation of the fibre layers	mm
δ_{pp}	Shear deformation of the fibre layers	mm
ε_{yy}	Strain distribution ahead of crack tip	mm/mm
$\varepsilon_{yy,notch}$	Strain distribution ahead of crack tip in a laminate containing notches	mm/mm
$\varepsilon_{yy,M(T)}$	Strain distribution ahead of crack tip in a M(T) laminate	mm/mm
$\sigma_{applied}$	Total applied stress in laminate	MPa
$\sigma_{m,applied}$,σ_m	Stress in the metal layers due to far-field applied load	MPa
$\sigma_{m,cur}$	Curing stress in the metal layers	MPa
$\sigma_{f,applied}$	Far-field load in the fibre layers	MPa
σ_{nom}	Nominal stress	MPa
$\sigma_{bending}$	Bending stress	MPa
$\sigma_{westergaard}$	Westergaard stress	MPa
$\sigma_{westergaard,M(T)}$	Westergaard stress for M(T) specimen	MPa
σ_{yy}	Westergaard stress distribution ahead of crack tip	MPa
$\sigma_{yy,f}$	Westergaard stress distribution ahead of crack tip in a panel with finite width	MPa
σ_{ys}	Yield strength	MPa
σ_{notch}	Stress at the discretely notched area	MPa
β	Correction factor	–
β_{Isida}	Correction factor derived by Isida	–
λ	Nomarlized crack length	–
λ	Nomarlized crack length	–
φ	Thickness ratio	–

SUBSCRIPT

1	the variable is related to crack tip 1

2	the variable is related to crack tip 2
$i1$	the variable is related to crack i
$i1$	the variable is related to the crack tip 1 of crack i
$i2$	the variable is related to the crack tip 2 of crack i
$bypass$	the variable is related to bypass load
$pin, bearing$	the variable is related to a pair of pin bearing loads
pin, ff	the variable is related to the far-field load that equials a pin bearing load

ACRONYMS

COD	Crack Opening Displacement
DIC	Digital Image Correlation
FML	Fibre Metal Laminate
CLT	Classic Lamiante Theory
MVF	Metal Volume Fraction
LOV	Limite of Validity
MSD	Multiple-site Damage
WFD	Widespread Fatigue Damage
FEM	Finite Element Modelling
LEFM	Linear Elastic Fracture Mechanics
SIF	Stress Intensity Factor

List of Figures

List of Tables

1

INTRODUCTION

New materials are always desirable to improve the performance of the aircraft while decreasing the structural weight. However, the adoption of new materials for new aircraft structural design has to comply with strict airworthiness regulations which have a safety-focused conservative attitude. The success of damage tolerant Fibre Metal Laminates (FMLs) has been proven by their application as a fuselage skin materials on the Airbus A380 jumbo passenger aircraft. However, new application can bring new challenges. The damage tolerant behaviour of FMLs are desirable for applications on narrow-body aircraft where structures are thinner and the demands for fatigue life are higher. Furthermore, changes in safety regulations and requirements are constantly raising the bar in terms of the needed understanding and predictability of material performance. This thesis examines these challenges in the context of multiple site damage of FML structures.

Parts of this chapter have been published in Proceedings of 28th ICAF [1].

1

1.1. FIBRE METAL LAMINATE

1.1.1. DAMAGE TOLERANT MATERIAL TECHNOLOGY

Fibre Metal Laminates (FMLs) are hybrid laminates comprising thin metallic sheets alternately bonded to fibre reinforced prepreg layers. A typical FML layup is illustrated in Fig. 1.1. The FML concept originally evolved from bonded metal laminates which exhibited an improved damage tolerant behaviour over monolithic metal structures due to their layered nature. Fatigue resistant fibre layers were later added to the bond line of thin metal layers to further increase the resistance of the metal layers to fatigue cracking [2].

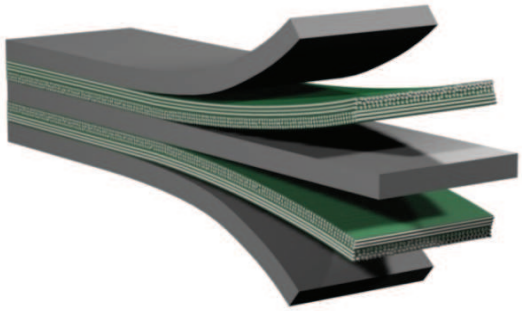

Figure 1.1: Typical FML layup [3]

One of the main advantages of this hybrid material configuration is that it expresses many of the desirable traits of its metal and composite constituent materials while simultaneously compensating for some of their disadvantages. Metals, particularly aluminium, have been widely applied as aircraft skin structures and their behaviour are quite well understood. Metals are tolerant to design features in forms of fastener holes and other cutouts due to their inherent ductility. They, however, are susceptible to fatigue cracking. Composites, on the other hand, are brittle in nature, which makes them susceptible to holes and cut-outs. In spite of their brittle nature, composites are relatively insensitive to fatigue compared to metals [4]. The combination of metal constituent and composite constituent in one laminate system leads to hybrid FML being able to be machined and assembled in a similar manner as metals, and possessing superior fatigue resistance in comparison with monolithic metals.

A key characteristic of FMLs is their damage tolerance behaviour: very high resistance against fatigue crack growth and longer critical crack length as a result of significant residual strength in case of fatigue damage. The high growth resistance enables longer inspection intervals while the longer critical crack length allows less sophisticated and thus less costly inspection techniques to be applied to detect the damages in FMLs. They are very desirable in the context of damage tolerance design philosophy utilised in the aerospace sector, since the damage tolerance philosophy relies on detection and

repair of damages to ensure the structural integrity and flight safety [5].

Their superior damage tolerance behaviour can be attributed to the bridging mechanism offered by the intact fatigue resistant fibres in the wake of fatigue cracks. A schematic illustration of the bridging mechanism is shown in Fig. 1.2. The intact bridging fibres act as a secondary load path and restrain the crack opening in the metal layers. As a result, load redistributes from the cracked metal layers to the bridging fibres. This load redistribution reduces the stresses experienced at the crack tip in the metal layers and thus the driving force for the crack. Moreover, the load redistribution also introduces cyclic shear stresses at the interfaces between metal layers and fibre layers, resulting in delamination growth at the interfaces. The delaminaton growth allows more delaminated fibre length to deform in order to accommodate the crack opening in the metal layers without over-straining the fibres, thus protecting the fibres from fracture [6].

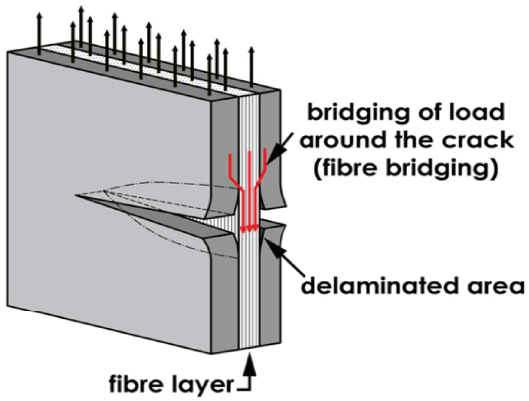

Figure 1.2: Bridging mechanism

The development and continued refinement of FMLs and their variants has been driven heavily by the improved damage tolerance via the fibre bridging mechanism. The first generation of FML coming into being was ARALL in the early 1970s. ARALL consisted of thin 2024-T3 layers bonded to aramid-epoxy composite layers alternately. ARALL requires laminate stretching after cure to mitigate the poor compressive properties of the aramid fibres, which limits its application in service [7]. Later in 1980s, glass fibres were introduced in place of aramid fibres to FMLs, leading to the variant of FMLs well known as Glare. The introduction of glass fibres alleviated the need for post-stretching since the the stability of glass fibres in compression is superior to that of aramid fibres [7]. Instead of dealing with unlimited mix of potential aluminium thicknesses and orientations of S2-glass fibres embedded in an FM 94 adhesive system, several standard Glare grades have been established and are summarised in Table 1.1. Glare has been successfully applied as a skin material in the upper fuselage structures on the wide-body Airbus A380 due to its superior damage tolerance and slow crack growth rate.

Table 1.1: Standard Glare grades [8]

Glare grade	sub	Alloy	Metal thickness [mm]	Prepreg orientation	Main beneficial characteristics
Glare 1	-	7475-T761	0.3-0.4	0/0	Fatigue, strength, yield stress
Glare 2	A	2024-T3	0.2-0.5	0/0	fatigue, strength
	B	2024-T3	0.2-0.5	90/90	fatigue, strength
Glare 3	-	2024-T3	0.2-0.5	0/90	fatigue, impact
Glare 4	A	2024-T3	0.2-0.5	0/90/0	fatigue, 0° strength
	B	2024-T3	0.2-0.5	90/0/90	fatigue, 90° strength
Glare 5	-	2024-T3	0.2-0.5	0/90/90/0	impact
Glare 6	A	2024-T3	0.2-0.5	±45	shear, off-axis properties
	B	2024-T3	0.2-0.5	∓45	shear, off-axis properties

1.1.2. ANALYSIS TOOLS FOR FMLS

During the course of developing the FML material technology, efforts have been made to develop analysis tools to understand and characterise the fatigue behaviour of FMLs with the aim to further explore the damage tolerance benefits of FMLs. These analysis tools include analytical models for fatigue crack initiation prediction and fatigue crack growth prediction [3, 6, 9, 10].

Prediction of fatigue crack initiation in FMLs is based upon the crack initiation behaviour of monolithic metal constituent material. The fibre bridging mechanism is not present during the crack initiation phase in FMLs, the actual stress cycles in the metal layers can be calculated using the Classical Laminate Theory (CLT) and S-N data for the given monolithic metal can be used to determine the fatigue crack initiation life [9, 10].

The fibre bridging mechanism, on the other hand, is present during the crack growth phase in FMLs, which has to be properly accounted for in order to be able to develop damage tolerance tools with the capability of accurately predicting the crack growth in the metal layers. Early crack growth prediction models for FMLs adopted phenomenological approaches by treating an FML as a bulk material analogous to the prediction models for monolithic metals [11–15]. These empirical models could not adequately capture the impact of the fibre bridging mechanism on the crack growth behaviour in the metal layers [16], since they neglected the composite nature of FMLs.

A breakthrough was achieved in the development of the damage tolerance tools for FMLs when the composite nature of FMLs were embraced: analysing the interaction between cracked metal layers and fibre layers, and simultaneously predicting the coupled delamination growth at the metal/composite interfaces and crack growth in the metal layers. Marissen obtained an analytical solution for ARALL FMLs based on the assumptions of a fixed elliptical delamination shape and a constant bridging stress distribution along the delamination front [17]. These two major assumptions were later found inconsistent, making it inappropriate for other FMLs. However, Marissen's model already

shed light on how the analysis of the coupled damage mechanisms in FMLs could be approached. Alderliesten further built on Marissen's work by discretising the delamination shape over the cracked metal layers into bar elements and implementing the displacement compatibility between crack opening in the metal layers and bridging fibre deformation at every bar elements, allowing a realistic bridging stress distribution and thus the coupled delamination growth and crack growth to be calculated [3, 6]. Extensions have been made based on Alderliesten's model to further explore the damage tolerance properties of FMLs, such as residual strength [18], variable amplitude loading [19–21], and generalised laminate configurations subjected to tension and bending [7].

1.2. MOTIVATION FOR THIS WORK

The damage tolerance properties of FMLs and the corresponding well developed damage tolerance analysis tools were presented in the previous section. Nevertheless, it is crucial to develop an analytical model for predicting fatigue crack growth behaviour in FMLs with multiple-site damage scenarios for the following reasons:

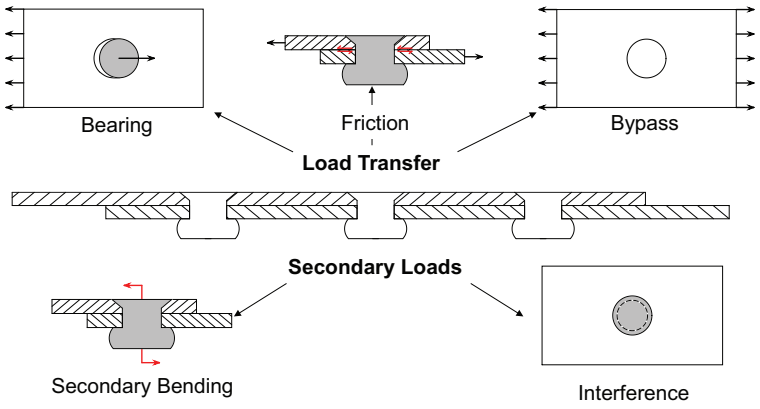

Figure 1.3: Stress components in a mechanically fastened joint [4]

First, although damage tolerance philosophy is recommended by the airworthiness regulations for the design of primary aircraft structures, its compatibility with an indefinite structural life is an identified deficiency. The philosophy continually ensures structural integrity through detection and repair of damages; however, it does not define a limit of validity of the approach in terms of structural life. There is a risk that widespread fatigue damage (WFD) within one structure arises over time. A classic example of the occurrence of WFD is the Aloha Airline Flight 243 that suffered explosive decompression as a result of sudden link-up of small fatigue cracks initiating from adjacent rivet holes in a longitudinal lap joint [22]. In order to combat the possibility of the WFD failure caused by crack growth at multiple sites within one structural element, i.e., multiple-site damage (MSD) scenario, the airworthiness regulations were revised in 2010 to include the definition of a Limit of Validity (LOV). The LOV is a period of structural life prior to which WFD will not occur, placing limits on the damage tolerance philosophy [23, 24]. It is therefore crucial to examine MSD crack growth behaviour of fibre metal laminates

even though they are every successful in the context of damage tolerance philosophy.

Second, MSD can potentially occur in FML structures, particularly mechanically fastened FML joints. The ductility provided by the metal constituent in FMLs makes them suitable for the application of mechanical joining techniques [4]. Relatively small FML panels can be mechanically jointed together to form large scale fuselage skin structures. Non-symmetric lap or butt joints, where secondary bending could occur, are normally adopted due to the aerodynamic requirements of the fuselage. In Fig. 1.3, the stress components in a non-symmetric mechanically fastened joint are illustrated. The stress rising contributors like pin bearing, open hole subjected to bypass loading, deteriorated peak tensile stress at the faying surface as a result of secondary bending, as well as fretting resulting from friction, make such joints vulnerable to multiple crack initiations at fastener hole edges or around hole edges in a critical fastener row.

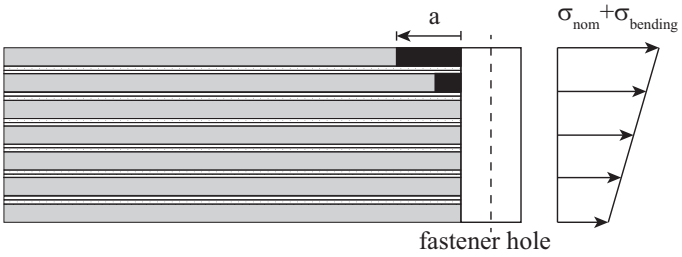

(a) Part through crack configuration in a thick laminate

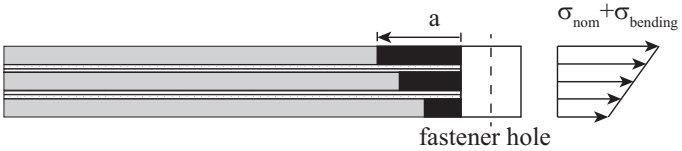

(b) Through thickness crack configuration in a thin laminate

Figure 1.4: Fatigue crack scenarios in FMLs

It is important to make a distinction between the crack configuration in thick jointed laminates and that in thin jointed laminates. A schematic illustration of respective crack configurations in a thick FML and a thin FML is shown in Fig. 1.4, the associated through-thickness stress distributions resulting from superposed tensile stress and secondary bending are also illustrated.

Thick laminates need to be used as a fuselage skin material for wide-body airplanes where the pressurisation loads in the skin are higher than that of narrow-body airplanes, for instance the application of Glare as fuselage skin on the Airbus 380. As shown in Fig. 1.4(a), secondary bending results in through-thickness stress distribution. Although secondary bending deteriorates the peak tensile stress at the faying metal layer, resulting in the earliest crack initiation at this layer, the fibre layers provide a barrier which prevents the crack from growing in the thickness direction. A crack has to initiate separately in the next metal layer with less tensile stress while the remaining metal layers have sig-

nificantly long crack free time as a result of the decreasing tensile stress. The crack free metal layers, together with the intact fibre layers, provide the same bridging mechanism as the fibre bridging. Depending on the number of crack free metal layers and the crack free longevity, the bridging can be efficient enough to stop crack growth in the cracked layers. In other words, the redundancy for the through-thickness crack is potentially so high that a part-through crack configuration can only form in thick laminates. In this case, the presence of part-through MSD cracks seems not a concern. Results from the full-scale fatigue tests on Airbus 380 aircraft show few crack initiation sites and extremely slow crack growth afterwards in the thick skin laminates, a number of cracks were arrested after some growth due to the bridging mechanism [25].

The relatively lower pressurisation loads in a narrow-body airplane with smaller fuselage diameter permits the use of thin laminates. In spite of the barrier to through-thickness crack growth provided by the fibre layers in thin laminates, the redundancy for the through-thickness crack growth can be low enough that all the metal layers are cracked (see Fig. 1.4(b)). Multiple through-thickness cracks in one fastener row can grow with accelerated rate in consequence of crack interaction.

The approach in this research will aim at analysing the MSD crack growth in thin FMLs for the potential application of such damage tolerant laminates on narrow-body airplanes.

Third, analytical damage tolerance models tend to analyse the crack growth behaviour of isolated symmetric cracks in FMLs. The major limitation of these damage tolerance tools for analysing MSD is that the crack interaction cannot be captured, leading to very non-conservative predictions. Finite element modelling (FEM) is versatile and can be adopted for analysing MSD problem in FMLs. However one has to keep in mind that MSD in FMLs is a fatigue issue, which involves iteration of calculating the states of MSD cracks. FEM can only be adopted at the expense of computational efficiency. Therefore an analytical approach with high computational efficiency is sought in this work for MSD crack growth prediction in FMLs.

1.3. OBJECTIVES OF THIS WORK

The objective of this work is to develop computationally efficient methodologies for predicting crack growth behaviour in FML joints containing MSD cracks. This objective is met by achieving the following sub-objectives:

- Develop an analytical model that enables analysis of MSD crack growth behaviour in flat FMLs subjected to far-field tension
- Develop a prediction model for fatigue crack growth behaviour in FMLs subjected to tension and pin bearing

Far-field tension is present in the form of bypass loading in FML joints and pin bearing is resulting from the load transfer from one jointed FML to another. These two are the major loading components affecting MSD crack growth behaviour in FML joints.

Secondary bending is another significant influence on fatigue crack growth in FML joints. The influence of secondary bending will be analysed qualitatively, not analytically incorporated into the prediction model. The reason is that analysing the effect of

secondary bending on crack growth behaviour in FMLs leads to the employment of the analytical model of Wilson [7], which could be a computationally consuming approach. It is argued in this work that the effect of secondary bending on MSD crack growth behaviour in FMLs should be evaluated by employing correction factors in order to obtain a fast and efficient estimation.

1.4. NATURE OF FATIGUE IN FMLS

MSD problem in monolithic metals has been extensively studied [26–33]. However, these methods from open literature for monolithic metals are inappropriate to be applied for FMLs as the fibre constituent leads to FMLs having different nature of fatigue crack growth compared to their monolithic metal counterparts. The nature of fatigue in FMLs is explained in comparison with that in monolithic metals to shed light on what important aspects have to be considered in analysing MSD in FMLs.

As a result of their hybrid nature, FMLs have different fatigue behaviour compared to monolithic metal. The fatigue resistant fibres which remain intact in the wake of fatigue cracks in metal layers in FMLs act as a second load path and restrain the opening of the cracks. Due to this bridging mechanism, the driving force for the crack is considerably reduced and the crack growth in FMLs is quite slow in comparison with monolithic metal. The bridging mechanism, however, is not effective in the crack initiation phase for FMLs [9]. In addition, the cyclic stress in the metal layer of FMLs is a superposition of the stress induced by the applied load and the curing stress [9, 10]. These two factors result in a quite short initiation life for FMLs.

Fig. 1.5 shows the contributions of the initiation life and crack growth life to the total fatigue life for FMLs and monolithic aluminium. The differences in contributions are typical for FMLs and monolithic metals [9]. As a result of the very fast crack growth in monolithic metal, the crack growth life only accounts for a very small part of its fatigue life. On the contrary, the superior fatigue crack growth resistance of FMLs results in a considerably long crack growth life which covers the main part of the total fatigue life.

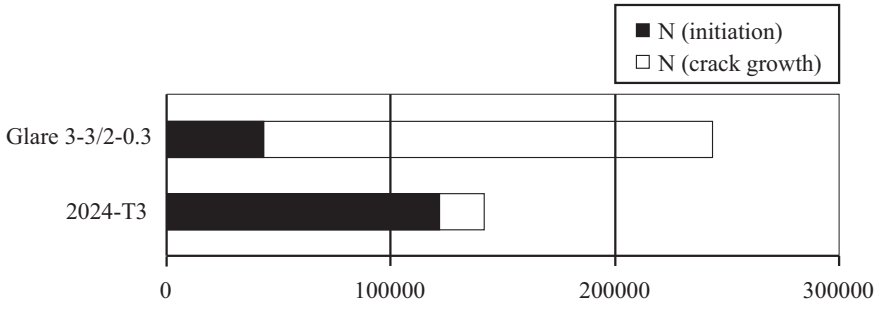

Figure 1.5: Fatigue life comparison for FMLs and monolithic aluminium [9]

The difference in ratio of crack growth life to overall fatigue life for metals and FMLs has implications on the fatigue behaviour of such materials in an MSD scenario. In order to discuss these differences, the influence of MSD cracks will be divided into two categories: load redistribution effects and crack-tip interaction effects. Crack tip interaction

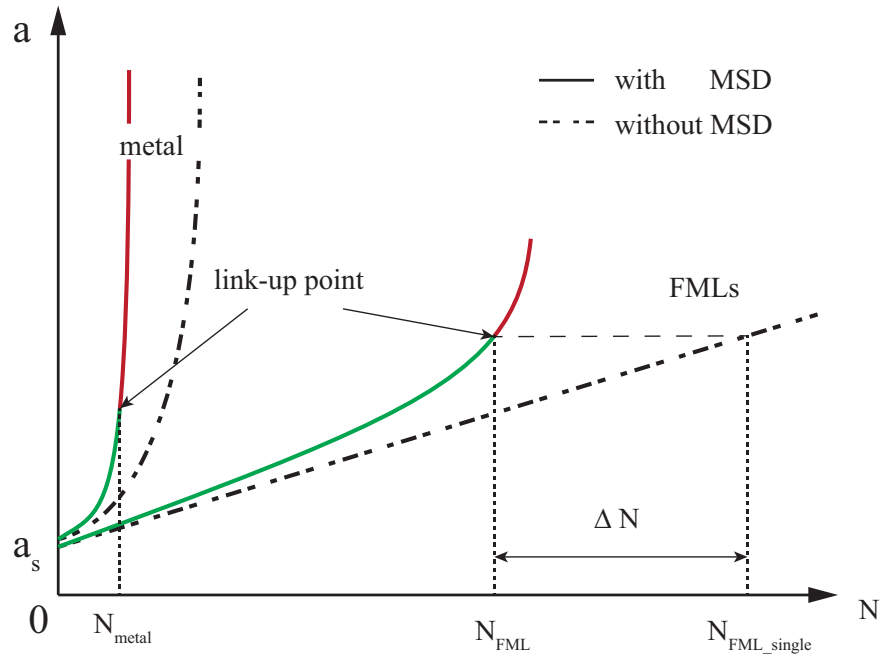

Figure 1.6: Schematic comparison of crack growth with MSD and without MSD for FMLs and metal

effects occur when the proximity of multiple crack tips results in an interaction of the stress singularities in front of the crack tips. For two cracks approaching each other, this tends to result in rapid fatigue propagation and ultimately linkup of the cracks. Load redistribution effects occur due to a loss in component stiffness due to the presence of multiple damages. These effects will be present over the entire range of damage sizes and proximities (i.e., they are also present when crack-tip interaction effects are present), although they are easier to describe for cracks sufficiently far that crack-tip interaction effects are negligible. In such a case, the crack propagation of one crack will be increased due to the increase in stress in the undamaged region of the component resulting from other damaged regions.

The relative crack growth behaviour of metals and FMLs, with and without MSD, is shown schematically in Fig. 1.6. The relatively rapid crack growth behaviour of the metal implies that cracks in an MSD scenario will grow towards each other relatively quickly resulting in early link-up. Crack link-up will rapidly increase the size of the primary crack, resulting in a reduction of fatigue life. The reduction in crack growth life is thus heavily influenced by crack-tip interaction effects. Conversely, the slower fatigue crack growth rate in FMLs combined with the shorter crack initiation life means that a significant portion of the MSD crack growth life in FMLs can occur well before the presence of crack-tip interaction effects. During this time, the cumulative effects of load redistribution resulting from the presence of multiple damages can result in a significant reduction in fatigue life (ΔN).

1

1.5. THE ALDERLIESTEN CRACK GROWTH MODEL

This work will be based on the analytical model proposed by Alderliesten for predicting isolated central cracks for FMLs, for the sake of conciseness and computational efficiency. The Alderliesten model is summarised here in order to provide a baseline and to aid in explaining what modifications and extensions have to be made to analyse the crack growth behaviour in FML joints containing complex MSD crack scenario, subjected to complex loading system.

Using the Linear Elastic Fracture Mechanics (LEFM) together with the principles of superposition and displacement compatibility, Alderliesten has successfully made the prediction of coupled propagation of cracks in the metal layers and delaminations at metal/composites interfaces [3, 6]. Both the crack extension and delamination extension are determined with LEFM methods. The stress intensity factor (Eq. 5.1) at the crack tip is used to characterise the crack extension in the metal layers while the strain energy release rate (Eq. 5.2) is applied to estimate the extension of delamination. For both crack growth resistance and delamination extension resistance of FMLs, experimentally determined Paris relations are applied to determine respective growth rates with the corresponding stress intensity factor and strain energy release rate [3, 6].

$$K_{total} = K_{ff} + K_{br} \tag{1.1}$$

The stress intensity factor, K_{total}, at the crack tip in an FML is calculated using the principle of superposition, as expressed in Eq. 5.1. K_{ff} is due to the stresses in the metal layers comprising the stress resulting from the far-field applied stress and the tensile residual stress resulting from the mismatch in thermal coefficients of the metal and fibre constituents, while K_{br} is due to the bridging stress distribution in the intact bridging fibres in the wake of a through-thickness fatigue crack. K_{total} therefore is a function of the bridging stress distribution. The strain energy release rate, G, is also a function of the bridging stress distribution (see Eq. 5.2). The bridging stress distribution therefore needs to be determined at first in order to resolve the crack extension and delamination growth.

$$G = \frac{n_f t_f}{2jE_f}\left(\frac{n_m t_m E_m}{n_m t_m E_m + n_f t_f E_f}\right)(S_f(x) + S_{br}(x))^2 \tag{1.2}$$

The bridging stress distribution along the crack is resolved by implementing the displacement compatibility between the crack opening in the metal layers and the deformation of bridging fibres over delaminated length [3, 6]. Since the fibre layers are bonded to the metal layers at the delamination front, the opening displacement of the fatigue cracked metal layers should be identical to the deformation of the bridging fibres over the delaminated length. See Eq. 5.3. The opening displacement of the cracked metal layers, which is given on the left side of Eq. 5.3, consists of opening displacement , v_{ff}, due to the stresses in the metal layers and closing displacement, v_{br}, due to the bridging stresses in the bridging fibres. On the right side of Eq. 5.3, the deformation of the bridging fibres over the delaminated length includes elongation of the bridging fibre layers resulting from the bridging stresses, δ_f, and shear deformation of the prepreg layers, δ_{pp}.

$$v_{ff}(x) - v_{br}(x) = \delta_{pp}(x) + \delta_f(x) \tag{1.3}$$

For a central crack in an FML, the stress intensity factor, K_{ff} and the crack opening term v_{ff} due to the far-field stress in the metal layers can be given with the monolithic metal panel solutions, which are given by Alderliesten as Eq. 1.4 and Eq. 1.5 respectively. σ_m represents the far-field stress in the metal layers, which can be calculated with the CLT [9, 10]. E_m represents the Young's modulus of the metal. The coordinate x is illustrated in Fig. 1.7.

$$K_{ff} = \sigma_m \sqrt{\pi a} \tag{1.4}$$

$$v_{ff} = 2\frac{\sigma_m}{E_m}\sqrt{a^2 - x^2} \tag{1.5}$$

While the stress intensity factor, K_{br}, and the crack closing term, v_{br}, due to the bridging stress distribution are expressed as integrals of the respective stress intensity factor and crack opening due to symmetric point-loads (see Fig. 1.7) along the delamination boundary.

Alderliesten approximates K_{br} with the following equation:

$$K_{br} = \int_{a_s}^{a} K_{br}(x_i)\,dx_i \tag{1.6}$$

with

$$K_{br}(x_i) = \frac{2P}{\sqrt{\pi a}} \frac{a}{\sqrt{a^2 - x_i^2 + b^2(x_i)}} \left(1 + \frac{1}{2}(1+\nu)\frac{b^2(x_i)}{a^2 - x_i^2 + b^2(x_i)}\right) \tag{1.7}$$

while v_{br} is given as:

$$v_{br} = \int_{a_s}^{a} v(x, x_i)\,dx_i \tag{1.8}$$

with $v(x, x_i)$ denoting the crack opening at location x due to symmetric point-loads acting at location x_i (Fig. 1.7).

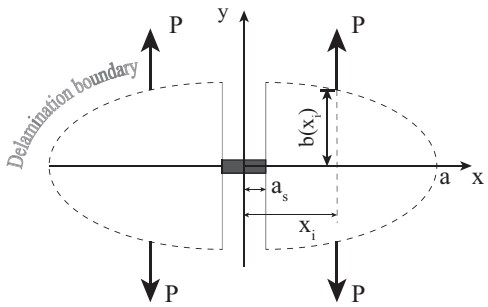

Figure 1.7: Illustration of symmetric point-loads acting at the delamination boundary $b(x_i)$ and at locations x_i [3]

It becomes obvious that the displacement of the metal crack and the delaminated length of the bridging fibres vary along the crack flank. Alderliesten evenly divides the delamination shape into bar elements to implement Eq. 5.3 at each bar location for solving the bridging stress. Fig. 1.8 schematically illustrates the division of the delamination shape. Moreover, the crack closing component, v_{br}, at one bar location is not only a function of the bridging stress at the bar element location, but also affected by the bridging stress at each bar element (Eq. 1.8). As a result, the displacement compatibility has to be implemented simultaneously for all the bar elements, forming a system of linear equations which can be solved with linear algebra. The size of the matrix for the system of linear equations is equal to the number of the bar elements.

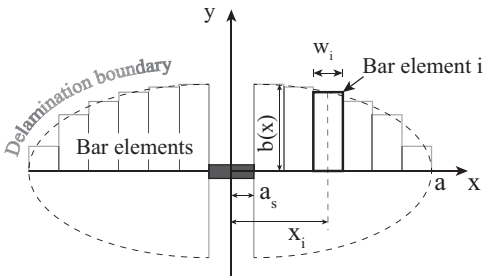

Figure 1.8: Discretization for calculating the bridging stress distribution [3]

Alderliesten implements the model in a numerical program. The overall structure of the program is shown in Fig. 1.9. It is worth noting that Eqs. 1.4-1.8 are developed for symmetric crack scenarios in FMLs.

1.6. ISSUES IN DIRECT EXTENDING THE ALDERLIESTEN MODEL FOR MSD SCENARIOS

Based on the description in the preceding section, it is essential to calculate the bridging stress distribution by simultaneously implementing the displacement compatibility at all bar elements. In consequence, extending the Alderliesten model to simultaneously solve all crack states of FMLs containing MSD scenarios faces several issues. To explain these issues, an example of an MSD scenario in an FML is schematically illustrated in Fig. 1.10.

The first issue is to calculate the crack opening displacements (CODs) for a row of cracks depending on the configuration. For evenly spaced cracks subjected to far-field tensile stress, the CODs are can be found in [34]. However, non-evenly spaced cracks are more common in real structures, such as the illustrated case in Fig. 1.10, which can be attributed to the fact that the boundary conditions for all the crack tips are not the same in a real structure with a finite width. As a result, the growth behaviour of a crack tip can differ from the rest, leading to non-evenly spaced cracks whose CODs are difficult to derive. In addition, the crack closing displacement, v_{br}, at a bar element in one crack due to the bridging stresses, such as the bar element i in Fig. 1.10, should be coupled with the bridging stress distributions over all cracks. Derivation of an analytical equation for

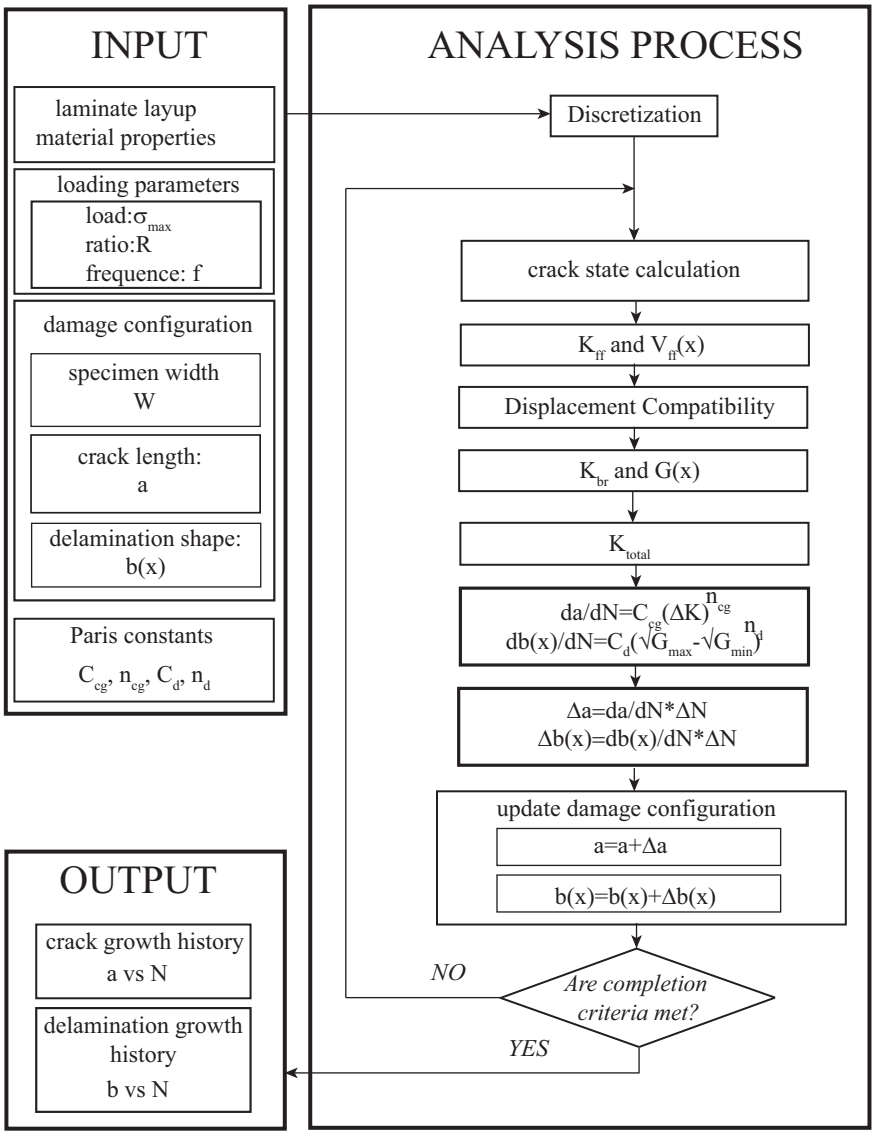

Figure 1.9: Flow diagram for the Alderliesten model (adapted from [3])

this v_{br} is extremely challenging.

The second issue is the computational efficiency of simultaneous prediction of the bridging stress at all bar elements over multiple cracks. As in the example illustrated in Fig. 1.10, the closing displacement, v_{br}, of bar element i should be a function of the bridging stresses at all bar elements of Crack 1, Crack 2 and Crack 3. Thus a matrix whose size could be around 3 times larger than that for one crack configuration needs to be constructed in order to solve for the bridging stresses simultaneously. Depending on

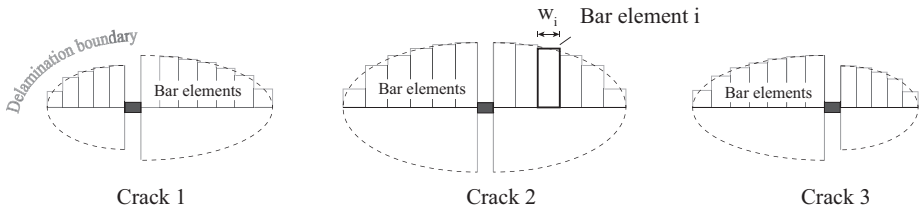

Figure 1.10: Discretization of delamination shapes for all cracks [1]

the number of cracks and the length of each crack of a generic MSD configuration in an FML, the much larger matrix constructed to predict bridging stress distribution results in computational inefficiency.

The third issue could be that the Alderliesten model cannot analyse the non-symmetric crack opening and non-symmetric delamination shapes for two crack tips of an asymmetric crack in an MSD scenario. The Alderliesten model has to be extended to incorporate the non-symmetry effects.

1.7. ALTERNATIVE APPROACH FOR PREDICTING CRACK GROWTH IN FMLS WITH MSD SCENARIOS

In the face of the issues and limitation in direct extension of the Alderliesten model for MSD crack growth in FMLs, a simplified MSD prediction approach for FMLs is an alternative, i.e., to solve each crack state by idealising the effect of other cracks in terms of reduction in overall stiffness.

The overall stiffness of a structure is related to the material stiffness (Young's modulus) and geometric stiffness of the structure [35]. The material stiffness of a panel is an inherent property which cannot be changed merely by the presence of a crack. However, the presence of a crack can decrease the geometric stiffness of a structure by reducing the net sectional area, resulting in larger deformation under the same loading condition as the remaining material has to carry the entire applied load. As a result, the crack growth rate increases with the increasing crack length according to LEFM. In case the cracked panel is reinforced by stiffeners which increase the effective stiffness of the cracked panel, the deformation is restrained. The crack growth rate decreases when the crack grow towards an adjacent stiffener as a result of the load redistribution from the cracked skin to the stiffeners [35]. Another example is that the crack growth in FMLs is much slower compared to that of a crack in a monolithic metal panel because the intact bridging fibres partially compensate the geometric stiffness reduction in the metal layers [8].

The reverse case of a cracked panel reinforced by stiffeners is the presence of adjacent cracks in the panel. In addition to one single crack in a monolithic metal panel, the presence of collinear adjacent cracks prohibitively decreases the effective stiffness of the panel as no other material could compensate the stiffness reductions. As a result, the crack growth rate of the single metal crack prematurely soars up. By contrast, the effect of the presence of adjacent MSD cracks on the growth behaviour of a single crack

in FMLs is not as pronounced as in metal. This is attributed to the compensation made by the intact fibres in the wake of MSD cracks to the stiffness reductions in metal layers. Nevertheless, the presence of MSD cracks in FMLs still results in reductions in the geometric stiffness which lead to load redistribution from the locations of MSD cracks to the single crack.

Modelling the effects of adjacent MSD cracks on a single crack in terms of load redistribution mechanism in FMLs permits solving the state of the single crack without knowing all the crack opening of other cracks, and solves a relatively small matrix only for the single crack every step. This process can be iterated until all crack states have been calculated for a given MSD configuration.

One task arising in this alternative approach is to calculate the non-symmetry effects on the crack growth behaviour of a non-symmetric crack in an FML: to derive K_{ff} and v_{ff} solutions for an eccentric crack in the metal layer, obtain K_{br} and v_{br} solutions for a non-symmetric delamination shape with respect to the crack centre. A few more steps are needed prior to being able to analyse MSD crack growth behaviour in FMLs.

1.8. THESIS OVERVIEW

Considering the objectives of this work and the alternative approach for MSD in FMLs, an overview of its structure is given in Fig. 1.11. Each chapter will address one issue that is needed to approach the objective of this work, they are summarised in the following:

Chapter 2 - Load redistribution mechanism. This chapter will describe the development of an analytical model that captures the effects of load redistribution caused by reductions in geometric stiffness on the crack growth behaviour in FMLs, verify whether or not modelling the load redistribution mechanism is a feasible means of analysing crack growth behaviour in FMLs containing multiple cracks.

Chapter 3 - COD and stress intensity factor solutions for eccentric cracks in metals. Based on the Westergaard stress function for crack problem in metals, three solutions will be developed in order to obtain the optimal COD solution and K solution for a non-symmetric crack in a metal panel.

Chapter 4 - Non-symmetric crack growth in FMLs. The COD and K solution obtained in Chapter 3 will be applied to calculate the states of non-symmetric cracks in the metal layers due to the stress in the metal layers. A solution for calculating the stress intensity factor and crack closing due to fibre bridging in non-symmetric delamination shapes with respect to the crack centre will be developed to account for influence of non-symmetric delamination shapes on the crack growth behaviour in the metal layers.

Chapter 5 - MSD in flat FMLs. An analytical model for MSD crack growth prediction in FMLs subjected to far-field tensile loading will be developed based on the model in Chapter 2 and the model in Chapter 4. The load redistribution mechanism and non-symmetric growth behaviour in FMLs containing multiple cracks can be simultaneously analysed.

Chapter 6 - Pin loading effects. In this chapter, the crack growth behaviour in FMLs subjected to tension and pin loading will be analytically predicted.

Chapter 7 - MSD in FML joints. The fulfilment of this work's objective will be evaluated. The output of a methodology based on the model in Chapter 5 and the model in Chapter 6 for MSD in FML joints will be compared to test data. Areas where the method-

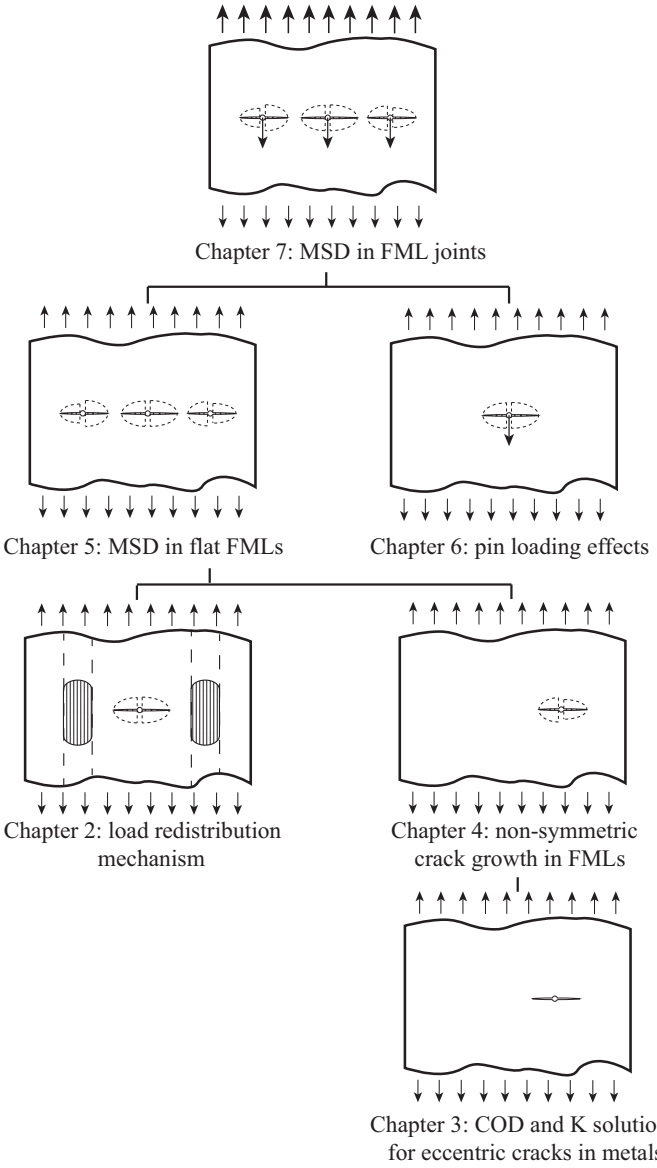

Figure 1.11: Structure of this research

ology falls short will be specifically discussed. How the model can be further developed to fulfil the objective will be described.

Chapter 8 - Discussion and conclusions. A detailed discussion on the assumptions made in the development of this work and their consequences on the model output, the overall performance of the models developed in this research and final conclusions will

be provided in this chapter.

REFERENCES

[1] W. Wang, C. Rans, R. Alderliesten, and R. Benedictus, *Philosophy of multiple-site damage analysis for fibre metal laminate structures,* in *Proceedings of 28th Symposium of the International Committee on Aeronautical Fatigue ICAF 2015, Helsinki, Finland* (2015).

[2] A. Vlot, *Glare:History of the Development of a New Aircraft Material* (Kluwer Academic Publisher, Dordrecht, The Netherlands, 2001).

[3] R. C. Alderliesten, *Fatigue crack propagation and delamination growth in GLARE*, Ph.D. thesis, Delft University of Technology, Delft, the Netherlands (2005).

[4] C. D. Rans, *2 - bolted joints in glass reinforced aluminium (glare) and other hybrid fibre metal laminates (fml), in Composite Joints and Connections*, in Composite Joints and Connections (2011).

[5] W. Wang, C. Rans, R. C. Alderliesten, and R. Benedictus, *Predicting the influence of discretely notched layers on fatigue crack growth in fibre metal laminates,* Engineering Fracture Mechanics **145**, 1 (2015).

[6] R. C. Alderliesten, *Analytical prediction model for fatigue crack propagation and delamination growth in glare,* International Journal of Fatigue **29**, 628 (2007).

[7] G. Wilson, *Fatigue Crack Growth Prediction for generalized fiber metal laminates and hybrid materials*, Ph.D. thesis, Delft University of Technology, Delft, the Netherlands (2013).

[8] A. Vlot and J. W. Gunnink, *Fibre Metal Laminates-An Introduction* (Kluwer Academic Publisher, Dordrecht, The Netherlands, 2001).

[9] J. J. Homan, *Fatigue initiation in fibre metal laminates,* International Journal of Fatigue **28**, 366 (2006).

[10] S. Spronk, I. Şen, and R. Alderliesten, *Predicting fatigue crack initiation in fibre metal laminates based on metal fatigue test data,* International Journal of Fatigue **70**, 428 (2015).

[11] T. Takamatsu, T. Matsumura, N. Ogura, T. Shimokawa, and Y. Kakuta, *Fatigue crack growth properties of a glare3-5/4 fiber/metal laminate,* Engineering Fracture Mechanics **63**, 253 (1999).

[12] R. Toi, *An empirical crack growth model for fiber/metal laminates,* in *Proceedings of the 18th symposium of the international committee on aeronautical fatigue* (Melbourne,Australia, 1995) pp. 899–909.

[13] T. Takamatsu, T. Matsumura, N. Ogura, T. Shimokawa, and Y. Kakuta, *Fatigue crack growth of a glare3-5/4 fiber/metal laminate and validity of methods for analysing results,* in *20th symposium international committee on aeronautical fatigue* (Bellevue Washington, USA, 1999).

[14] Y.-J. Guo and X.-R. Wu, *A phenomenological model for predicting crack growth in fiber-reinforced metal laminates under constant-amplitude loading,* Composites Science and Technology **59**, 1825 (1999).

[15] T. Takamatsu, T. Shimokawa, T. Matsumura, Y. Miyoshi, and Y. Tanabe, *Evaluation of fatigue crack growth behavior of glare3 fiber/metal laminates using a compliance method,* Engineering Fracture Mechanics **70**, 2603 (2003).

[16] R. C. Alderliesten, *Development of an empirical fatigue crack growth prediction model for the fibre metal laminate glare*, Master thesis, Delft University of Technology, Delft, the Netherlands (1999).

[17] R. Marissen, *Fatigue crack growth in ARALL. A hybrid aluminium-aramid composite material: Crack growth mechanisms and quantitative predictions of the crack growth rates*, Ph.D. thesis, Delft University of Technology, Delft, the Netherlands (1988).

[18] R. Rodi, *The Residual Strength Failure Sequence in Fibre Metal Laminates*, Ph.D. thesis, Delft University of Technology, Delft, the Netherlands (2012).

[19] S. Khan, *Fatigue Crack and Delamination Growth in Fibre Metal Laminates under Variable Amplitude Loading,* Ph.D. thesis, Delft University of Technology, Delft, the Netherlands (2013).

[20] S. U. Khan, R. C. Alderliesten, C. D. Rans, and R. Benedictus, *Application of a modified wheeler model to predict fatigue crack growth in fibre metal laminates under variable amplitude loading,* Engineering Fracture Mechanics **77**, 1400 (2010).

[21] S. U. Khan, R. C. Alderliesten, and R. Benedictus, *Delamination in fiber metal laminates (glare) during fatigue crack growth under variable amplitude loading,* International Journal of Fatigue **33**, 1292 (2011).

[22] W. Hendricks, *The aloha airlines accident — a new era for aging aircraft,* in *Structural Integrity of Aging Airplanes*, Springer Series in Computational Mechanics, edited by S. N. Atluri, S. G. Sampath, and P. Tong (Springer Berlin Heidelberg, 1991) Chap. 11, pp. 153–165.

[23] *Federal register/vol. 77, no. 101, thursday may 24, 2012/ rules and regulations,* .

[24] R. Eastin, *'wfd'-what is it and what's 'lov' got to do with it?* International Journal of Fatigue **31**, 1012 (2009).

[25] T. Beumler, *Moc for a380 hybrid structure,* in *Proceedings of the 2008 aircraft structural integrity program conference* (San Antonio, USA, 2008).

[26] D. Chang and A. Kotousov, *A strip yield model for two collinear cracks,* Engineering Fracture Mechanics **90**, 121 (2012).

[27] R. A. Collins and D. J. Cartwright, *On the development of the strip yield model for the assessment of multiple site damage,* Theoretical and Applied Fracture Mechanics **25**, 167 (1996).

[28] R. A. Collins and D. J. Cartwright, *An analytical solution for two equal-length collinear strip yield cracks,* Engineering Fracture Mechanics **68**, 915 (2001).

[29] D. S. Dugdale, *Yielding of steel sheets containing slits,* Journal of the Mechanics and Physics of Solids **8**, 100 (1960).

[30] H. R. Millwater, *A simple and accurate method for computing stress intensity factors of collinear interacting cracks,* Aerospace Science and Technology **14**, 542 (2010).

[31] S. Pitt and R. Jones, *Multiple-site and widespread fatigue damage in aging aircraft,* Engineering Failure Analysis **4**, 237 (1997).

[32] D. P. Rooke, *Stress intensity factors for cracks at a row of holes,* International Journal of Fracture **18**, R31 (1982).

[33] X. R. Wu and W. Xu, *Strip yield crack analysis for multiple site damage in infinite and finite panels – a weight function approach,* Engineering Fracture Mechanics **78**, 2585 (2011).

[34] H. Tada, P. C. Paris, and G. R. Irwin, *The stress analysis of cracks handbook* (ASME, New York, 2000).

[35] C. Rans, R. Rodi, and R. C. Alderliesten, *Analytical prediction of mode i stress intensity factors for cracked panels containing bonded stiffeners,* Engineering Fracture Mechanics **97**, 12 (2013).

2

PREDICTING THE INFLUENCE OF DISCRETELY NOTCHED LAYERS ON FATIGUE CRACK GROWTH IN FIBRE METAL LAMINATES

This paper presents an analytical model for fatigue crack growth prediction in Fibre Metal Laminates (FMLs) containing discretely notched layers. This model serves as a precursor in the development of a simplified prediction methodology for modelling the effect of load redistribution on a single crack in FMLs containing Multiple-site Damage (MSD) scenario. The model mainly focuses on capturing the influence of load distribution around discretely notched layers on the growth behaviour of an adjacent crack in an FML panel. The utilised approach in the model is the use of linear elastic fracture mechanics (LEFM) in conjunction with the principle of superposition and displacement compatibility. The proposed model is also validated using experimental data.

This chapter has been published in Engineering Fracture Mechanics **145**, 1-14 (2015) [1].

2.1. INTRODUCTION

The design philosophies used to ensure the integrity of aircraft structures over their lifetime have evolved over time. Currently, the design philosophy known as damage tolerance is recommended by the airworthiness regulations for the design of primary aircraft structures [2, 3]. Goranson defines damage tolerance as *the ability of structure to sustain anticipated loads in the presence of fatigue, corrosion or accidental damage until such damage is detected, through inspections or malfunctions, and repaired* [2]. Although this definition is generally agreed upon, various interpretations on the implementation of damage tolerance exist, particularly related to the determination of inspection intervals for metallic and composite aircraft structures. For the case of metallic structures, inspection intervals are set based upon a detection window defined as the service life required for a damage to grow from a detectable size (based on inspection capabilities) to a critical size (based on limit load carrying capability). Central to this is the concept of slow-growth and the ability to predict damage growth behaviour. Conversely, a no-growth approach is typically adopted in composite structures whereby damage growth under service conditions is not permitted and inspection intervals are specified based on the statistical likelihood of damage-causing events. This paper focuses on the slow-growth interpretation most commonly adopted for metallic structures.

A flaw identified in the damage tolerance design philosophy is its compatibility with an indefinite structural life. The philosophy focuses on detection and repair of damages through continued maintenance; however, it does not define a limit to the validity of this approach in terms of structural life. As damage tolerance analyses tend to focus on the evolution of singular or isolated damage states, there is a risk that they will be invalidated over time due to the occurrence of widespread fatigue damage within a structure. The classic example of this occurring is the Aloha Airlines Flight 243 that on April 28, 1988 suffered explosive decompression in flight due to the sudden link-up of small fatigue cracks at adjacent rivet holes in a longitudinal lap joint [4].

To combat the possibility of another failure due to widespread fatigue damage, the aircraft regulatory authorities have revised the regulations in 2010 with new rules pertaining to Ageing airplane safety *widespread fatigue damage* [5]. This revision included the definition of a Limit of Validity (LOV) of the engineering data (including the damage tolerance analyses) which support the continuing structural maintenance of an aircraft. These new regulations effectively require the aircraft OEMs to establish a firm limit to the operational life of a given aircraft type (within a given type certificate) that is substantiated with test evidence and analysis. As a result, there is a renewed interest in robust and efficient analysis methods for predicting Widespread Fatigue Damage (WFD) and its effects.

Fibre Metal Laminates are a class of hybrid metal-composite materials that evolved out of bonded metal laminate structures in the aerospace sector [6]. These materials were developed and refined for their superior crack growth resistance and critical damage size that complimented the damage tolerance design philosophy utilized in the aerospace sector. This growth resistance enables longer inspection intervals while the larger critical damage size enables the application of less sophisticated (and thus less costly) inspection techniques. These properties led to the successful application of FMLs as a fuselage skin material on the Airbus A380 passenger jet [6], and make FMLs a strong

material candidate in future transport aircraft.

In light of the new LOV requirement placing limits on damage tolerance and the success of FMLs in the context of damage tolerance, it is crucial to examine the WFD behaviour of FML structures. The open literature contains robust fatigue crack growth prediction methodology that has been developed for constant amplitude loading by Alderliesten [7, 8], and subsequently refined for variable amplitude loading [9–11] and for part-through cracks [12]. The robustness of these model even permits the prediction of FML crack growth material based upon individual constituent material behaviour [13]. However, directly applying these models for predicting the WFD crack growth behaviour of FMLs is cumbersome and computationally cost-ineffective due to a load redistribution calculation that will be elaborated on further in Section 2. Thus, a simplified approach for dealing with WFD prediction in FML structures is needed.

This paper presents and validates a precursor model for predicting the WFD behaviour of FML structures: crack growth adjacent to a discretely notched layers in an FML panel. This model is developed with the intention of applying it to model the load redistribution effects on a single crack in an FML panel containing WFD. Section 2.2 provides a brief description of the current state of the art of FML crack growth prediction and highlights the difficulty in directly applying this approach for WFD and motivating the proposed precursor model. Section 2.3 describes the development of the FML WFD precursor model while Section 2.4 presents an experimental program. Section 2.5 provides the validation of the model using experimental data.

2.2. BACKGROUND: STATE OF THE ART IN FML CRACK GROWTH PREDICTION

2.2.1. FATIGUE CRACK GROWTH BEHAVIOUR IN FMLS

Fatigue crack propagation in FMLs comprises crack growth in metal layers and delamination at the interfaces between metal layers and prepreg layers [7, 8]. FMLs derive their superior crack growth resistance due to the fibre bridging mechanism. Fig. 2.1 depicts this mechanism. The fatigue resistant fibres remain intact while fatigue cracks are present in metal layers of FMLs and act as a secondary load path over the crack. Partial load is transferred from the crack tip in the cracked metal layers into intact fibre layers. Consequently less stress is transferred around the crack tip in metal layers and the corresponding stress intensity factors at the crack tips therefore are reduced. In addition, this bridging mechanism introduces cyclic shear stresses at the interfaces between metal layers and fibre layers, which could induce delamination growth at the interfaces.

Alderliesten has developed an analytical model to predict the coupled crack propagation in metal layers and delamination growth at the interface between metal layer and fibre layer in FMLs, based on LEFM, superposition and displacement compatibility [7, 8]. The overall approach of his model will be summarized here for a given initial crack and delamination geometry. For a more in-depth review, please refer to [7, 8].

Crack extension in the metal layers is calculated using classical LEFM based on a cyclic crack tip stress intensity factor (ΔK) and an experimentally derived Paris relation for the crack growth resistance of the metallic material. The stress intensity factor at a given load is decomposed into two terms using superposition. The first term, K_∞, rep-

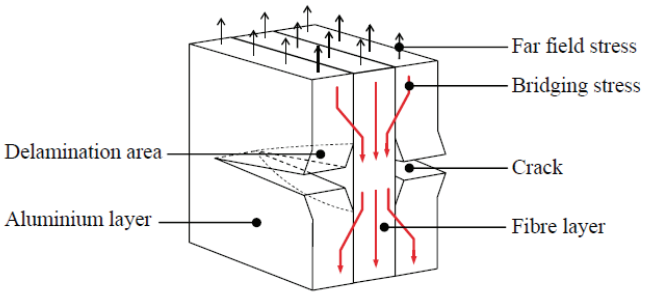

Figure 2.1: Bridging Mechanism

resents the stress intensity factor in the cracked metal layers due to the far-field applied load. The reduction in the stress intensity factor at the crack tip due to the fibre bridging mechanism, K_{br}, can be superimposed onto the far-field case, resulting a total stress intensity factor:

$$K_{total} = K_{\infty} + K_{br} \tag{2.1}$$

Extension of the interface delamination is similarly calculated using LEFM with an experimentally derived Paris relation for the delamination growth resistance. Due to the complexity of describing the stress state at an interface between two dissimilar materials (and thus calculating K), the Paris relation is described in terms of the strain energy release rate, G. As G varies along the delamination front, according to the local bridging stress state (Eq. 2.2), Alderliesten subdivides the delamination into columns perpendicular to the crack and makes the assumption that delamination growth occurs only in this direction. Propagation of the delamination within the crack growth direction is assumed to be tied to the crack tip [14].

$$G = \frac{n_f t_f}{2jE_f}\left(\frac{n_m t_m E_m}{n_m t_m E_m + n_f t_f E_f}\right)(S_f + S_{br})^2 \tag{2.2}$$

The extension of the metal fatigue crack and interface delamination can only be resolved once the bridging stress distribution is determined. Alderliesten calculates the bridging stress distribution along the crack length for a given fatigue crack and delamination geometry by applying displacement compatibility. Over the cracked region of the FMLs, the crack opening in the metal layers (as a result of crack opening due to the far-field load, v_{∞}, and crack closing due to the bridging stresses , v_{br}) must be identical to the elongation and deformation of the prepreg layers over the delaminated length, δ_f, plus the shear deformation of the fibre layer, δ_{br}.

$$v_{\infty}(x) - v_{br}(x) = \delta_f(x) + \delta_{pp}(x) \tag{2.3}$$

In this equation, v_{br}, δ_f, and δ_{br} all depend on the bridging stress distribution. This equation can only be solved numerically with a square matrix whose size is consistent with the number of even subdivision columns in the delamination shape [7, 8].

2.2.2. CHALLENGES IN PREDICTING MSD GROWTH IN FMLS

From previous description of FMLs crack growth model, it becomes apparent that the crack opening displacement of cracks in metal layers and using a matrix to numerically calculate the bridging stress distribution are two essential elements in implementation of displacement compatibility. To solve all crack states of FMLs containing MSD scenario simultaneously with the Alderliesten crack growth model therefore faces these two major challenges: 1) the crack opening displacement for each crack is very difficult to be derived analytically. 2) Each crack has a matrix to be solved and these cracks are coupled with each other. To solve bridging stress distributions for all cracks constructs a very large matrix, depending on the number of cracks, which is computationally inefficient. These two challenges make the use of FMLs crack growth model for MSD scenario problematic. Consequently, a simplified MSD prediction model for FMLs is an alternative, i.e. to solve each crack state by idealising the effect of other cracks in terms of reduction in overall stiffness.

The overall stiffness of a structure depends not only on the material stiffness (Young's modulus) but also geometric stiffness of the structure [15]. The presence of a crack in a panel reduces geometric stiffness because of a reduction in the net sectional area. This reduction in geometric stiffness results in an increase of the panel deformation because the cracked panel continues to carry the entire applied load. In an unstiffened metal panel, as no additional structural element compensates the reduction in geometric stiffness, a crack in the panel easily gains high crack growth rate according to LEFM. On the contrary, geometric stiffness reduction in cracked metal layers is compensated partially by the intact fibres over the crack in FMLs. Thus the crack growth rate of a crack in FMLs is almost stable for significant large portion of the crack growth life [6].

In the case of MSD scenario, the influences of multiple cracks adjacent on a single crack can be divided into crack tip interaction effects and load redistribution effects. Crack tip interaction effects are attributed to the interaction of the stress singularities in front of two approaching crack tips, which result in rapid fatigue growth and link-up of cracks. Load redistribution effects are attributed to the geometric stiffness reduction in the presence of MSD cracks. These effects are present over the whole fatigue growth life. Because the nature of slow crack growth behaviour in FMLs, a significant portion of MSD crack growth life in FMLs can occur before crack tip interaction effects are present. Over this period, the crack tip interaction effects can be neglected and the cumulative effects of load redistribution can result in significant decrease in fatigue life of FMLs.

Modelling the effects of adjacent MSD cracks on a single crack as local reductions in geometric stiffness in FMLs permits solving the single crack state without knowing all the crack opening displacement of other cracks, and provides a more efficient numerical solution that only one relatively small matrix for the single crack is solved every step. This process can be iterated until all crack states have been calculated.

2.2.3. ANALOGY BETWEEN AN ADJACENT FATIGUE CRACK AND DISCRETELY NOTCHED LAYERS

Since this precursor model is proposed with the intention of utilising it to model the load redistribution effects on a single crack in an FML panel with MSD cracks, it mainly focuses on modelling the effects of load redistribution caused by geometric stiffness re-

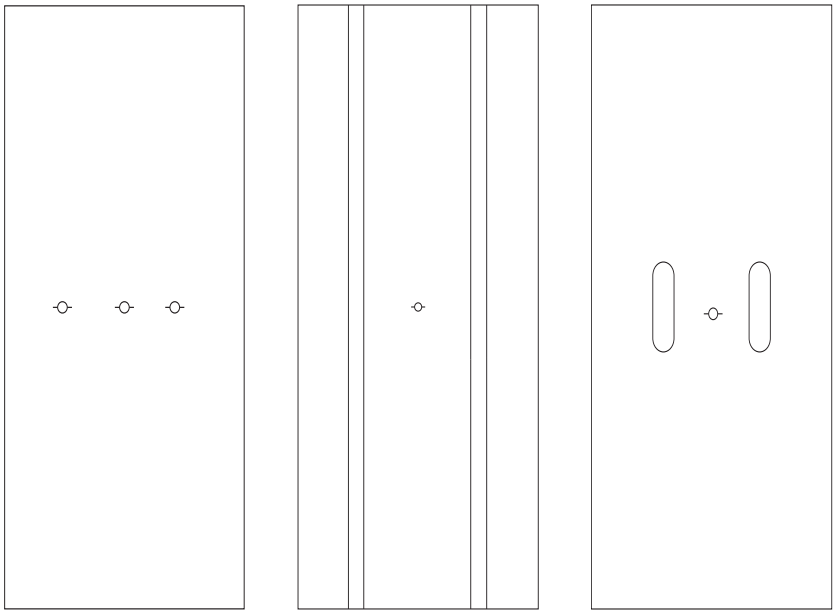

Figure 2.2: Analogy between real MSD (a), removal of whold strips (b), removal of partial strips (c)

ductions on an adjacent crack growth in this paper. The geometric stiffness reduction can be achieve by real MSD cracks or by removal of material ahead of the crack tip in FMLs.

For a central crack with two other crack symmetrically located on both sides in an FML panel, shown in Fig. 2.2(a), the effects of load redistribution caused by other two cracks on the central crack growth change along fatigue loading. This is because the adjacent cracks also grow under fatigue, making the validation of the proposed method in terms of capturing load redistribution due to the stiffness reduction difficult with this configuration.

Alternatively, the stiffness reductions at both sides of the central crack can be achieved by removing material ahead of the crack tips. As shown in Fig. 2.2(b), two entire strips of metal or fibre layers are symmetrically removed. This configuration also results in load redistribution with stable reduction in geometric stiffness at the locations of the strips under fatigue loading. However, removing the entire strip of metal layers in FMLs to achieve fixed stiffness reduction is not practical from a manufacturing perspective. Besides, differences in coefficient of thermal expansion between metal layers and fibre layers could also introduce other possible adverse effects during the high temperature and high pressure curing cycle in an autoclave.

The stiffness reductions therefore are chosen to be achieved by discretely notched layers. These artificial notches can be achieved by exclusive removal of partial strips of metal layers or fibre layers, as depicted in Fig. 2.2(c). If partial metal strips are removed,

the length of the artificial notch should be relatively long so that the stress concentrations at the edges are as low as possible because no additional cracks at the notch edges are desirable. The removal of fibre layers does not initiate any cracks at the notch edges. These artificial notches simulate the reductions in geometric stiffness that can be created by fatigue cracks, allowing the effect of stiffness reduction on a single fatigue crack in FMLs via load redistribution methodology to be studied.

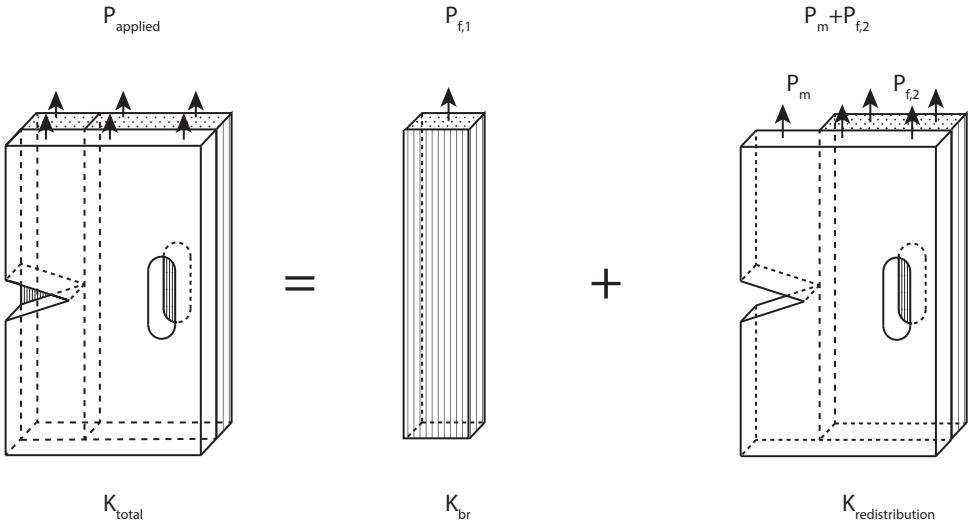

Figure 2.3: Decomposition of load in FML

2.3. MODEL DEVELOPMENT

A central cracked FML panel with two artificial discretely notched layers symmetrically located at both sides of the central crack is considered in this paper, as illustrated in Fig. 2.2(c). The modelling relies on the principle of superposition and LEFM. The overall stress intensity factor, K_{total}, for the central crack in this case can be determined by superimposing the stress intensity factor due to bridging mechanism of fibres over the crack, K_{br}, and the stress intensity factor in cracked metal layer attributed to the far-field applied load and load redistribution resulting from the presence of a notch in front, $K_{redistribution}$. To aid in calculation of individual stress intensity factor term, the applied far-field load in FML is also decomposed into two parts: load transmitted in intact fibres over the crack, and load transmitted in remaining metal layers and fibre layers, which is schematically illustrated in Fig. 2.3.

$$K_{total} = K_{redistribution} + K_{br} \tag{2.4}$$

The far-field applied stress in the laminate can be calculated if the applied load and the configuration of the FML panel is known, see Eq. 2.5. The applied stress in metal layer, $\sigma_{m,applied}$, and in fibre layer, $\sigma_{f,applied}$, can be calculated using the classic laminate theory detailed in [16, 17].

$$\sigma_{applied} = \frac{P_{applied}}{n_m t_m W + n_f t_f W} \tag{2.5}$$

where the subscript m refers to metal layer and f refers to fibre layer, n denotes the number of specified layers, t represents thickness of each layer.

The far-field load transmitted by intact fibres over the crack, and by remaining metal layers and fibre layers are given below:

$$P_{f,1} = \sigma_{f,applied} n_f t_f a \tag{2.6}$$

$$P_m = \sigma_{m,applied} n_m t_m W \tag{2.7}$$

$$P_{f,2} = \sigma_{f,applied} n_f t_f (W - a) \tag{2.8}$$

2.3.1. MODELLING LOAD REDISTRIBUTION DUE TO THE PRESENCE OF NOTCHES

The presence of notches in metal layers decreases the effective stiffness at the notched area, which results in load transfer from the notched area to surrounding material, as depicted in Fig. 2.4. This load transfer is characterized with the implementation of displacement compatibility which is enforced by assuming an isostrain condition between the artificial notched area and surrounding material. This compatibility condition is also applied by Barsoum and Ravi Chandran in analysing stress intensity factors in layered and functionally graded materials [18, 19]. The transferred load can vary as a function of the crack length.

According to the classic laminate theory, the isostrain condition among intact metal layers and fibre layers in FMLs must be valid. The stress distribution ahead of the crack tip in metal layers can be characterised by the Westergaard stress distribution [20], it is therefore assumed that the stress distribution ahead of the crack tip for the whole laminate follows the same distribution in metal layers. Fig. 2.5 depicts the stress distribution in the intact FML ahead of the crack tip, which is expressed as

$$\sigma_{yy} = \frac{\sigma_{westergaard}}{\sqrt{1-(a/x)^2}} \tag{2.9}$$

for $a < x < x_l$ and $x_r < x < W$, where the value of $\sigma_{westergaard}$ is still unknown due to the fact that it is affected by $F_{transferred}$ which is still not determined. Other quantities mentioned in Eq. 2.9 are denoted in Fig. 2.5.

According to the assumption that the isostrain condition is also valid between the discretely notched area and surrounding laminate, the stress distribution for $x_l < x < x_r$ is then given as Eq. 2.10. The stress distribution at the notch area is schematically depicted in Fig. 2.5.

$$\sigma_{notch} = \frac{E_{notch}}{E_{FML}} \frac{\sigma_{westergaard}}{\sqrt{1-(a/x)^2}} \tag{2.10}$$

with E_{notch} being the Young's modulus of the remaining material at the notched area and E_{FML} the Young's modulus of the FML panel.

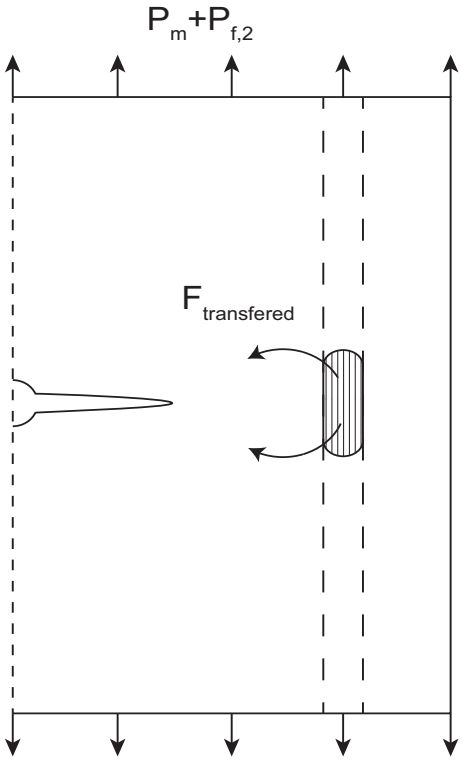

Figure 2.4: Illustration of load redistribution due to notch

As shown in Fig. 2.5(a), when the crack tip is far away from the left edge of the artificial notch, the Westergaard stress distribution at the notch is smooth and the value is low, the stress reduction due to reduction in the effective stiffness at the notch is therefore small, which means less load transfer between the two parts. However, when the crack tip approaches the edge, due to the high stress value and steep gradient, the stress reduction at the notch is higher resulting in higher load transferred to the crack tip, see Fig. 2.5(b).

The applied far-field loads in the metal layers and fibre layers excluding the intact fibres over the crack, shown in Fig. 2.5, are transmitted through the remaining material at the crack plane, i.e. the intact FML and fibre layers at notched area. Based on the load equilibrium, the applied far-field load is equal to the loads transmitted by the remaining material at the crack plane which can be calculated by integrating the stress distribution in Eqs. 2.9 and 2.10.

$$P_m + P_{f,2} = \int_a^{x_l} \sigma_{yy}\, t_{FML}\, \mathrm{d}x + \int_{x_l}^{x_r} \sigma_{notch}\, t_{notch}\, \mathrm{d}x + \int_{x_r}^{W} \sigma_{yy}\, t_{FML}\, \mathrm{d}x \tag{2.11}$$

where t_{FML} and t_{notch} represent thickness of the FML and total fibre layers at the artificial notch respectively.

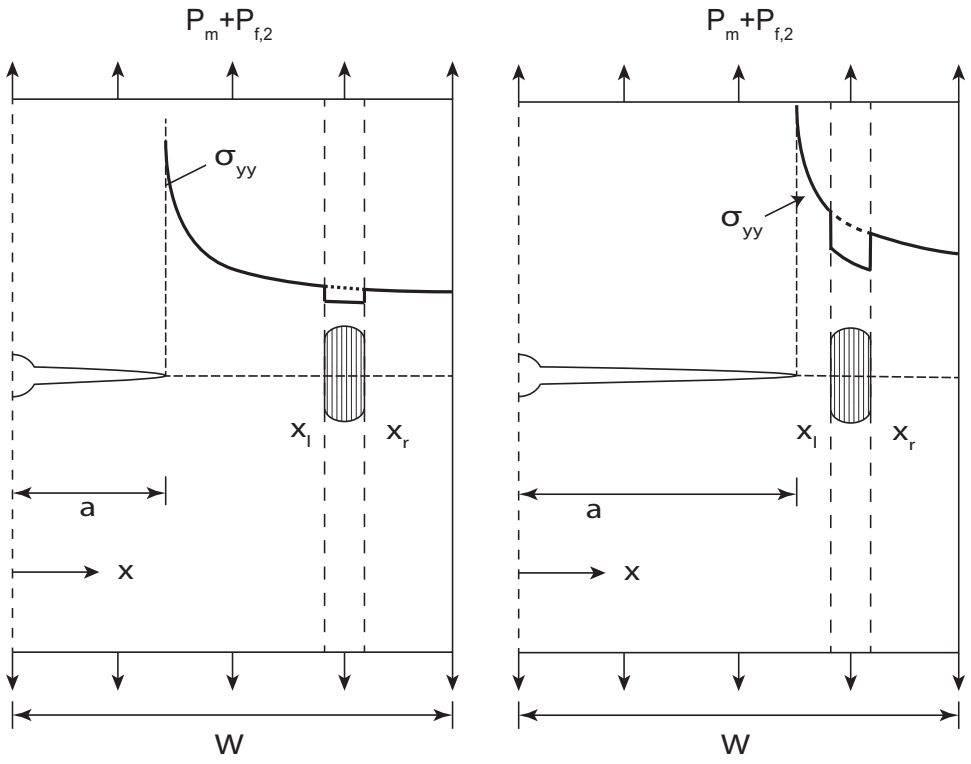

Figure 2.5: Illustration of stress distribution at cracked section

Substitute Eq. 2.9 and Eq. 2.10 into Eq. 2.11 and rewrite the equation for $\sigma_{westergaard}$:

$$\sigma_{westergaard} = \frac{P_m + P_{f,2}}{\int_a^{x_l} \frac{t_{FML}}{\sqrt{1-(a/x)^2}}\,\mathrm{d}x + \int_{x_l}^{x_r} \frac{E_{notch}}{E_{FML}} \frac{t_{notch}}{\sqrt{1-(a/x)^2}}\,\mathrm{d}x + \int_{x_r}^{W} \frac{t_{FML}}{\sqrt{1-(a/x)^2}}\,\mathrm{d}x} \tag{2.12}$$

The stress in metal layers is then determined in terms of $\sigma_{westergaard}$ using the classic laminate theory [16, 17]. This stress, denoted as σ_m, is attributed to the applied far-field load and the load redistribution caused by the notch. Based on the LEFM theory, the corresponding stress intensity factor can be given

$$K_{redistribution} = \sigma_m \sqrt{\pi a} \tag{2.13}$$

It has to be noticed that in the Alderliesten model, the Dixon correction factor is implemented to account for the boundary condition. However, in the methodology presented in this paper, the boundary effect has been taken into consideration using the Westergaard stress distribution. The Dixon correction therefore should not be used again.

2.3.2. MODELLING LOAD REDISTRIBUTION DUE TO THE BRIDGING FIBRES

The intact fibres bridging the crack restrict the crack opening displacement resulting from the applied far-field load and the redistributed load. Consequently, partial load in metal layers is transferred into the intact fibres resulting in a reduction in stress intensity factor at the crack tip. The calculation of the bridging stress σ_{br} in the intact bridging fibres follows the same displacement compatibility method used by Alderliesten [7, 8], see Eq.(2.3). It is noteworthy that only the bridging stress in the bridging fibres is accounted for when calculating the crack closing displacement, v_{br}, and corresponding stress intensity factor, K_{br}. For detailed calculation, one can refer to [7, 8].

2.3.3. CRACK GROWTH MODEL AND DELAMINATION GROWTH MODEL

Crack growth rate in metal layers can be estimated with the empirical Paris relation:

$$\frac{da}{dN} = C_{cg}(\Delta K)^{n_{cg}} \tag{2.14}$$

values of material constants are $C_{cg} = 2.17 \cdot 10^{-12}$ and $n_{cg} = 2.94$.

Similarly, delamination growth rate is estimated using the Paris relation based on the strain energy release rate:

$$\frac{db}{dN} = C_d(\sqrt{G_{max}} - \sqrt{G_{min}})^{n_d} \tag{2.15}$$

where the material constants are derived from experimental data [8]. The values are $C_d = 0.05$ and $n_d = 7.5$.

2.4. TEST PROGRAM

2.4.1. MATERIAL AND SPECIMENS

The tested FMLs were Glare 3-3/2-0.4 panels. The lay-up for the tested Glare is defined as [Al/0/90/Al/90/0/Al], where Al refers to a 2024-T3 aluminium layer, and 0 and 90 refer to unidirectional prepreg layers and their orientation. The prepreg layer consists of S2-glass fibres embedded in FM94 epoxy resin. The principle properties of Glare constituents are given in Table 2.1.

Table 2.1: Material properties

	Al	**Prepreg**
Young's modulus $E_x[GPa]$	72.4	48.9
Young's modulus $E_y[GPa]$	72.4	5.5
Shear modulus $G_{xy}[GPa]$	27.6	5.55
Poisson's ratio v_{xy}	0.33	0.33
Poisson's ratio v_{yx}	0.33	0.0371
Thickness of single layer$[mm]$	0.4	0.133
Thermal expansion coefficient[1/°C]	$22 \cdot 10^{-6}$	$6.1 \cdot 10^{-6}(0°)$ $26.2 \cdot 10^{-6}(90°)$

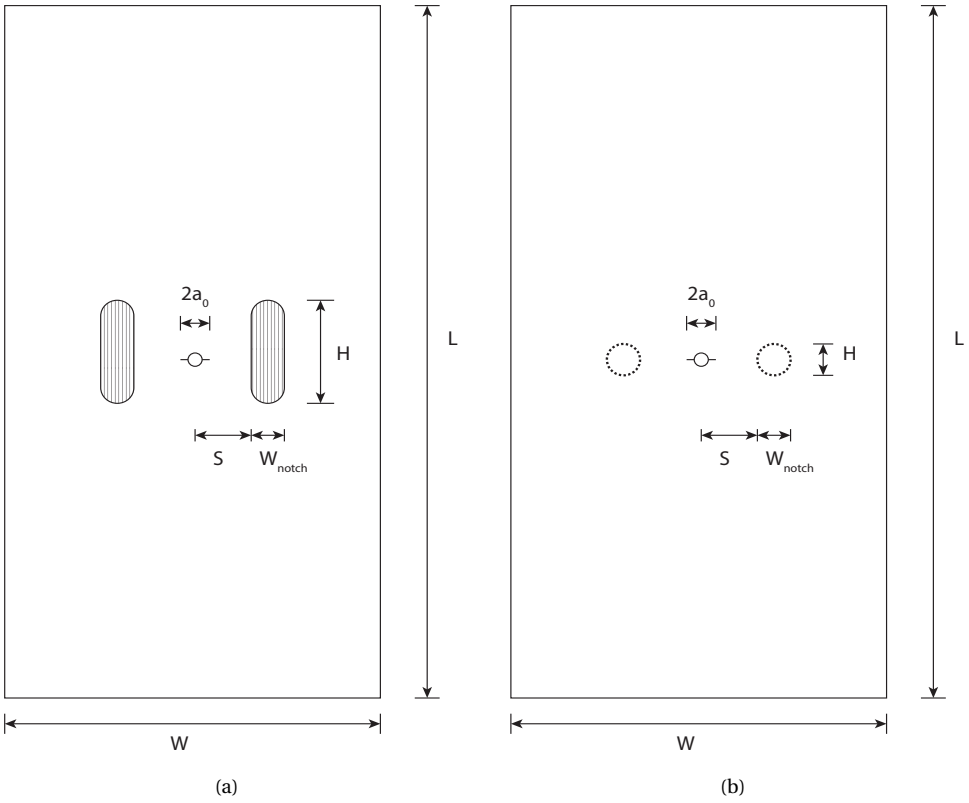

Figure 2.6: Geometry for specimens with notches in Al layers (a), specimens with notches in prepreg layers (b)

With the intention to achieve different stiffness reduction at the location of the artificial notch, two kinds of discrete notches were manufactured in specimens: Glare panels containing round-end slots exclusively in aluminium layers whose configuration is schematically depicted in Fig. 2.6(a) with corresponding dimensions given as type 2 and 3 in Table 2.2, and Glare panels with circular notches exclusively in fibre layers whose configuration is given in Fig. 2.6(b) and its dimensions are given as type 4 in Table 2.2. 3 layers of aluminium are removed for notch configuration depicted in Fig. 2.6(a) and 2 composites layers are removed for notch configuration in Fig. 2.6(b). Standard M(T) Glare panels were also made to serve as baseline, type 1 in Table 2.2 denotes its specific dimensions.

The M(T) specimens were made by laminating three intact layers of aluminium and two cross-plies in between. For specimens with artificial notches in aluminium layers, rectangular aluminium panels were cut at first. Then two holes were drilled at opposite corners of the panels. Two pins were put in the holes to align and fix three aluminium panels when the artificial notches were milled. Once aluminium panels with corresponding slots were ready, they were laminated with prepreg layers in which two

pin holes were also made as in aluminium panels so that two pins could be used to align the artificial notches in different layers during curing. For specimens with notches in fibre layers, circular notches instead of slots were punched. As prepreg plies have very low rigidity, it is difficult to cut slot notches using a punch whose head is circular. In addition, the influence of manufacturing slots or circular notches in fibre layers on stiffness reduction is minor. Two pin holes were also made at opposite corners in both aluminium layers and prepreg plies so that pins could also be applied to align notches in different fibre layers during curing. After curing process, the panels were C-scanned to check whether the notches in different layers were aligned.

The assembled 2024-T3 layers and prepreg layers were put into an autoclave to perform the curing process at a maximum temperature of 120 °C and maximum pressure of 6 bars. Each specimen was drilled a hole of 3 mm diameter with two saw-cuts of 1.5 mm on both sides resulting in a total initial saw-cut length of $2a_0 = 6$ mm.

Table 2.2: Specimen configuration

Type	**W**(mm)	**L**(mm)	$2a_0$(mm)	W_{notch}(mm)	**H**(mm)	**S**(mm)
1	140	300	6	-	-	-
2	140	300	6	8	16	26
3	140	300	6	4	12	26
4	140	300	6	8	8	26

2.4.2. FATIGUE TEST

Fatigue testing was conducted under constant amplitude fatigue loading conditions with a maximum applied stress of 140 MPa, stress ratio of $R = 0.05$, and testing frequency of 10 Hz. Testing was carried out on an MTS 810 servo hydraulic test frame containing pin hole grips and an 250 kN load-cell (model 661. 22D-01). The test set-up is given in Fig. 2.7. The test was stopped after a number of cycles and the maximum load was applied so that the crack was fully open. Then the crack length was measured using a monocular microscope with an precision of 0.1 mm. After both crack length and corresponding cycle number were recorded, the test was resumed. Each crack increment was kept around 0.5 mm in order to get abundant test data and reduce testing scatter. Crack growth rates were calculated using a 7-point incremental polynomial method recommended in the ASTM E647-00 [21] for processing crack growth measurements.

2.4.3. TEST FOR ISOSTRAIN MODEL VALIDATION

The stress distribution ahead of the crack tip, which is characterised with the Westergaard stress distribution method, is of great interest in modelling the load redistribution. However, only the corresponding strain distribution can be obtained in a test environment. The experimental strain measurement technique chosen for this study is the Digital Image Correlation (DIC). The DIC method [22, 23] obtains the deformation field on the surface of an specimen by tracking deformation of a random pattern in the image of the specimen without deformation (source image) and the image of the deformed specimen (target image). This deformation field can be post-processed to calculate the

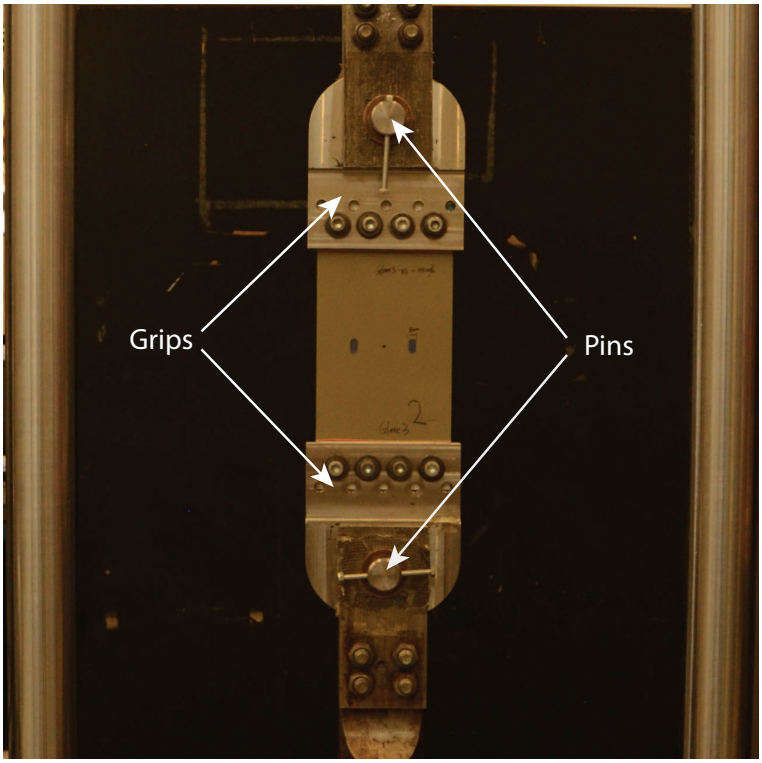

Figure 2.7: Test set-up

corresponding strain field on the surface of the test specimen. Using this method, it is possible to easily visualise and quantify the crack tip strain field and the corresponding influence of the notches present in the test specimens used in this study. All DIC strain measurements presented in this paper were made using the VIC-3D™ DIC system offered by Correlated Solutions.

DIC strain measurements were made for a M(T) specimen and a specimen with notches of 8mm wide in aluminium layers. To measure the strain distribution in front of the crack tip without interference by the bridging fibres, the cracks in both specimens were made by saw-cut, as a result the fibres were also cut in the saw-cut region. The collection of reference and loaded images for DIC processing was performed under static loading conditions. To facilitate correlation of the images by the DIC system, a flat white base coat of paint and an airbrushed speckle pattern of black paint were applied to the measurement area. The subset size for image correlation is $21 \cdot 21$ pixels and the step is 5.

2.5. MODEL VALIDATION

The experimental data is utilised to validate the prediction methodology described. First, the predicted strain distribution ahead of the crack tip is compared to that experimen-

tally obtained using the DIC method. Second, the predicted crack growth rates are compared with experimentally obtained results.

2.5.1. COMPARISON BETWEEN PREDICTED STRAIN DISTRIBUTION AND DIC TEST RESULTS

For the M(T) specimen including fibres cut in the saw-cut region, the stress distribution ahead of the crack tip can be characterised with Eq. 2.9. The load equilibrium between the applied load and load transferred at the net section area is expressed as

$$P_{applied,M(T)} = t_{FML} W \int_a^W \frac{\sigma_{westergaard}}{\sqrt{1-(a/x)^2}} \, \mathrm{d}x \tag{2.16}$$

which can be rearranged to solve $\sigma_{westergaard,M(T)}$:

$$\sigma_{westergaard,M(T)} = \frac{P_{applied,M(T)}}{t_{FML} W \sqrt{1-(2a/W)^2}} \tag{2.17}$$

The strain distribution in front of the crack tip can then be calculated with Westergaard stress divided by the Young's modulus of the laminate:

$$\varepsilon_{yy,M(T)} = \frac{P_{applied,M(T)}}{t_{FML} E_{FML} W \sqrt{1-(2a/W)^2} \sqrt{1-(a/x)^2}} \tag{2.18}$$

The strain distribution in front of the crack tip of the notched specimen is given in the same way

$$\begin{aligned} \varepsilon_{yy,notch} = & \frac{1}{E_{FML}\sqrt{1-(a/x)^2}} \\ & \cdot \frac{P_{applied,notch}}{\int_a^{x_l} \frac{t_{FML}}{\sqrt{1-(a/x)^2}} \mathrm{d}x + \int_{x_l}^{x_r} \frac{E_{notch}}{E_{FML}} \frac{t_{notch}}{\sqrt{1-(a/x)^2}} \mathrm{d}x + \int_{x_r}^{W} \frac{t_{FML}}{\sqrt{1-(a/x)^2}} \mathrm{d}x} \end{aligned} \tag{2.19}$$

The predicted and measured strain distributions on both side of the central crack are compared in Fig. 2.8. From Fig. 2.8(a), it can be seen that the predicted strain distribution correlates with DIC measurement very well, which proves that using Westergaard stress method to characterise the stress distribution ahead of a crack tip in a laminate is a valid method.

Fig. 2.8(b) gives the strain distribution for the specimen containing notches in aluminium layers, the blue and red lines indicate the locations of the edges of right and left side notches respectively. This misalignment is due to a manufacturing error. However, the corresponding prediction for these two notch cases overlap with the prediction for notch edges at $26mm$ and $34mm$ (the average locations of left and right side notch edges with respect to crack centre). Since the strain distribution around the notch area is quite smooth based on the prediction method, the influence of the locations of notches on prediction results is therefore significantly small. The DIC measurements reveal smooth variation of the strain distribution between the notch area and surrounding laminate, which verifies the assumption that isostrain between these two areas. In addition, the

DIC measurements show that the strain rises near the notch edges which are due to stress concentration. However, the influence of this deviation of the measured strain from the predicted strain based on neglecting the stress concentration at the notch area upon the load redistribution is minor. The reason for that is due to the low Young's modulus and very small thickness of the fibre layers at the notched area. Therefore, the assumption of isostrain condition between the notch area and surrounding laminate, and neglecting the stress concentration at notch edges are reasonably verified.

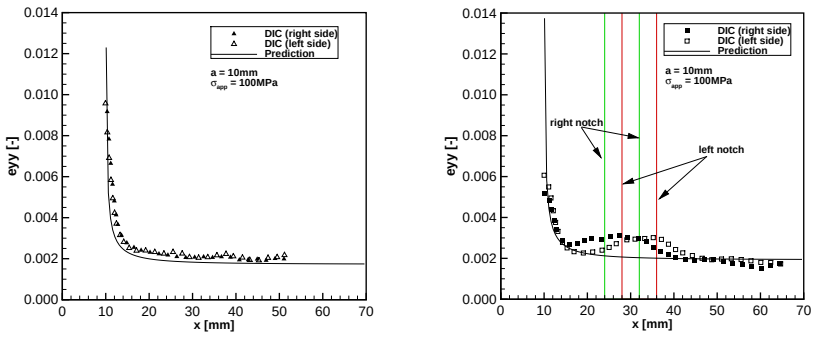

(a) (b)

Figure 2.8: Strain distribution ahead of the crack tip in M(T) specimen (a), in notched specimen (b)

2.5.2. CRACK GROWTH RATES COMPARISON

Several predicted crack growth rates for Glare 3 with different notch configurations are given together with corresponding experimental results. The crack growth rates are plotted versus the crack length measured from the crack centre.

In Fig. 2.9, the crack growth rates for Glare 3 containing 8mm wide notches in aluminium layers or in fibre layers are given together with their corresponding prediction results. The specific configurations of the specimens are given in Fig. 2.6 and corresponding dimensions for the notches are give as Type 2 and Type 4 in Table 2.2 respectively. The test result and prediction of the Alderliesten crack growth model for the M(T) specimen (Type 1 in Table 2.2) are also given to highlight the effect of stiffness reduction on crack growth rate. The grey area represents the location of the artificial notch. The maximum applied stress level is $140MPa$. The overall predicted crack growth rates correlate quite well with the observed crack growth rates. As can be seen from Table 2.1, the thickness and Young's modulus of aluminium layer are much higher than fibre prepreg layer, the reduction in effective stiffness caused by removal of aluminium layers is therefore higher than removal of fibre layers. Consequently, the specimen containing notches in aluminium layers has higher initial crack growth rate and gains greater crack growth rate with crack length. Whereas, due to a small stiffness reduction caused by removing the fibre layers, the corresponding crack growth rate almost keeps identical to that of the M(T) result over its most propagation and only accelerates a little when the crack tip reaches the edge of the artificial notch.

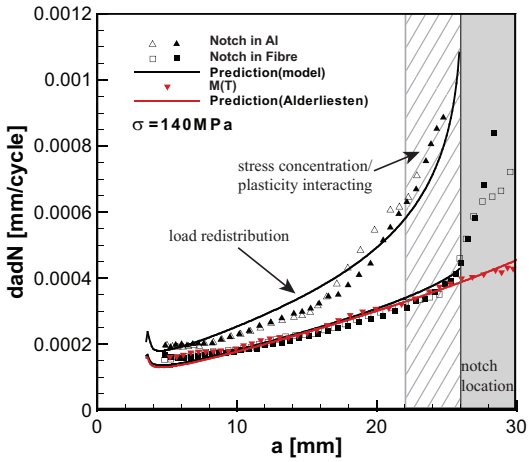

Figure 2.9: Comparison between predicted and experimental crack growth rate for Glare 3-3/2 with notches in Al layers or fibre layers with $\sigma_{max} = 140MPa$

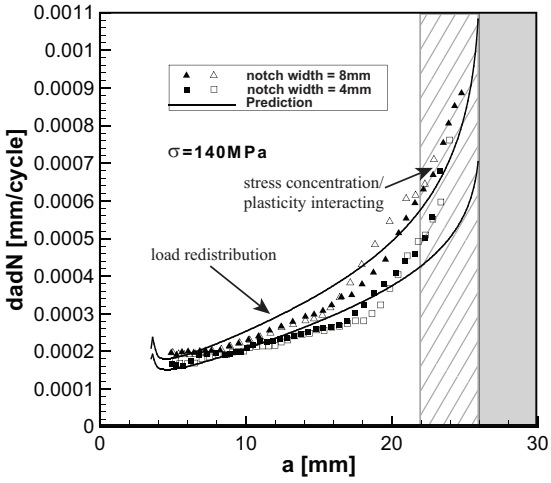

Figure 2.10: Crack growth rates for Glare 3-3/2 panels with different notches of 8mm and 4mm wide in Al layers under $\sigma_{max} = 140MPa$

The predictions were stopped when the crack tip reached the notch edge. The corresponding test on the specimen containing notches in aluminium layers also stopped at this point, while the test on the specimen with notches in fibre layers was continued after the crack exceeded the notch edge. From the test results shown in Fig. 2.9, the crack grows much faster at the notch area in the comparison with the results for the M(T) specimen in which the crack opening is always restrained by the bridging fibres. Even

though the crack opening in the aluminium layer in the specimen containing notches in fibre layers is constrained by the bridging fibres from the saw-cut to the notch edge, the crack growth rate increases rapidly once the crack exceeds the notch edge, as can be seen in Fig. 2.9. This proves that the bridging mechanism of fibres just behind the crack tip plays a key role in reducing the corresponding stress intensity factor.

The initial discrepancy of the prediction can be attributed to the inaccuracy of presumed delamination size in the beginning. The initially calculated bridging stress and delamination extension are sensitive to this initially assumed delamination size and the subsequent calculation is also affected [7]. Then the calculation converges after a very small crack extension.

The crack growth rates for specimens under maximum applied load of 140 MPa but with notch width of 8mm and 4 mm in aluminium layers (Type 2 and Type 3 in Table 2.2) are given together with the corresponding predicted results in Fig. 2.10. For both cases, the crack accelerates when it approaches the edge of the artificial notch. The specimen with wider notches which result in larger stiffness reductions has greater crack acceleration, which is also captured by the prediction method.

For specimens with notched aluminium layers in Fig. 2.9 and Fig. 2.10, stress concentration occurs at the notch edges. Calculation of the notch root stress concentration and corresponding plasticity beyonds the scope of this paper. However, the effects of interaction between the stress singulatrity in front of the crack tip and notch root stress concentration (or plasticity interacting) are present when the crack tip approaches the notch edge. This interaction occurs only over a small portion of the crack size, which is depicted in Fig. 2.9 and Fig. 2.10. For the major portion of the crack propagation, only load redistribution effects are present. Neglecting the notch root stress concentration results in larger load redistribution for the crack and larger stress intensity factors, resulting in conservative prediction results.The division of these two portions is roughly based on the experimental measurements given in Fig. 2.8(b)

2.6. DISCUSSION

In preceding sections, the validation shows that using the Westergaard stress distribution adequately captured the stress state in front of the crack tip and the model described in this paper gives a good prediction for each case. Especially, the proposed model estimates the crack growth acceleration very well when the crack gets close to the edge of the artificial notch. Still some aspects regarding the model's limitation and its potential to be extended to address fatigue crack growth in FMLs containing MSD need to be discussed.

2.6.1. LIMITATION OF THE PROPOSED MODEL

In the presented analytical model, the length of the artificial notch is ignored by assuming no stress concentration at the edges of the artificial notches. So the proposed model is a simplification of modelling a notch as a complete removal of a very long strip of material. The DIC results indicate that there are stress concentrations at the artificial notch edges. However, the influence of the stress concentration on the load redistribution in the analytical model is minor. Neglecting the stress concentration at notch edges results

in higher stress intensity factor and thus conservative prediction results. As a result, this analytical model still provides good predictions.

Due to the fact that the precursor model is based on the Westergaard stress method, it can only be extended to study the collinear cracks scenario in FMLs.

2.6.2. POTENTIAL OF EXTENDING THIS ANALYTICAL MODEL TO A MSD PREDICTION MODEL IN FMLS

The model presented in this paper successfully captures the effect of load redistribution due to stiffness reduction, achieved by artificial notches, on the growth behaviour of the adjacent crack. The crack growth accelerates when the crack tip approaches the location of the stiffness reduction as more loads are redistributed to the crack tip. This investigation approves the potential of idealising the effect of an adjacent crack on the fatigue growth behaviour of a single crack as stiffness reduction when addressing fatigue crack growth in FMLs containing MSD scenarios. However, it is noteworthy that the stiffness reductions caused by cracks are becoming larger during fatigue loading. This phenomenon is similar to the effect of a wider artificial notch on the growth behaviour of the adjacent crack, which is illustrated in Fig. 2.10. This analytical model therefore has the potentiality to be extended to a simplified model for MSD prediction in FMLs.

2.7. CONCLUSION

An analytical model for predicting crack acceleration due to discretely notched layers based on linear elastic fracture mechanics (LEFM), the principle of superposition and displacement compatibility has been presented. From the DIC investigation it is concluded that the implementation of the Westergaard stress distribution is applicable. The load redistribution around the artificial notch has been captured through applying the Westergaard stress distribution and isostrain condition. Although the simplification of modelling a notch as a complete removal of a long strip of aluminium or fibre material is not a true physical representation of the problem, it still provided good predictions. Load redistribution is adequately captured by the non-physical representation. The crack acceleration can be attributed to the effect of this load redistribution on the adjacent crack.

This paper serves as the first step that intends to develop a simplified prediction methodology for crack growth rates of MSD cracks in FMLs. It is concluded that capturing the effect of load redistribution around an artificial notch on the fatigue growth behaviour of an adjacent crack is a feasible way to study crack acceleration. It shows promise for incorporating the load redistribution of adjacent cracks in an MSD scenario for predicting fatigue crack grow behaviour of each crack in FMLs.

REFERENCES

[1] W. Wang, C. Rans, R. C. Alderliesten, and R. Benedictus, *Predicting the influence of discretely notched layers on fatigue crack growth in fibre metal laminates*, Engineering Fracture Mechanics **145**, 1 (2015).

[2] U. Goranson, *Damage tolerance facts and fiction*, in *International conference on*

damage tolerance of aircraft structures (Delft University of Technology, Delft, the Netherlands, 2007).

[3] B. Nesterenko and G. Nesterenko, *Analysis of requirements on fatigue and damage tolerance for civil transport airplanes,* in *26th Symposium of the international committee on aeronautical fatigue, ICAF 2011*, edited by J. Komorowski (Springer) pp. 39–59.

[4] W. Hendricks, *The aloha airlines accident — a new era for aging aircraft,* in *Structural Integrity of Aging Airplanes*, Springer Series in Computational Mechanics, edited by S. N. Atluri, S. G. Sampath, and P. Tong (Springer Berlin Heidelberg, 1991) Chap. 11, pp. 153–165.

[5] *Federal register/vol. 77, no. 101, thursday may 24, 2012/ rules and regulations,* .

[6] A. Vlot and J. W. Gunnink, *Fibre Metal Laminates-An Introduction* (Kluwer Academic Publisher, Dordrecht, The Netherlands, 2001).

[7] R. C. Alderliesten, *Fatigue crack propagation and delamination growth in GLARE,* Ph.D. thesis, Delft University of Technology, Delft, the Netherlands (2005).

[8] R. C. Alderliesten, *Analytical prediction model for fatigue crack propagation and delamination growth in glare,* International Journal of Fatigue **29**, 628 (2007).

[9] S. Khan, *Fatigue Crack and Delamination Growth in Fibre Metal Laminates under Variable Amplitude Loading,* Ph.D. thesis, Delft University of Technology, Delft, the Netherlands (2013).

[10] S. U. Khan, R. C. Alderliesten, C. D. Rans, and R. Benedictus, *Application of a modified wheeler model to predict fatigue crack growth in fibre metal laminates under variable amplitude loading,* Engineering Fracture Mechanics **77**, 1400 (2010).

[11] S. U. Khan, R. C. Alderliesten, and R. Benedictus, *Delamination in fiber metal laminates (glare) during fatigue crack growth under variable amplitude loading,* International Journal of Fatigue **33**, 1292 (2011).

[12] G. Wilson, *Fatigue Crack Growth Prediction for generalized fiber metal laminates and hybrid materials*, Ph.D. thesis, Delft University of Technology, Delft, the Netherlands (2013).

[13] R. C. Alderliesten, C. Rans, and R. Benedictus, *The applicability of magnesium based fibre metal laminates in aerospace structures,* Composites Science and Technology **68**, 2983 (2008), nanocomposites - Processing, Characterization, Properties, Applications and Modelling, selected papers from Nanocomposite Special Symposium of ACCM-5, with regular papers.

[14] R. C. Alderliesten, J. Schijve, and S. v. d. Zwaag, *Application of the energy release rate approach for delamination growth in glare,* Engineering Fracture Mechanics **73**, 697 (2006).

[15] C. Rans, R. Rodi, and R. C. Alderliesten, *Analytical prediction of mode i stress intensity factors for cracked panels containing bonded stiffeners,* Engineering Fracture Mechanics **97**, 12 (2013).

[16] J. J. Homan, *Fatigue initiation in fibre metal laminates,* International Journal of Fatigue **28**, 366 (2006).

[17] S. Spronk, I. Şen, and R. Alderliesten, *Predicting fatigue crack initiation in fibre metal laminates based on metal fatigue test data,* International Journal of Fatigue **70**, 428 (2015).

[18] I. Barsoum and K. S. Ravi Chandran, *Stress intensity factor solutions for cracks in finite-width three layer laminates with and without residual stress effects,* Engineering Fracture Mechanics **70**, 2015 (2003).

[19] K. S. Ravi Chandran and I. Barsoum, *Determination of stress intensity factor solutions for cracks in finite-width functionally graded materials,* International Journal of Fracture **121**, 183 (2003).

[20] H. Westergaard, *Bearing pressure and cracks.* Journal of Applied Mechanics **6**, 49 (1939).

[21] E647-00, ASTM, *Standard test method for measurement of fatigue crack growth rates,* (2011).

[22] H. Lemmen, R. C. Alderliesten, R. Benedictus, J. Hofstede, and R. Rodi, *The power of digital image correlation for detailed elastic-plastic strain measurements,* (2008).

[23] R. Rodi, R. C. Alderliesten, and R. Benedictus, *Crack-tip behavior in fiber/metal laminates by means of digital-image correlation,* Journal of Aircraft **47**, 1636 (2010).

3

TOWARDS THE ANALYSIS OF BUILT-UP STRUCTURES CONTAINING ECCENTRIC CRACKS: ANALYTICAL SOLUTIONS FOR CRACK OPENING DISPLACEMENTS OF ECCENTRIC CRACKS

In the context of the thin-walled metallic aerospace structures, the added resistance to crack propagation offered by a built-up structure is desirable from a damage tolerance standpoint. The analysis of fatigue cracking in such structures, however, is limited by the lack of crack opening solutions. This paper develops analytical models that calculate crack opening displacements (CODs) for a more general cracking scenario, i.e., non-symmetric cracks. The proposed models are based on the Westergaard stress functions. It is then found that the COD solution of one model is particularly useful. The potential significance of the obtained solutions lies in analysing fatigue cracking in built-up structures containing non-symmetric cracks. The crack opening solution is particularly useful in estimating the load transfer between cracked body and intact bridging structures in built-up structures using the principle of displacement compatibility.

This chapter is to be submitted to European Journal of Mechanics - A/Solids [1]

3.1. INTRODUCTION

The damage tolerance design philosophy is currently recommended by airworthiness regulations to ensure the aviation safety and the integrity of aircraft structures [2]. The concept of slow growth and the ability to predict damage growth behaviour are essentials in the implementation of damage tolerance for metallic structures [3]. Due to the prevalence of thin-walled structures in aerospace applications and their sensitivity to fatigue damage, the added resistance to crack propagation offered by the built-up structures is very desirable. The structural elements in built-up structures provide multiple load paths, which could lead to load transfer from cracked elements to intact elements in case of fatigue damage. This load transfer results in reduced driving force for the crack to propagate in particular elements.

The damage tolerant built-up structures can be manufactured with two main different joining techniques: traditional mechanical fastening and adhesive bonding. Analytical models have been developed based on fracture mechanics, the principle of superposition and displacement compatibility to exploit the damage tolerance benefits of built-up structures [3–7]. The superposition method of Poe [4] for riveted structures has been adapted to analyse adhesively bonded stiffened panels [5, 6]. The treatment of adhesive interface as discrete adhesive elements analogous to individual fasteners in these models makes predicting crack growth in panels underneath bonded stiffeners difficult. To overcome the difficulties posed by discretisation, Rans et al. [3] has developed a new analytical model by breaking down a complex cracked stiffened panel into cracked components on which different bonded stiffener conditions have influence. Alderliesten [7] has also successfully described the crack growth behaviour in Fibre Metal Laminates by treating the laminated material as an adhesively bonded built-up structure instead of as a single material.

It is worth noting that the principle of displacement compatibility is of significance in analysing the load redistribution in cracked built-up structures. Central to this principle is to understand the deformation behaviour of cracked bodies in such structures. The cracked elements deform in compliance with the structural deformation of intact elements in a built-up structure under applied load, therefore load transfers from less stiff cracked elements to other elements. The lack of analytical solutions for the deformation behaviour of eccentrically cracked panels hinders the analysis ability to estimate the crack growth behaviour in complex built-up structures. This restraint is highlighted in the course of analysing crack growth in hybrid Fibre Metal Laminates with Multiple-site Damage scenario where non-symmetric cracks present [8]. The non-symmetric cracks have non-symmetric crack opening displacements, resulting in non-symmetric load redistribution between the cracked metal layers and the intact bridging fibres. Under fatigue loading, asymmetric delamination shapes are formed for two crack tips of a non-symmetric crack at the metal/composites interface as a result of the asymmetric load transfer. This asymmetric delamination growth affects the crack propagation behaviour in the metal layers, and vice versa [8]. This non-symmetric crack growth behaviour in built-up FMLs has to be studied.

Another solution to analysing the crack growth behaviour in built-up structures is to adopt finite element modelling (FEM) techniques, such as the study by Zhang et al. [9]. FEM techniques do provide a means to analyse crack opening and corresponding

crack growth behaviour, however, FEM lacks the simplicity and flexibility compared to the analytical models.

The goal of this paper is to obtain a better understanding of the deformation behaviour of eccentrically cracked panels. This paper proposes analytical models for calculating the crack opening displacement of a non-symmetric crack in a metallic panel based on the Westergaard stress function [10]. The Westergaard stress function is simplified to provide solutions for crack opening displacement and stress-strain field in the line of a non-symmetric crack. The stress intensity factor solutions arising from the simplified Westergaard stress function are compared to the analytical results of Isida [11] to show the validity of the proposed models. FEM is applied to validate the COD solutions and stress-strain distributions ahead of crack tips calculated by the proposed models. In Section 3.5, one simplified load transfer model for a laminated structure is given to illustrate the usage of COD in analysing the cracking in built-up structures.

3.2. THE WESTERGAARD FUNCTION METHOD

The Westergaard function method is a very convenient methodology to characterise the entire stress and strain fields for cracked body. The Westergaard functions can also be simplified to their near-tip solutions, i.e., stress intensity factor (SIF) solutions which provide the stress and strain distributions at the crack tip vicinities. In some instances, however, it is desirable to know the entire stress-strain field ahead of the crack tip. Load redistribution due to stiffness variation (either geometric or material stiffness) can be resolved from such a stress-strain field, such as the analysis of crack growth behaviour in a stiffened panel conducted by Rans [3].

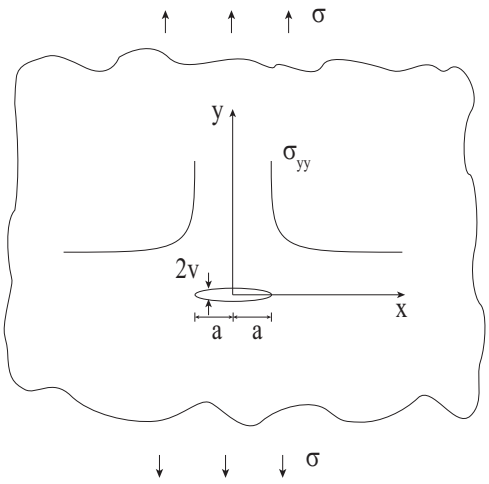

Figure 3.1: Illustration of stress distribution and crack opening in an infinite panel

The closed-form Westergaard solutions are strictly applicable to infinite plate crack problems except for Mode III crack problems [12, 13]; nevertheless they can be modified to provide meaningful solutions for a finite panel with a crack [3, 14, 15]. Barsoum et al.

[14, 15] predict the stress intensity factor for cracks in finite width functionally graded material containing layers with different stiffness using this method. With the same assumption, Rans [3] predicts the crack growth in stiffened metallic panels.

The Westergaard function [10] for Mode I crack problem in infinite panel is given by

$$Z_I(z) = \frac{\sigma}{\sqrt{1-(a/z)^2}} \tag{3.1}$$

where $z = x + i \cdot y$ is a complex number indicating a location in the xy-coordinates plane illustrated in Fig. 3.1, σ is far-field applied stress and a is half crack length. Then the stresses can be given as [16]:

$$\sigma_x = ReZ_I - y \cdot ImZ_I^{'} - \sigma \tag{3.2}$$

$$\sigma_y = ReZ_I + y \cdot ImZ_I^{'} \tag{3.3}$$

$$\tau_{xy} = -y \cdot ReZ_I^{'} \tag{3.4}$$

The stress distribution ahead of the crack tip along the crack plane, i.e., along $y = 0$, is of particular interest and can be expressed as

$$\sigma_{yy} = \frac{\sigma}{\sqrt{1-(a/x)^2}} \tag{3.5}$$

where x is the distance from the crack centre.

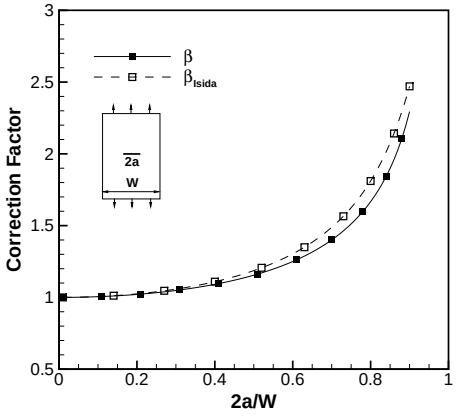

Figure 3.2: Comparison of correction factors for a central crack in finite panel

The corresponding crack opening displacement within the crack length (Fig. 3.1) is given [12, 13]:

$$2v = \frac{4\sigma}{E}\sqrt{a^2 - x^2} \tag{3.6}$$

and the stress intensity factor at the crack tip is expressed as

$$K = \sigma\sqrt{\pi a} \tag{3.7}$$

For one central crack embedded in a finite panel, the stress ahead of the crack tip along crack plane can be assumed to follow the Westergaard stress distribution [17]:

$$\sigma_{yy,f} = \frac{\sigma \cdot \beta}{\sqrt{1-(a/x)^2}} \tag{3.8}$$

here the introduction of the correction factor β is to account for the influence of the finite width boundary condition. The correction factor β is a function of crack length and panel width. This variable can be calculated using the load equilibrium between the crack section and far-field. For a finite panel of width W, the load equilibrium can be expressed as:

$$\sigma \cdot W = 2\int_a^{W/2} \frac{\sigma \cdot \beta}{\sqrt{1-(a/x)^2}} dx \tag{3.9}$$

Solving the integral for a uniform stress state and rearranging for β:

$$\beta = \frac{1}{\sqrt{1-(2a/W)^2}} \tag{3.10}$$

and the corresponding crack opening displacement and stress intensity factor for a central crack in a finite panel can be given as following respectively:

$$2v_f = \frac{4\beta\sigma}{E}\sqrt{a^2-x^2} \tag{3.11}$$

$$K = \beta\sigma\sqrt{\pi a} \tag{3.12}$$

The correction factor β is plotted in Fig. 3.2 against the ratio between the crack length and specimen width. In order to show the validity of the solution from the simplified Westergaard stress function, the obtained correction factor for SIF is compared to that derived by Isida. see Fig.3.2. Good correlation can be observed.

It is worth noting that a finite panel with a central crack under Mode I loading possesses a symmetric axis passing through the crack centre in loading direction. The Westergaard stress distributions in front of two crack tips, crack opening displacement configuration are symmetric with respect to this symmetric axis (or crack centre). Especially it can be seen in Eqs. 3.8, 3.12, 3.11 that these variables are functions of the crack length a which is measured from the crack centre, also the location of maximum crack opening, to the crack tip.

The presence of an eccentric crack in a finite panel under Mode I loading eliminates the symmetric condition possessed by a centrally cracked panel. As a result, the COD configuration and the stress distributions (stress-strain fields) ahead of the non-symmetric crack tips are expected to be asymmetric with respect to its crack centre. The analysis of this non-symmetric deformation behaviour in an eccentrically cracked panel is detailed in the following section.

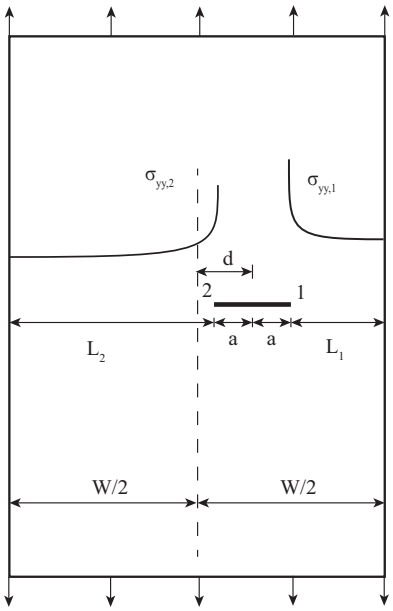

Figure 3.3: Illustration of eccentric crack configuration and different stress distributions in front of two crack tips

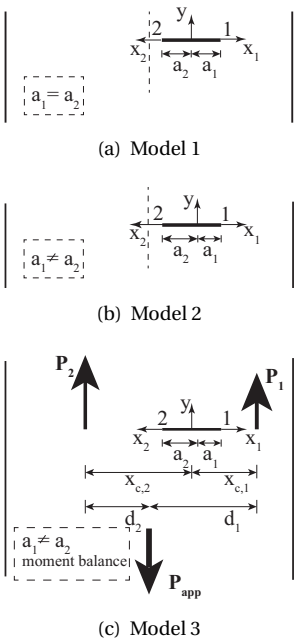

Figure 3.4: Comparison of the 3 models

3.3. MODELS FOR CALCULATING COD OF A NON-SYMMETRIC CRACK

The generalised approach for modelling the COD of a non-symmetric crack is as follows. First, it is assumed that the Westergaard stress distribution (Eq. 3.8) and associated COD solution (Eq. 3.11) are applicable to both crack tips in the non-symmetric crack. Due to the non-symmetry, a different magnitude of the Westergaard stress distribution is expected in front of each crack tip as illustrated by the difference in $\sigma_{yy,1}$ and $\sigma_{yy,2}$ in Fig. 3.3. This difference can be captured by a difference in the β factor for each crack tip. These β factors are obtained by integrating the Westergaard stress distribution and equating it to the applied load.

In applying this generalised approach, assumptions need to be made regarding the definition of crack length and the load distribution in the cracked panel. When defining the half-crack lengths, one needs to keep in mind that the COD solution arising from the Westergaard stress distribution describes a half crack with a maximum displacement at the root of the crack ($x = 0$). Thus, the definition of the datum for measuring the crack length artificially prescribes the point of maximum COD for the crack. Load redistribution is also a key factor to consider. The presence of a crack changes the stiffness of a panel and can cause load to be preferentially carried by one or the other sides of the panel. This affects the load equilibrium expressed in Eq. 3.9. Three different cases were considered which are all illustrated in Fig. 3.4.

In Model 1, the datum for the crack length definition is assumed to be in the centre

of the crack ($a_1 = a_2$) and the resultant of the Westergaard stress distribution is assumed to be equal to the applied load acting over the half-width of the panel defined from the crack datum (i.e., no load redistribution in the panel). This is illustrated in Fig. 3.4(a). A consequence of the assumed crack datum is that the maximum COD will occur in the centre of the crack, and due to the difference in β for each crack tip, there will be a discontinuity in COD at this point. Besides, the variation in SIF is a result of the reduction of the net-section of the panel in the crack plane alone.

In Model 2, the presence of the discontinuity of COD in Model 1 is corrected. The datum for the crack length definition is allowed to deviate from the centre of the crack such that the COD of both cracks are equal at the crack datum. This is illustrated in Fig. 3.4(b). Assumptions regarding the load distribution remain the same as in Model 1.

Finally, in Model 3, the possibility of load redistribution is examined. If the boundary conditions for loading do not provide rotational constraint (i.e., a pin-clevis connection), the resultant load on either side of the crack will redistribute to maintain moment equilibrium in the panel as illustrated in Fig. 3.4(c). This load redistribution case is considered in this model with the same crack datum definition procedure as Model 2.

The eccentricity convention [11] is used in this paper to define the location of a non-symmetric crack. As illustrated in Fig. 3.3, the width of the panel is W and the total crack length is denoted as $2a$. Distance from crack centre to the centre of the panel is d. Then the eccentricity, e, is defined as:

$$e = 2d/W \tag{3.13}$$

The distances from crack tip 1 and 2 to their corresponding edges ahead (Fig. 3.3) can be calculated:

$$L_1 = \frac{W}{2}(1-e) - a \tag{3.14}$$

$$L_2 = \frac{W}{2}(1+e) - a \tag{3.15}$$

Then the normalized crack length is given as:

$$\lambda = \frac{a}{L_1 + a} \tag{3.16}$$

3.3.1. MODEL 1: SYMMETRIC CRACK LENGTHS DEFINITION AND LOAD EQUILIBRIUM METHOD

As shown in Fig. 3.3, one eccentric crack is embedded in a panel under far-field tensile loading. For this model, the crack length, a, is defined as the length from the crack centre to the crack tip ($a_1 = a_2$ in Fig. 3.4(a)). The stress distributions in front of the crack tips are then given as the Westergaard stress distribution respectively:

$$\sigma_{yy,1} = \frac{\sigma \cdot \beta_1}{\sqrt{1-(a/x_1)^2}} \tag{3.17}$$

$$\sigma_{yy,2} = \frac{\sigma \cdot \beta_2}{\sqrt{1-(a/x_2)^2}} \tag{3.18}$$

where x is the distance from the crack centre.

Integrations of the stress distributions give the loads carried by the uncracked material in front of the crack tips respectively:

$$P_1 = \int_a^{w_1} \sigma_{yy,1} dx_1 \cdot t \tag{3.19}$$

$$P_2 = \int_a^{w_2} \sigma_{yy,2} dx_2 \cdot t \tag{3.20}$$

where $w_1 = L_1 + a$ and $w_2 = L_2 + a$ and t denotes the thickness of the panel.

For this model, this load equilibrium between the crack section and far-field is implemented in the following way:

$$P_1 = \sigma \cdot w_1 \cdot t \tag{3.21}$$

$$P_2 = \sigma \cdot w_2 \cdot t \tag{3.22}$$

This means of implementing load equilibrium assumes no load redistribution in two half-width panels defined by the crack datum in this model. From Eqs. 3.17-3.22, the correction factors β_1 and β_2 can be easily determined:

$$\beta_1 = \frac{1}{\sqrt{1-(a/w_1)^2}} \tag{3.23}$$

$$\beta_2 = \frac{1}{\sqrt{1-(a/w_2)^2}} \tag{3.24}$$

From the analysis in previous section, these two correction factors are also correction factors for the stress intensity factors of the two crack tips respectively.

In Fig. 3.5, the calculated correction factors together with Isida's results are plotted against normalised crack length, λ, for several typical eccentricities to show the validity of this model. For crack tip 1, the β_1 curves calculated with the proposed Model 1 overlap with each other for all eccentricities. It can be observed that the predicted results correlate well with Isida's prediction results. However, the correction factors for crack tip 2 are underestimated for all eccentricities. Especially for eccentricities lager than 0.6, the predicted results almost keep constant with crack length. This can be attributed to the fact that the influence of the boundary ahead of crack tip 1 on crack tip 2 is neglected.

The crack opening displacements can be also calculated according to the Westergaard method. The opening configuration of the half crack for tip 1 is given:

$$2v_1 = \frac{4\beta_1\sigma}{E}\sqrt{a^2 - x_1^2} \tag{3.25}$$

and COD for crack tip 2 is given by:

$$2v_2 = \frac{4\beta_2\sigma}{E}\sqrt{a^2 - x_2^2} \tag{3.26}$$

Then it becomes obvious that the calculated maximum crack opening displacements at $x_1 = x_2 = 0$ are not identical for an eccentric crack, which violates the physics of this crack problem. It is then concluded that Model 1 cannot be used to calculate the crack opening displacement configuration for a non-symmetric crack. The analysis process proves that the definition of crack datum at the crack centre can lead to the computed displacement incompatibility. In other words, the maximum crack opening location is not the crack centre for non-symmetric cracks.

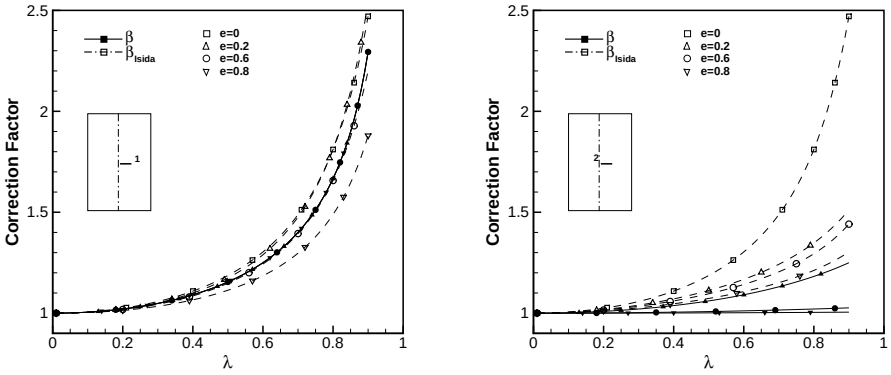

(a) crack tip 1 (b) crack tip 2

Figure 3.5: Correction factors comparison of Model 1

3.3.2. MODEL 2: NON-SYMMETRIC CRACK LENGTHS DEFINITION AND LOAD EQUILIBRIUM METHOD

The definition of the crack length, a, in Model 1 leads to the displacement incompatibility at the location of crack centre. It is therefore reasonable to define the crack length from the crack tip to the location of maximum crack opening displacement instead of to the crack centre. The location of the maximum crack opening is still an unknown parameter for a non-symmetric crack.

In this model, the total crack length is given as $2a$ and two crack lengths a_1 and a_2 are the lengths between the location of maximum crack opening displacement and crack tip 1 and 2 respectively, resulting in non-symmetric crack lengths (see Fig. 3.4(b)). The sum of the two crack lengths is equal to the total crack length:

$$a_1 + a_2 = 2a \tag{3.27}$$

The Westergaard stress distributions in front of the crack tips are expressed as

$$\sigma_{yy,1} = \frac{\sigma_1}{\sqrt{1-(a_1/x_1)^2}} \tag{3.28}$$

$$\sigma_{yy,2} = \frac{\sigma_2}{\sqrt{1-(a_2/x_2)^2}} \tag{3.29}$$

where x_1, x_2 are from the maximum crack opening location (Fig. 3.4(b)) and σ_1, σ_2 are to be determined.

In this case, the loads carried by the uncracked material in front of the crack tips can be calculated in a similar way as Eqs. 3.19-3.20:

$$P_1 = \int_{a_1}^{w_1} \sigma_{yy,1} dx_1 \cdot t \tag{3.30}$$

$$P_2 = \int_{a_2}^{w_2} \sigma_{yy,2} dx_2 \cdot t \tag{3.31}$$

but with $w_1 = L_1 + a_1$ and $w_2 = L_2 + a_2$, denoting that w_1 and w_2 are distances between maximum crack opening location and two free edges respectively.

The load equilibrium is also implemented in a similar way as in Model 1:

$$P_1 = \sigma \cdot w_1 \cdot t \tag{3.32}$$

$$P_2 = \sigma \cdot w_2 \cdot t \tag{3.33}$$

It is notable that no load redistributes between the two half-width panels defined by the crack datum in this model either. The crack datum definition in this model prescribes two different half-width panels compared to Model 1.

Furthermore, the maximum crack opening displacement should be equal for the two half cracks at $x_1 = x_2 = 0$, which can be expressed as:

$$\frac{4\sigma_1}{E}\sqrt{a_1^2 - 0^2} = \frac{4\sigma_2}{E}\sqrt{a_2^2 - 0^2} \tag{3.34}$$

All the unknown variables can be determined by solving the system of Eqs. 3.27-3.34 simultaneously in a numerical way as their analytical solutions are extremely difficult to be derived.

Then the SIF solutions for the two crack tips can be expressed as following

$$K_1 = \sigma_1 \sqrt{\pi a_1} \tag{3.35}$$

$$K_2 = \sigma_2 \sqrt{\pi a_2} \tag{3.36}$$

In order to compare with Isida's prediction, the correction factors are calculated as:

$$\beta_1 = \frac{K_1}{\sigma\sqrt{\pi a}} = \frac{\sigma_1\sqrt{\pi a_1}}{\sigma\sqrt{\pi a}} \tag{3.37}$$

$$\beta_2 = \frac{K_2}{\sigma\sqrt{\pi a}} = \frac{\sigma_2\sqrt{\pi a_2}}{\sigma\sqrt{\pi a}} \tag{3.38}$$

The comparison is given in Fig. 3.6. The predicted correction factors for crack tip 1 and 2 are both underestimated when crack length increases, especially for the prediction of crack tip 1.

In fact, the implementation of the load equilibrium in these two models does not consider the load redistribution due to the stiffness difference in both sides of an eccentrically cracked panel. The presence of a non-symmetric crack changes the stiffness of a panel and the load is preferentially carried by the one or the other sides of the panel. These effects of load redistribution are accounted for in Model 3.

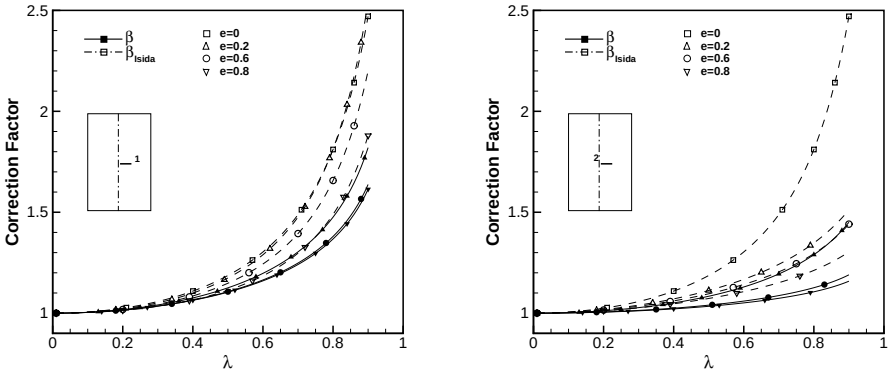

(a) crack tip 1 (b) crack tip 2

Figure 3.6: Correction factors comparison of Model 2

3.3.3. MODEL 3: LOAD EQUILIBRIUM AND MOMENT EQUILIBRIUM METHOD

The possibility of load redistribution is examined in this model. The stress distributions in front of the crack tips are assumed as the same as in Model 2, i.e. Eqs. 3.28 and 3.29. The definition of crack datum remains the same. Crack displacement compatibility at maximum crack opening location is implemented as Eq. 3.34.

The loads carried by the material in front of crack tip 1 and crack tip 2 are given as Eqs. 3.30 and 3.31, the implementation of load equilibrium is expressed in following manner for this model:

$$P_1 + P_2 = P_{app} \tag{3.39}$$

with $P_{app} = \sigma \cdot wt$ being the total applied far-field load.

In addition, the load on either side of the crack, P_1 and P_2, redistributes to maintain the moment equilibrium in the panel (Fig. 3.4(c)).

The location of the equivalent load P_1 for the stress distribution in front of crack tip 1 is the centroid of the distribution shape in its own coordinates.

$$x_{c,1} = \frac{\int_{a_1}^{w_1} \sigma_{yy,1} x_1 dx_1}{\int_{a_1}^{w_1} \sigma_{yy,1} dx_1} \tag{3.40}$$

and the location of the equivalent load P_2 is

$$x_{c,2} = \frac{\int_{a_2}^{w_2} \sigma_{yy,2} x_2 dx_2}{\int_{a_2}^{w_2} \sigma_{yy,2} dx_2} \tag{3.41}$$

Then the mathematical description of the moment equilibrium is given as:

$$P_1 d_1 = P_2 d_2 \tag{3.42}$$

where d_1 and d_2 are distances from locations of P_1 and P_2 to the panel centre respectively (Fig. 3.4(c)) and are expressed as:

$$d_1 = a + d + x_{c,1} - a_1 \tag{3.43}$$

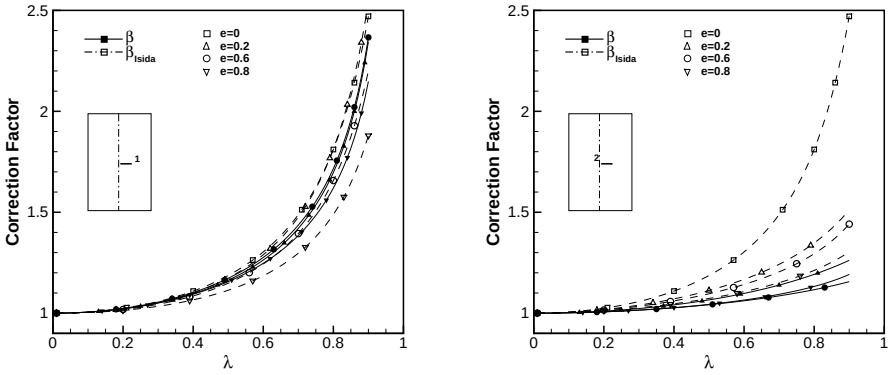

(a) crack tip 1 (b) crack tip 2

Figure 3.7: Correction factors comparison of Model 3

$$d_2 = a - d + x_{c,2} - a_2 \tag{3.44}$$

Numerically solving the system of these equations provides all the results. The correction factors are also given in the same manner as Eqs. 3.37 and 3.38. The comparison for some typical eccentricities and normalised crack lengths is made in Fig. 3.7.

From the comparison in Fig. 3.7, it can be seen that the correlation for crack tip 1 is very good for different eccentricities. For crack tip 2, the correction factors are underestimated for all the eccentricities. The error becomes larger as the crack length increases, especially for $\lambda > 0.6$. However, crack tip 1 is much more critical than crack tip 2. Accurate prediction of stress intensity factor for crack tip 1 is much more critical then. Besides, the proposed Model 3 should provide sufficiently accurate prediction results for practical structures in aircraft industry as the thin walled structures normally are very wide. The possibility of the appearance of an extreme crack configuration with both high eccentricity and high λ should be very low.

Table 3.1: Parameters used in FEA models

	values
Young's Modulus	72400[MPa]
Poission's Ratio	0.33
Thickness	0.4[mm]
Width	200[mm]
Length	300[mm]
Stress	100[MPa]

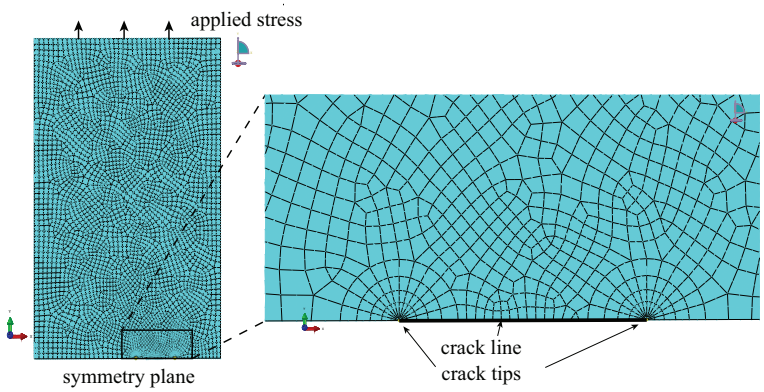

Figure 3.8: Mesh of the FEA model for an Al 2024-T3 panel with an eccentric crack

3.4. VERIFICATION

The near tip solutions of the Westergaard stress distributions, SIF results, for eccentric cracks have been validated with the analytical results of Isida. This section verifies the predicted deformation behaviour of eccentrically cracked panels from Model 2 and Model 3. The crack opening displacement and stress-strain field in front of crack tips are of particular interest. Due to the fact that Model 1 is not able to predict a continuous crack opening displacement configuration for a non-symmetric crack, only the crack opening displacements predicted by Model 2 and Model 3 are compared to FEM results. The Westergaard stress distributions and stress intensity factor results predicted by Model 2 and Model 3 are also compared to FEM results in order to present an intuitive validation of the usage of the Westergaard method.

3.4.1. FINITE ELEMENT ANALYSIS

ABAQUS FEM analysis is applied to calculate crack opening displacement configurations, stress distribution in front of two crack tips and stress intensity factors for cracks in metal panels with finite width. The FEA results are used to verify the results derived from the models proposed in Section 3.3.

The material properties of Al 2024-T3 were used to model the metal panels in ABAQUS code package, see Table 3.1. The metal panels were modelled using 3-D shell planar. Half-symmetry was applied, only upper half of the panels were modelled. The bottom edge where the crack was defined was assigned the symmetry plane and the stress was applied on the upper edge. Fig. 3.8 shows these details and the mesh of the structure and refined mesh for the crack tip zone. Contour integral evaluation technique was applied to calculate the stress intensity factors for the crack tips, the crack tip zones were meshed using $S8R5$ elements. The rest of the structure used $S8R$ elements. Table 3.1 summarizes the parameters used in FEA models.

3.4.2. COMPARISON

As the half-symmetry condition was applied in FEM modelling, so the crack opening displacements predicted by Model 2 and Model 3 for a_1 and a_2 are given as following respectively in order to conveniently make the comparison:

$$v_1 = \frac{2\sigma_1}{E}\sqrt{a_1^2 - x_1^2} \tag{3.45}$$

$$v_2 = \frac{2\sigma_2}{E}\sqrt{a_2^2 - x_2^2} \tag{3.46}$$

The studied case is an Al 2024 – $T3$ panel with the configuration and loading parameters given in Table 3.1. In Fig. 3.9, the crack opening displacements for a crack of 40 mm with different eccentricities are given. $x = 0$ in the figure denotes crack tip 2 and $x = 40$ indicates crack tip 1. The dashed vertical lines denote the analytically calculated maximum crack opening locations in Fig. 3.9. As can be seen, the crack opening for the case of $e = 0.1$ is almost the same as the central crack. Predictions from Model 2 and Model 3 for eccentricities of 0 and 0.1 correlate with FEA results very well. It is interesting that the crack opening increases with increasing eccentricity for the same crack length. Both models captures this phenomenon, but Model 3 provides better prediction results.

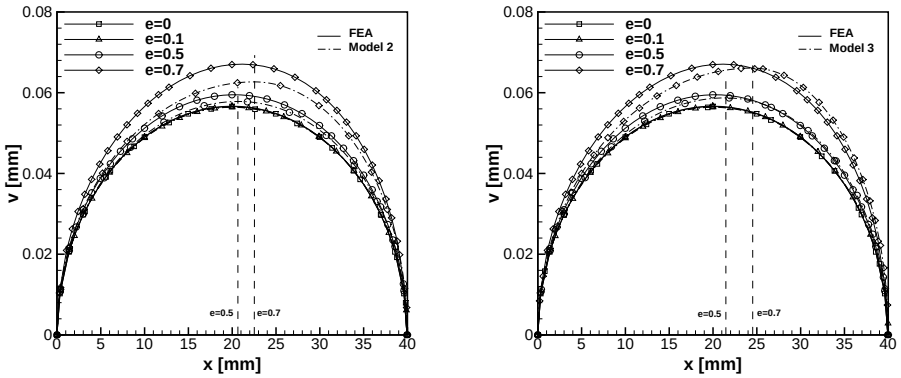

(a) Model 2

(b) Model 3

Figure 3.9: COD comparison

The predicted stress distributions in front of crack tips are also compared to FEA results. Only one case is studied to verify the assumption of the Westergaard stress distribution in front of crack tips, as shown in Fig. 3.10. The points highlighted with dashed circulars is due to the singularity at the node of a transition from a triangular element to a quadrilateral element (Fig. 3.8), i.e. a calculation error occurs at this node in front of the crack tip. Nevertheless the overall trend of stress distributions are the same. Only slight difference can be observed between Model 2 and Model 3.

Although the predicted correction factors for stress intensity factors are compared to Isida's results, the direct comparison between predicted stress intensity factors and FEA results is given in Fig. 3.11.

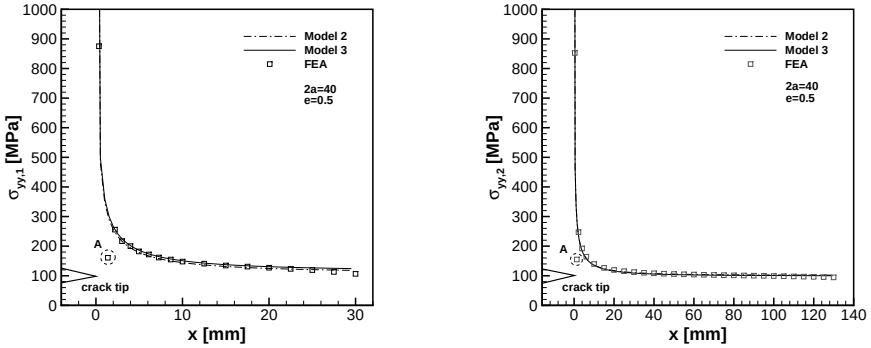

(a) in front of crack tip 1

(b) in front of crack tip 2

Figure 3.10: Stress distribution comparison

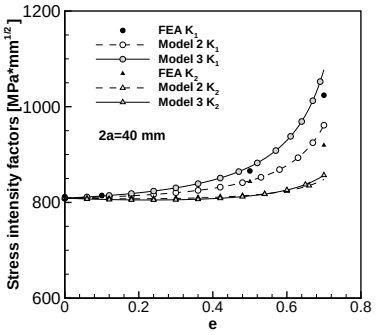

Figure 3.11: Comparison of stress intensity factors

3.5. DISCUSSION

Based on the comparisons and modelling process, Model 3 is the most appropriate means of modelling deformation behaviour in an eccentrically crack panel. The assumptions regarding the stress distributions in front of eccentric crack tips and the definition of crack datum for measuring crack length are reasonable. Furthermore, the COD solutions and stress distributions in Model 3 have the potential to be extended to account for load redistributions caused by stiffness variations in front of crack tips [8], such as analysis of fatigue cracking in complex built-up structures with non-symmetric cracks.

3.5.1. A SIMPLIFIED EXAMPLE OF MODELLING LOAD TRANSFER IN A BUILD-UP STRUCTURE

An example of modelling load transfer from the cracked body to intact components in a build-up structure using Model 3 and the principle of displacement compatibility is presented in order to illustrate the impact of non-symmetric crack configuration on

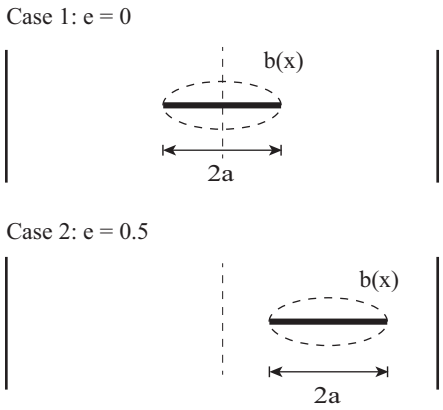

Figure 3.12: Illustration of two crack cases

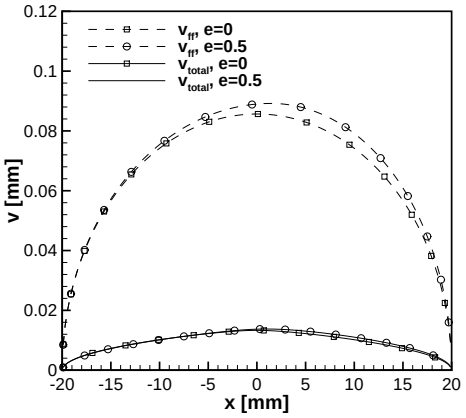

Figure 3.13: Comparison of crack opening displacements

the analysis of cracking in such complex structures. A very simple fibre metal laminate (FML) made of one 2024-T3 aluminium layer in the middle and two layers of S-2 glass fibres in loading direction bonded on both sides of the metal layer is used as a build-up structure since the fatigue resistant fibres keep intact in the wake of a fatigue crack in the middle metal layer, these intact fibres restrain the opening of the crack in the metal layer. The generalised approach for calculating SIF in these structures can be found in [7, 18]. The properties of the materials used for this laminate is given in Table 3.2. Considering the case that the laminate has been cured at a maximum pressure of 6 bars and a maximum temperature of 120 °C, and is under 100 MPa far-field applied stress, the stress in metal layer, S_m, and stress in fibre layer, S_f, can be calculated with the Classic Laminate Theory [19], that is $S_m = 151.9$ MPa and $S_f = 21.95$ MPa.

Table 3.2: Material properties

	Al	**Prepreg**
Young's modulus $E_x[GPa]$	72.4	48.9
Young's modulus $E_y[GPa]$	72.4	5.5
Shear modulus $G_{xy}[GPa]$	27.6	5.55
Poisson's ratio υ_{xy}	0.33	0.33
Poisson's ratio υ_{yx}	0.33	0.0371
Thickness of single layer$[mm]$	0.4	0.133
Width$[mm]$	200	200
Thermal expansion coefficient[1/°C]	$22 \cdot 10^{-6}$	$6.1 \cdot 10^{-6}(0°)$ $26.2 \cdot 10^{-6}(90°)$

Two crack cases in the laminate are compared, one case with $e = 0$ and another one with $e = 0.5$ (see Fig. 3.12). The total crack length, $2a$, is 40 mm for both cases and they have the same delamination shapes which is denoted as $b(x)$ (see Eq. 3.47 and Fig. 3.14).

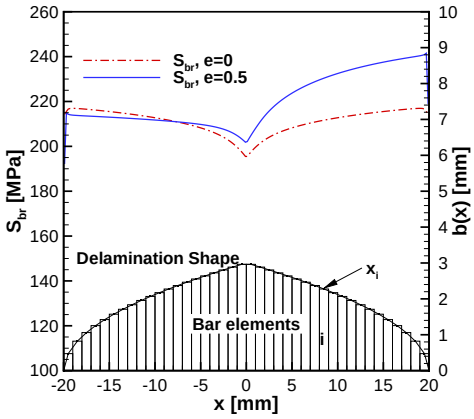

Figure 3.14: Delamination shape and S_{br}

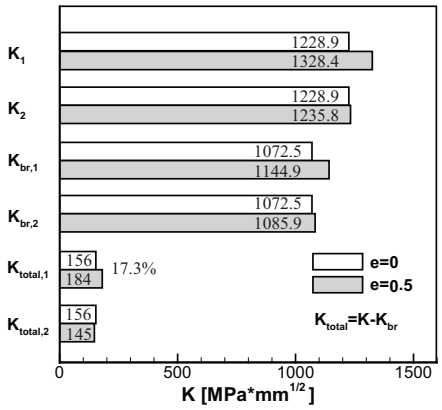

Figure 3.15: Comparison of stress intensity factors

The delamination shape is discretised into bar elements with width of 0.2mm for each one (Fig. 3.14). At each bar element, the fibres restrain the opening of the crack, so the displacement of the crack should be compatible with the fibre deformation [7, 18]. For simplicity of illustration, this displacement compatibility is implemented between the crack opening and the fibre elongation without considering shear deformation of fibre prepreg for each bar element (see Eq. 3.48).

$$b(x) = 3\sqrt{1 - \frac{|x|}{a}} \tag{3.47}$$

$$v_{ff}(x) - v_{br}(x) = \frac{S_f + S_{br}(x)}{E_f} b(x) \tag{3.48}$$

where x denotes the location of the middle point of a bar element, v_{ff} is the crack opening in the metal layer due to the far-field applied load, v_{br} is the crack closing due to the bridging stress distribution, $S_{br}(x)$. The right side of Eq. 3.48 is the fibre elongation. It then becomes obvious that S_{br} is the resultant stress due to the load transfer from cracked metal layer into the intact fibre layers [7, 18].

$v_{ff}(x)$ and the SIFs for two crack tips (K_1, K_2) can be calculated using Model 3 with S_m in the metal layer (Fig. 3.13), the Westergaard stress function for two points loading on Page 5.6 in [13] is used to calculate $v_{br}(x)$. The equation can be solved for S_{br} at each middle point (x_i in Fig. 3.14). The Westergaard method for two points loading can then be used to calculate the resultant bridging stress intensity factor, K_{br}, for each crack tip. The detailed calculation method can be referred to [7, 18].

The calculated crack openings are presented in Fig. 3.13, where $v_{total} = v_{ff} - v_{br}$. The obtained S_{br} for each crack case is presented in Fig. 3.14 and corresponding SIFs in Fig. 3.15. Case 2 ($e = 0.5$) has larger crack opening displacement compared to Case 1 which is a symmetric crack configuration. In such a built-up structure, the larger crack opening displacement leads to larger bridging stress distribution in intact fibres especially for $0 < x_i < 20$ (larger load transfer). Even though the larger load transfer occurs

for Case 2, the resultant SIF for crack tip 1 ($K_{total,1}$) of Case 2 is still 17.3% higher than Case 1. Besides, this larger load transfer between the cracked metal layer and intact fibre layers could result in larger delamination under fatigue loading in reality, further reducing the load bearing capability of the structure.

3.6. CONCLUSION

This paper develops analytical models to investigate the deformation behaviour in eccentrically cracked panels. The Westergaard stress function is simplified to calculate the opening displacement in the crack and the stress distributions ahead of two crack tips. The stress intensity factor solutions arising from the proposed models are compared to analytical results from Isida. Based on the validation, Model 3 is the best means of modelling crack opening and stress intensity factor.

It is found that the crack length for a non-symmetric crack should be defined as the length from the maximum crack opening location to the crack tip in the context of the Westergaard stress distribution. The load on either side of a non-symmetric crack redistributes, as a result of stiffness difference in the panel, to maintain the moment equilibrium. The results from Model 3 are accurate for the critical crack tip while the stress intensity factor for another tip is a bit underestimated for cracks with very high eccentricity and length.

The deformation of eccentrically cracked panels obtained from this paper can be very useful in analysing cracking behaviour in complex built-up structures, especially for analysing fatigue problem. The significance of understanding the deformation behaviour in such panels is substantiated in analysing load transfer in an eccentrically cracked laminated structure in this paper.

REFERENCES

[1] W. Wang, C. Rans, and R. Benedictus, *Towards the analysis of built-up structures containing eccentric cracks: Analytical solutions for crack opening displacements of eccentric cracks,* to be submitted to European Journal of Mechanics - A/Solids .

[2] U. Goranson, *Damage tolerance facts and fiction,* in *International conference on damage tolerance of aircraft structures* (Delft University of Technology, Delft, the Netherlands, 2007).

[3] C. Rans, R. Rodi, and R. C. Alderliesten, *Analytical prediction of mode i stress intensity factors for cracked panels containing bonded stiffeners,* Engineering Fracture Mechanics **97**, 12 (2013).

[4] J. C.C. Poe, *Stress-intensity factor for a cracked sheet with riveted and uniformly spaced stringers,* NASA Technical report R-358 (1971).

[5] T. Swift, *Fracture analysis of adhesively bonded cracked panels,* Journal of Engineering Materials and Technology **100**, 10 (1978), 10.1115/1.3443441.

[6] P. M. Toor, *A review of some damage tolerance design approaches for aircraft structures,* Engineering Fracture Mechanics **5**, 837 (1973).

[7] R. C. Alderliesten, *Analytical prediction model for fatigue crack propagation and delamination growth in glare,* International Journal of Fatigue **29**, 628 (2007).

[8] W. Wang, C. Rans, R. Alderliesten, and R. Benedictus, *Philosophy of multiple-site damage analysis for fibre metal laminate structures,* in *Proceedings of 28th Symposium of the International Committee on Aeronautical Fatigue ICAF 2015, Helsinki, Finland* (2015).

[9] X. Zhang, M. Boscolo, D. Figueroa-Gordon, G. Allegri, and P. E. Irving, *Fail-safe design of integral metallic aircraft structures reinforced by bonded crack retarders,* Engineering Fracture Mechanics **76**, 114 (2009).

[10] H. Westergaard, *Bearing pressure and cracks.* Journal of Applied Mechanics **6**, 49 (1939).

[11] M. Isida, *Stress-intensity factors for the tension of an eccentrically cracked strip,* Journal of Applied Mechanics **33**, 674 (1966), 10.1115/1.3625138.

[12] H. Tada, P. C. Paris, and G. R. Irwin, *The stress analysis of cracks handbook* (Del Research, Hellertown, 1973).

[13] H. Tada, P. C. Paris, and G. R. Irwin, *The stress analysis of cracks handbook* (ASME, New York, 2000).

[14] I. Barsoum and K. S. Ravi Chandran, *Stress intensity factor solutions for cracks in finite-width three layer laminates with and without residual stress effects,* Engineering Fracture Mechanics **70**, 2015 (2003).

[15] K. S. Ravi Chandran and I. Barsoum, *Determination of stress intensity factor solutions for cracks in finite-width functionally graded materials,* International Journal of Fracture **121**, 183 (2003).

[16] C. T. Sun and T. N. Farris, *On the completeness of the westergaard stress functions,* International Journal of Fracture **40**, 73 (1989).

[17] D. L. Chen, B. Weiss, and R. Stickler, *A new approach for the determination of stress intensity factors for finite width plate,* Engineering Fracture Mechanics **48**, 561 (1994).

[18] R. C. Alderliesten, *Fatigue crack propagation and delamination growth in GLARE,* Ph.D. thesis, Delft University of Technology, Delft, the Netherlands (2005).

[19] J. J. Homan, *Fatigue initiation in fibre metal laminates,* International Journal of Fatigue **28**, 366 (2006).

4

ANALYTICAL PREDICTION MODEL FOR NON-SYMMETRIC FATIGUE CRACK GROWTH IN FIBRE METAL LAMINATES

This paper proposes an analytical model for predicting the non-symmetric crack growth and accompanying delamination growth in FMLs. The general approach of this model applies Linear Elastic Fracture Mechanics, the principle of superposition, and displacement compatibility based on the understanding of deformation behaviour in eccentrically cracked metal panels. The non-symmetric crack growth behaviour of two crack tips and accompanying asymmetric load transfer from the eccentrically cracked metal layers to the intact bridging fibres are successfully predicted with the model. The predicted crack growth rates and delamination evolution are compared to test data, good correlation is observed.

This chapter is to be submitted to International Journal of Fatigue [1].

4.1. INTRODUCTION

Fibre Metal Laminates (FMLs) are composed of alternative metallic layers and fibre-reinforced polymer layers. The fatigue resistant fibre layers remain intact in the wake of fatigue cracks in metal layers in FMLs under cyclic loading, restraining the crack opening and acting as a second load path for the cracked metal layers. This bridging mechanism, shown in Fig. 4.1, dramatically reduces the stress severity at the crack tip and thus the crack growth in metal layers [2–4]. One variant of FMLs, Glare, has been successfully applied as fuselage skin material on Airbus A380. Its superior damage tolerance in comparison with monolithic metal panels significantly contributes to the successful application.

Alderliesten has studied symmetric crack growth in FMLs under Mode I fatigue loading based on Linear Elastic Fracture Mechanics (LEFM) [3, 4]. The fatigue damage mechanisms in FMLs involve fatigue crack growth in the metal layers and accompanying delamination at metal/composite interfaces. These two coupled damage mechanisms are investigated by Alderliesten through applying the principle of superposition and estimating the load transfer between the cracked metal layers and intact fibre layers with the principle of displacement compatibility. The load transfer can be attributed to the fact that the intact bridging fibres restrain the crack opening in the metal layers, which reduces the stresses experienced at the crack tip and introduces interface delamination. The Alderliesten model has been refined for variable amplitude loading [5–7] and for part-through cracks [8].

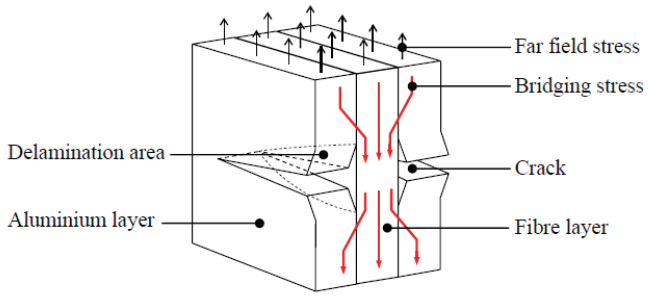

Figure 4.1: Illustration of bridging mechanism [9]

One limitation of the Alderliesten model is that it can not be applied to analyse non-symmetric crack cases in FMLs. However, non-symmetric fatigue crack cases can arise in FMLs in practice for several reasons, such as the scatter of crack initiation at hole edges and crack interaction in case of Multiple-site Damage (MSD) scenario [10] etc. One tip of a non-symmetric crack can grow faster than the other tip under fatigue loading. Therefore a prediction model is needed to extend the ability to analyse non-symmetric crack growth behaviour in FML structures, which is required to meet the damage tolerance requirement. In addition, another motivation for developing such a model is to analyse MSD crack growth behaviour in FMLs [10, 11]. As a result of crack interaction in an FML with MSD, a single crack may have asymmetric configuration involving crack tip

asymmetry and delamination asymmetry (see Fig. 4.2). The ability to calculate the non-symmetry effects on the states of a single crack, such as stress intensity factors and load transfer between cracked metal layers and intact bridging fibres, in an FML is therefore needed. The effects of adjacent MSD cracks on the state of the single crack in an FML can be estimated with the load redistribution mechanism according to the philosophy in [10, 11]. All crack states can be calculated by analysing each single crack in an FML with MSD scenario [10, 11].

Many attempts to address non-symmetric crack growth in finite metallic structures can be found in open literature [12–19], but no analytical prediction model for non-symmetric crack growth in FMLs has been found in open literature. One obstacle for developing such an analytical model is to understand the deformation behaviour of an eccentrically cracked panel. The crack opening displacement of a non-symmetric crack is of particular importance in analysing the load transfer between the cracked layers to intact bridging fibres in an FML.

This paper proposes an analytical model for predicting the fatigue crack growth of non-symmetric cracks in FMLs. The model is built upon the success of Alderliesten by applying LEFM, the principles of superposition and displacement compatibility. The implications of non-symmetry on fatigue cracking behaviour in FMLs are highlighted in comparison with the symmetric crack scenario in Section 4.2. The model development is detailed in Section 4.3 with focuses on the analysis of non-symmetry effects on stress intensity factors and crack opening displacement, and on the analysis of non-symmetric bridging calculation. Section 4.5 provides the validation of the proposed model with the test program detailed in Section 4.4.

4.2. COMPARISON OF SYMMETRIC AND NON-SYMMETRIC CRACK GROWTH BEHAVIOUR IN FMLS

In FMLs, fatigue crack growth in metal layers and delamination propagation at composite/metal interfaces take place simultaneously and interact with each other through the bridging mechanism. The growth behaviour of the two crack tips is affected not only by the free edge boundary conditions, but also the difference in delamination shapes for the tips. A symmetric fatigue crack configuration in an FML means crack tip symmetry (same boundary conditions) and delamination symmetry (no difference in delamination shapes for two crack tips), illustrated in Fig. 4.2(a). A non-symmetric crack configuration can be either delamination asymmetry (Fig. 4.2(b)), crack tip asymmetry (Fig. 4.2(c)), or a combination of both (Fig. 4.2(d))

The effects of non-symmetry on the crack state and delamination growth of a non-symmetric crack in an FML are discussed in comparison with the symmetric crack configuration in the following subsections.

4.2.1. EFFECTS ON STRESS INTENSITY FACTORS OF TWO CRACK TIPS

The stress state at a crack tip in a metallic panel can be characterised with the stress intensity factor experienced at the crack tip. According to Alderliesten [3, 4], the total stress intensity factor of the crack tip (K_{total}) in the metal layers of FMLs can be expressed

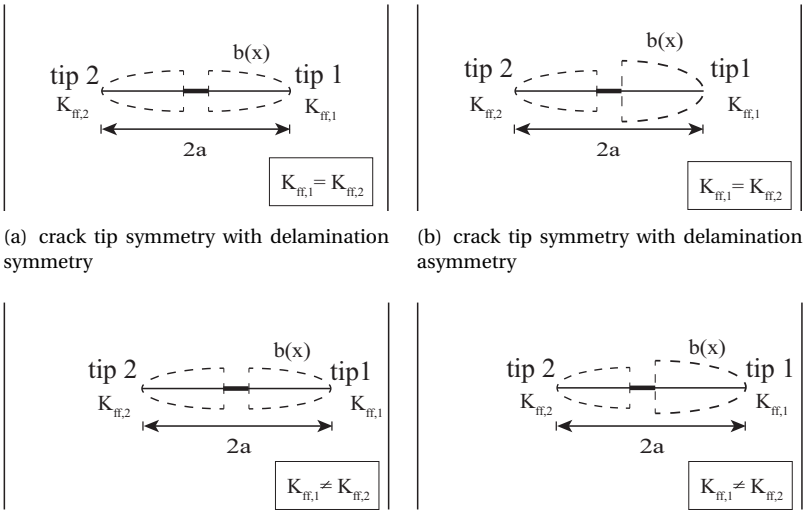

(a) crack tip symmetry with delamination symmetry

(b) crack tip symmetry with delamination asymmetry

(c) crack tip asymmetry with delamination symmetry

(d) crack tip asymmetry with delamination asymmetry

Figure 4.2: Comparison of symmetric and non-symmetric crack configurations in FMLs

based on the principle of superposition:

$$K_{total} = K_{ff} + K_{br} \tag{4.1}$$

in which K_{ff} is the stress intensity factor due to far-field stresses in metal layers and K_{br} is due to the bridging stress in intact bridging fibres. In other words, the load transfer from the cracked metal layer to the intact bridging fibres leads to a negative K_{br}, resulting in a smaller superposed stress intensity factor (K_{total}) experienced at the crack tip.

For two symmetric crack tips, the influence of free edge boundary conditions are the same, which leads to $K_{ff,1} = K_{ff,2}$. This symmetry is valid for the crack cases in Fig. 4.2(a) and Fig. 4.2(b). On the contrary, $K_{ff,1} \neq K_{ff,2}$ is valid for the cases of asymmetric crack tips in Fig. 4.2(c) and Fig. 4.2(d) [10, 12].

The symmetric delamination shapes for the symmetric crack tips in Fig. 4.2(a) lead to $K_{br,1} = K_{br,2}$ according to the study of Alderliesten [3]. Even though the K_{br} solution for non-symmetric delamination shapes are unknown yet, $K_{br,1} \neq K_{br,2}$ is expected as the difference in delaimination shapes can lead to non-symmetric bridging stress distribution along the crack. Despite the symmetric delamination shapes in Fig. 4.2(c), $K_{br,1} \neq K_{br,2}$, as a result of non-symmetric crack opening displacement, which is explained in next subsections.

It is then obvious that K_{total} is only the same for two tips if there is both crack tip and delamination symmetry. Either crack tip asymmetry or delamination asymmetry could lead to different total stress intensity factors for two tips. Thus different crack growth behaviour of two tips of a non-symmetric crack is expected in an FML. The proposed model should be capable of analysing these phenomena.

4.2.2. EFFECTS ON CRACK OPENING DISPLACEMENT

It is well known that a symmetric crack in a metal panel possesses a symmetric crack opening displacement with respect to its crack centre under uniform tensile loading, and that the maximum crack opening occurs at the crack centre. For an FML under Mode I far-field loading, the stresses in the metal layers can be calculated with Classical Laminate Theory (CLT). The symmetric crack opening displacement of a central crack under applied load can then be determined [3, 4].

However, the crack opening of a non-symmetric crack in an FML under Model I loading needs to be re-analysed. The study in [10] found that a non-symmetric crack in a finite metallic panel has a larger crack opening displacement than a central crack with the same length. In addition, the presence of a non-symmetric crack eliminates the symmetry possessed by a centrally cracked panel, the crack opening contour of a non-symmetric crack is asymmetric.

The difference in the crack opening displacements of a symmetric crack and a non-symmetric crack in FMLs due to far-field stresses implies different bridging stress distributions in the intact bridging fibres along the crack, which affects both the delamination growth at the metal/composite interfaces and crack growth in the metal layers. The effects are discussed in detail in the next subsection.

4.2.3. EFFECTS ON LOAD TRANSFER FROM CRACKED METAL LAYERS TO BRIDGING FIBRES

The intact fibres in the wake of fatigue cracks restrain the crack opening in the metal layers in FMLs, which introduces load transfer from the cracked metal layers to the fibre layers. The load transfer is achieved by shear at the metal/composite interfaces resulting in interface delamination growth.

The load transfer between the two bonded substances is estimated by Alderliesten using the principle of displacement compatibility, i.e., the sum of the crack opening due to far-field load (v_{ff}) and crack closing due to the load transfer (v_{br}) should be equal to the deformation of fibre prepreg layers including shear deformation (δ_{pp}) and fibre elongation (δ_f) [3, 4]. See the following equation:

$$v_{ff}(x) - v_{br}(x) = \delta_{pp}(x) + \delta_f(x) \tag{4.2}$$

where v_{br} and δ_f are functions of bridging stress distribution in bridging fibres ($S_{br}(x)$) and v_{ff} and δ_{pp} are functions of far-field stresses in metal layers [3, 4].

The bridging stress distributions for a symmetric case and a non-symmetric case are compared in Fig. 4.3 in order to illustrate how the difference in the crack opening displacements of both crack scenarios affects the load transfer [10]. For the symmetric crack case with symmetric delamination shapes, all the variables in Eq. 5.3 are symmetric with respect to the crack centre, a symmetric bridging stress distribution in the bridging fibres can be calculated with Eq. 5.3 [3]. Symmetric crack growth and symmetric delamination growth in FMLs can be predicted as well with the approach in [3].

In contrast, the non-symmetric case with the same delamination shapes has asymmetric v_{ff}, see Fig. 4.3. A relatively larger crack opening for one crack tip than another results in higher bridging stress according to the principle of displacement compatibility, as illustrated in Fig. 4.3. The higher bridging stress distribution indicates a larger

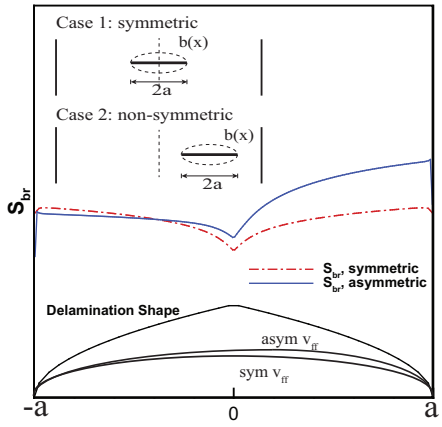

Figure 4.3: Illustration of bridging stress distributions for symmetric and non-symmetric crack cases [10]

K_{br} for the corresponding crack tip. Meanwhile the higher bridging stress distribution could promote larger delamination growth under fatigue loading, eventually resulting in a non-symmetric delamination shape. It is notable that the resultant K_{br} and K_{ff} are different, non-symmetric crack growth behaviours are therefore expected.

Based on the analysis, it can be argued that the crack tip asymmetry and delamination asymmetry interact with one another. A general crack configuration illustrated in Fig. 4.2(d) could be expected. The proposed model should be able to deal with the influence of non-symmetry resulting from both crack tip non-symmetry and the difference in delamination shapes.

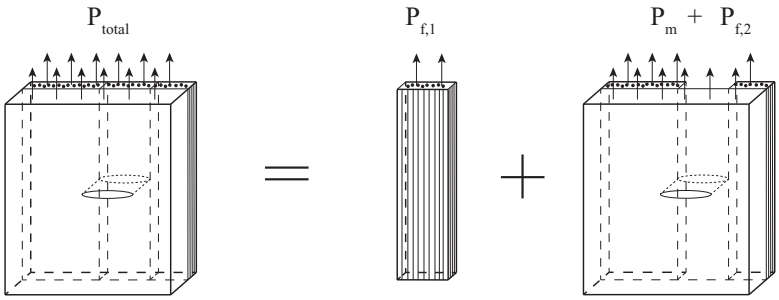

Figure 4.4: Decomposition of loads in FMLs system

4.3. MODEL DERIVATION

The general methodology that is based on LEFM, the principle of superposition and displacement compatibility used in [3, 4] for analysing symmetric cracks in FMLs can also be used for non-symmetric cracks. In comparison to symmetric cracks in FMLs, the physically different crack growth behaviour of non-symmetric cracks resulting from the asymmetric boundary conditions and difference in delamination shapes, however, need

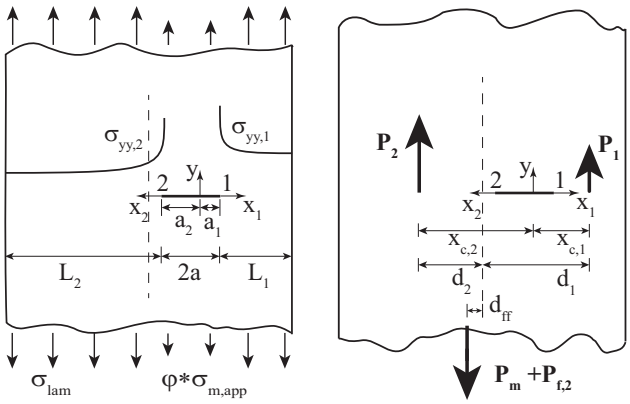

(a) actual stress distributions (b) equivalent loads

Figure 4.5: Illustration of equivalent loads for actual stress distributions

to be re-analysed. The core to this analysis is to calculate K_{ff} and K_{br} for each crack tip, and to derive the asymmetric crack opening displacement and the corresponding load transfer (S_{br}) which associates the crack growth and delamination growth.

In order to aid in calculating K_{ff} and K_{br} for each crack tip, the far-field applied load is decomposed using the principle of superposition, see Fig. 4.4. The stresses carried by metal layers, $\sigma_{m,app}$, and composite layers, $\sigma_{f,app}$, of an FML under total applied load P_{total} or applied stress σ_{lam} can be calculated with CLT [9, 20]. Then the load transmitted by the metal layers, P_m, and loads transmitted by fibres over the total crack length, $P_{f,1}$, and the rest fibres, $P_{f,2}$, can be respectively expressed as:

$$P_m = n_m t_m \sigma_{m,app} W \tag{4.3}$$

$$P_{f,1} = n_f t_f \sigma_{f,app} 2a \tag{4.4}$$

$$P_{f,2} = n_f t_f \sigma_{f,app} (W - 2a) \tag{4.5}$$

where W is the width of the panel and $2a$ is the total crack length. The subscripts m and f refer to metal layer and fibre layer respectively. n and t indicate the number of layers and their thickness.

4.3.1. K_{ff} CALCULATION

It is assumed that the stress distribution in front of a crack tip can be described with the Westergaard stress distribution in FMLs [11]. Since the non-symmetry results in different stress states at two crack tips of a non-symmetric crack, it is argued that the Westergaard stress distributions ahead of the two crack tips are different [10]. The different stress distributions are illustrated in Fig. 4.5(a).

The Westergaard stress distribution artificially defines a half crack length with a maximum opening displacement at the root [10]. In order to achieve a continuous crack opening displacement for a non-symmetric crack calculated with two different Westergaard stress distributions, two different crack lengths (a_1, a_2) are assumed, instead of

using the half crack length a of a crack with the length of $2a$ (Eqs. 4.6- 4.7). This method has been applied for calculating stress intensity factors and crack opening of an eccentric crack in a metal strip and is explained in detail in [10]. Thus the corresponding stress distributions in front of two crack tips in an eccentrically cracked FML can be given by:

$$\sigma_{yy,1} = \frac{\sigma_1}{\sqrt{1-(a_1/x_1)^2}} \tag{4.6}$$

$$\sigma_{yy,2} = \frac{\sigma_2}{\sqrt{1-(a_2/x_2)^2}} \tag{4.7}$$

where σ_1 and σ_2 are laminate stresses to be determined for the two crack tips. a_1 and a_2 are the assumed two crack lengths whose sum should be the total crack length (Eq. 4.8) and the corresponding x_1, x_2 coordinates are illustrated in Fig. 4.5(a).

$$a_1 + a_2 = 2a \tag{4.8}$$

Additionally, the crack opening at the root of two half crack lengths described with the Westergaard stress distribution should be the same in order to fulfil the physics of the crack problem, which is given analytically by [10]:

$$\frac{\sigma_1 S}{E_m} a_1 = \frac{\sigma_2 S}{E_m} a_2 \tag{4.9}$$

where S is the stiffness matrix for calculating the stresses in metal layers and can be calculated with CLT [9, 20].

At the cracked section of the panel, the loads carried by the intact materials are then given by:

$$P_1 = \int_{a_1}^{a_1+L1} \sigma_{yy,1} \mathrm{d}x_1 \cdot t_{lam} \tag{4.10}$$

$$P_2 = \int_{a_2}^{a_2+L_2} \sigma_{yy,2} \mathrm{d}x_2 \cdot t_{lam} \tag{4.11}$$

where L_1 and L_2 are the lengths of intact strips as illustrated in Fig. 4.5(a).

These two loads and the far-field load (Fig. 4.5(b)) should not only satisfy load equilibrium but also moment equilibrium [10]:

$$P_1 + P_2 = P_m + P_{f,2} \tag{4.12}$$

$$(P_m + P_{f,2}) d_{ff} + P_1 d_1 = P_2 d_2 \tag{4.13}$$

with d_{ff}, d_1 and d_2 being the distances between the corresponding equivalent loads and the vertical symmetric line of the laminate panel as illustrated in Fig. 4.5(b). These distances can be calculated based on their geometric relations.

The equivalent loads (P_1, P_2) of the Westergaard stress distributions ($\sigma_{yy,1}$, $\sigma_{yy,2}$) illustrated in Fig. 4.5 should be located at their centroids, respectively ($x_{c,1}$, $x_{c,2}$) [10]:

$$x_{c,1} = \frac{\int_{a_1}^{a_1+L_1} \sigma_{yy,1} x_1 \mathrm{d}x_1}{\int_{a_1}^{w_1} \sigma_{yy,1} \mathrm{d}x_1} \tag{4.14}$$

$$x_{c,2} = \frac{\int_{a_2}^{a_2+L_2} \sigma_{yy,2} x_2 \mathrm{d}x_2}{\int_{a_2}^{w_2} \sigma_{yy,2} \mathrm{d}x_2} \tag{4.15}$$

According to their geometrical relationship, d_1 and d_2 can be given by:

$$d_1 = \frac{W}{2} - (L_1 + a_1 - x_{c,1}) \tag{4.16}$$

$$d_2 = \frac{W}{2} - (L_2 + a_2 - x_{c,2}) \tag{4.17}$$

The location of the equivalent load of the far-field stress after decomposition can also be calculated by:

$$d_{ff} = \frac{W}{2} - \frac{\int_0^{L_2} \sigma_{lam} x \mathrm{d}x + \int_{L_2}^{L_2+2a} \varphi\sigma_{m,app} x \mathrm{d}x + \int_{L_2+2a}^{W} \sigma_{lam} x \mathrm{d}x}{\int_0^{L_2} \sigma_{lam} \mathrm{d}x + \int_{L_2}^{L_2+2a} \varphi\sigma_{m,app} \mathrm{d}x + \int_{L_2+2a}^{W} \sigma_{lam} \mathrm{d}x} \tag{4.18}$$

where $\varphi\sigma_{m,app}$ denotes that $\sigma_{m,app}$ is recalculated based on the whole laminate thickness, with φ being expressed as:

$$\varphi = \frac{n_m t_m}{t_{lam}} \tag{4.19}$$

Solving the system of Eqs. 4.6- 4.18 provides the results for all the relevant unknown parameters. Although an analytical solution is extremely hard to obtain, a numerical solution can be computed.

The curing process for manufacturing FMLs causes thermal residual stresses in the laminate due to the mismatched thermal expansion coefficients between the metal sheets and fibre layers. The tensile thermal residual stress for metal layers ($\sigma_{m,cur}$) is regarded as far-field stress when the crack is present [3, 4]. It is therefore assumed in this paper that the boundary condition has the same effects on the crack behaviour due to curing stress in metal layers as on the stress intensity factor due to far-field applied stress. Then the resultant stress intensity factors for the two crack tips can be expressed as:

$$K_{ff,1} = (\sigma_1 S + \frac{\sigma_1}{\sigma_{lam}} \sigma_{m,cur}) \sqrt{\pi a_1} \tag{4.20}$$

$$K_{ff,2} = (\sigma_2 S + \frac{\sigma_2}{\sigma_{lam}} \sigma_{m,cur}) \sqrt{\pi a_2} \tag{4.21}$$

4.3.2. CRACK OPENING DISPLACEMENT DERIVATION

The use of the Westergaard method provides the possibility of direct calculation of crack opening displacement [21, 22]. For a non-symmetric crack, the crack opening is calculated with two Westergaard functions defining two half crack lengths that is illustrated in Fig. 4.6 [10].

The crack opening displacements for the two half cracks (Fig. 4.6) due to the applied far-field stress and curing stress can be given by:

$$v_{ff,1} = \frac{2(\sigma_1 S + \frac{\sigma_1}{\sigma_{lam}} \sigma_{m,cur})}{E_m} \sqrt{a_1^2 - x_1^2} \tag{4.22}$$

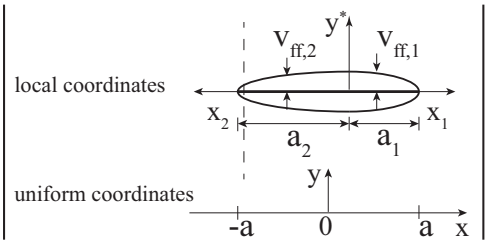

Figure 4.6: Illustration of crack opening displacement

$$v_{ff,2} = \frac{2(\sigma_2 S + \frac{\sigma_2}{\sigma_{lam}}\sigma_{m,cur})}{E_m}\sqrt{a_2^2 - x_2^2} \tag{4.23}$$

It is notable that the derived crack opening displacements are in local coordinates (Fig. 4.6). They need to be mapped to a uniform coordinates with $x = 0$ located at the crack centre in order to calculate the bridging stress distribution with the Westergaard method, see Fig. 4.6. As the mapped COD cannot be expressed by one analytical equation, it is denoted as $v_{ff}(x)$ in this paper.

4.3.3. S_{br} CALCULATION

It is believed that the same displacement compatibility between cracked metal layers and intact bridging fibre layers used by Alderliesten for the symmetric crack configuration [3, 4] can be used to calculate the bridging stress distribution for the non-symmetric crack configuration. Consider a generic damage configuration, illustrated in Fig. 4.7, where the delamination shape $b(x)$ and crack opening $v_{ff}(x)$ are asymmetric with respect to the crack centre. The dashed line in Fig. 4.7 represents a symmetric crack opening given as a reference.

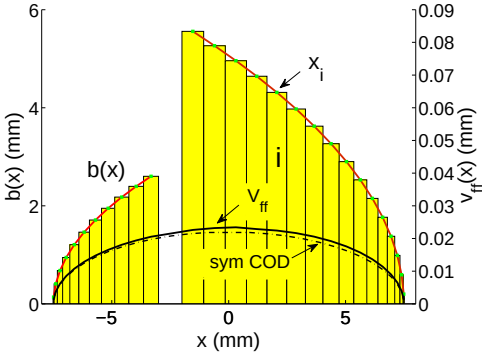

Figure 4.7: Illustration of delamination bars and crack opening

Similar to the method in [8], the delamination shape is divided into bar elements. Due to the known issue that the magnitude of the calculated K_{br} is much more sensitive to the bridging stresses in the bridging fibres very close to the crack tip than those in

other elements, the elements next to the crack tips are refined by assigning gradually smaller width, as shown in Fig. 4.7. Node x_i is the centre point of ith bar element where the bridging stress over width w_i is approximated by $S_{br}(x_i)w_i$ with $S_{br}(x_i)$ being the bridging stress at the node x_i.

Eq. 5.3 can be used to calculate the S_{br} distribution along the crack flank. $v_{ff}(x)$ for any location x in a uniform coordinates with its origin at the crack centre has been calculated in the preceding subsection. $v_{br}(x)$ can be calculated with the equation as follows:

$$v_{br}(x) = \sum_{-a<x_i<a} v(x, x_i) \tag{4.24}$$

where $v(x, x_i)$ denotes the crack opening at x due to a pair of point loads at x_i of the ith element (Fig. 4.7). For a cracked panel under a pair of point loads illustrated in Fig. 4.8, the analytical solution has been provided by Tata et al. [22].

$$v(x, x_i) = \frac{1}{G(1+\nu)} \mathrm{Im}\bar{Z}_I - \frac{b(x_i)}{2G} \mathrm{Re}Z_I \tag{4.25}$$

where Z_I and $\bar{Z}_I$ are the Westergaad stress functions and $b(x_i)$ is the delamination length at x_i, detailed information is given in Appendix B.

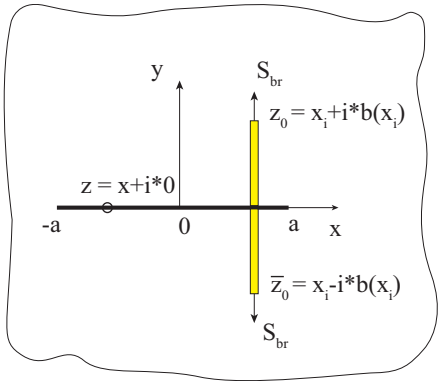

Figure 4.8: Two point bridging loads

The shear deformations of fibre layers for unidirectional plies and cross-ply layers have been calculated in [4], however the stress in the metal layers, S_{al} in the equations derived by Alderliesten, needs to be replaced by $\sigma_1 S + \frac{\sigma_1}{\sigma_{lam}}\sigma_{m,cur}$ or $\sigma_2 S + \frac{\sigma_2}{\sigma_{lam}}\sigma_{m,cur}$ for each half crack (a_1, a_2).

The fibre elongation can be calculated by

$$\delta_f(x) = \frac{S_f + S_{br}}{E} b(x) \tag{4.26}$$

where S_f is the sum of $\sigma_{f,app}$ and $\sigma_{f,cur}$ that is the curing stress in the fibre layers.

Due to the fact that $v_{br}(x)$ is related to the bridging stresses at all the elements, Eq. 5.3 has to be solved for all the bar elements simultaneously. A numerical solution can therefore be obtained [4].

$$S_{br}(x) = H^{-1}Q \tag{4.27}$$

where

$$H = \sum_{-a<x_i<a} \frac{v(x,x_i)}{S_{br}(x_i)} + \frac{b(x)}{E_f} \tag{4.28}$$

$$Q = v_{ff}(x) - \delta_{pp}(x) - \frac{S_f}{E_f} b(x) \tag{4.29}$$

4.3.4. K_{br} CALCULATION

The bridging stress is defined in this paper as the stress acting in the fibre layers. However, this bridging stress needs to be recalculated for the stress acting in each metal layer in order to calculate the K_{br} for each crack tip. The recalculation is given as [4]:

$$S_{br,m}(x) = S_{br}(x) \frac{n_f t_f}{n_m t_m} \tag{4.30}$$

Then the stress intensity factor for each crack tip due to the bridging stress distribution can be calculated by:

$$\begin{aligned} K_{br,1} = \sum_{-a<x_i<a} \frac{S_{br,m}(x_i)\, w(x_i)}{2\sqrt{\pi a}} \Big[\sqrt{\frac{a+z_0}{a-z_0}} + \sqrt{\frac{a+\bar{z}_0}{a-\bar{z}_0}} - \\ \alpha b(x_i) \Big(- \sqrt{\frac{a+z_0}{a-z_0}} \frac{a \cdot i}{(a+z_0)^2} + \sqrt{\frac{a+\bar{z}_0}{a-\bar{z}_0}} \frac{a \cdot i}{(a+\bar{z}_0)^2} \Big) \Big] \\ K_{br,2} = \sum_{-a<x_i<a} \frac{S_{br,m}(x_i)\, w(x_i)}{2\sqrt{\pi a}} \Big[\sqrt{\frac{a-z_0}{a+z_0}} + \sqrt{\frac{a-\bar{z}_0}{a+\bar{z}_0}} - \\ \alpha b(x_i) \Big(\sqrt{\frac{a-z_0}{a+z_0}} \frac{a \cdot i}{(a-z_0)^2} - \sqrt{\frac{a-\bar{z}_0}{a+\bar{z}_0}} \frac{a \cdot i}{(a-\bar{z}_0)^2} \Big) \Big] \end{aligned} \tag{4.31}$$

4.3.5. CRACK GROWTH MODEL AND DELAMINATION GROWTH MODEL

The fatigue crack growth rate in metal is predicted with the Paris relation after the stress intensity factor for each crack tip is obtained [4]:

$$\frac{da}{dN} = C_{cg} (K_{eff})^{n_{cg}} \tag{4.32}$$

where C_{cg} and n_{cg} are equation constants for Paris equation. For thin $2024-T3$ aluminium, the values are $C_{cg} = 2.17 \cdot 10^{-12}$ and $n_{cg} = 2.94$. K_{eff} is related to the range of K_{total} and the stress ratio R [23]:

$$K_{eff} = (0.55 + 0.33R + 0.12R^2)(1-R) \cdot \Delta K_{total} \tag{4.33}$$

For delamination growth at the interface between metal layers and fibre layers, the strain energy release rate G instead of K is employed as the driving force, simply because it is easier to calculate G at the interface of dissimilar materials [3, 4]. The strain energy release rate for each delamination column can be given in terms of stresses in bridging fibres:

$$G = \frac{n_f t_f}{2jE_f}\left(\frac{n_m t_m E_m}{n_m t_m E_m + n_f t_f E_f}\right)(S_f(x) + S_{br}(x))^2 \tag{4.34}$$

Then the interface delamination can also be calculated using the Paris relation [4]:

$$\frac{db}{dN} = C_d(\sqrt{G_{max}} - \sqrt{G_{min}})^{n_d} \tag{4.35}$$

with C_d and n_d being the Paris parameters. For the fibre metal laminate Glare, the values are $C_d = 0.05$ and $n_d = 7.5$.

4.4. EXPERIMENTAL PROCEDURE

4.4.1. MATERIAL AND MANUFACTURING

The FML materials used for validation tests are composed of layers of S2-glass fibres reinforced FM94 epoxy resin prepreg and 2024-T3 aluminium, which is known as Glare. The lay-up of the specimens is [Al/0/90/Al/90/0/Al] with 90 and 0 referring to the orientation of the prepreg layers with respect to the rolling direction of the aluminium. Table 4.1 provides the properties of the constituents.

Table 4.1: Material properties [11]

	Al	**Prepreg**
Young's modulus $E_x[GPa]$	72.4	48.9
Young's modulus $E_y[GPa]$	72.4	5.5
Shear modulus $G_{xy}[GPa]$	27.6	5.55
Poisson's ratio υ_{xy}	0.33	0.33
Poisson's ratio υ_{yx}	0.33	0.0371
Thickness of single layer$[mm]$	0.4	0.133
Thermal expansion coefficient[1/°C]	$22 \cdot 10^{-6}$	$6.1 \cdot 10^{-6}(0°)$ $26.2 \cdot 10^{-6}(90°)$

The aluminium layers and cross-plies were stacked together according to the lay-up, and then were put into an autoclave for curing. The curing process was carried out with a maximum temperature of 120 °C and maximum pressure of 6 bars. Then the Glare laminates were milled into the specimen size described in Fig. 4.9.

4.4.2. TEST MATRIX

In order to validate the proposed model for predicting non-symmetric fatigue crack growth in FMLs, the specimen configuration with initial non-symmetric saw-cuts that is illustrated in Fig. 4.9 was adopted. A circular hole with radius of 1.5 mm was applied to obtain saw-cuts from where the crack growth starts. The parameters of respective specimen configurations are given in Table 4.2, which comprise the test matrix. That the length of a saw-cut is equal to the hole radius means no initial saw-cut is applied at the corresponding hole edge in order to get a delayed crack growth and corresponding delamination growth. A symmetric crack configuration (sym-1) was tested as a reference for comparison.

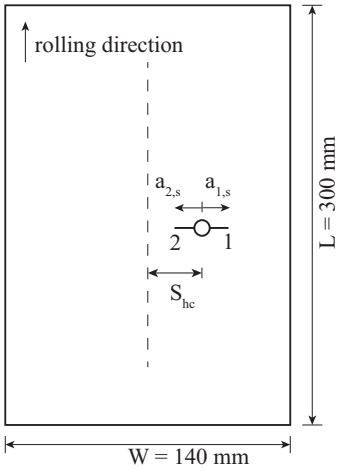

Figure 4.9: Specimen configuration

Table 4.2: Test matrix

Specimen	S_{hc} (mm)	$a_{1,s}$ (mm)	$a_{2,s}$ (mm)
sym-1	0	3	3
asym-1	0	7	1.5
asym-2	30	3	3

4.4.3. FATIGUE TEST

The test set-up is shown in Fig. 4.10. A MTS 810 servo hydraulic test frame with a 250 kN load-cell (model 661.22D-01) was used. The specimen was mounted on the test frame with pin-hole grips such that no rotation constraints were applied. All the fatigue tests were done under constant amplitude cyclic loading under force control. The maximum applied stress level was 120 MPa, the stress ratio was $R = 0.05$ and the frequency was $f = 10\ Hz$.

Cameras were used during the fatigue tests to take pictures which were post-processed to obtain the crack length and delamination shape evolution. The test was suspended after a certain number of fatigue cycles and the maximum stress was applied in order to get the maximum displacement of the crack opening and maximum deformation of the specimen. After that cameras took pictures of both sides of the specimen (see Fig. 4.10). The test was then resumed. This process was iterated until enough crack lengths were obtained in the specimen.

A strip of millimetre paper was bonded to the surface of the specimen facing a high resolution camera. The pictures captured by this camera were post-processed with ImageJ to obtain the crack lengths. The 7-point incremental polynomial method recommended in the ASTM E647-00 [24] was applied to derive crack growth rates with the crack lengths and corresponding cycles known.

The detection technique of the delamination shape adopted was the Digital Image

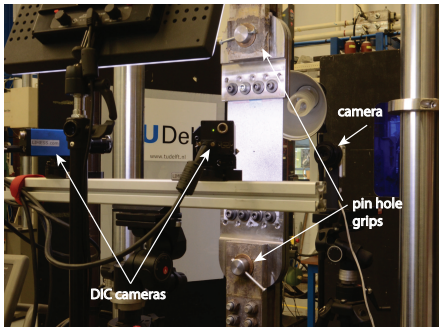

Figure 4.10: Test set up

Correlation (DIC) method [25–27]. The DIC method is known for measuring the strain distribution [25]. The DIC method obtains the deformation distribution by tracking the displacement of the random speckle patterns in the image of a deformed specimen under applied load and in the reference image of the specimen without any deformation. This displacement distribution is then processed to acquire the strain field. Due to the fact that the pieces of debonded aluminium carry negligible load while the bonded part still bears much more load, the evident difference in the strain distribution measured with DIC method between the delaminated part and bonded part makes the delamination front visible [26, 27].

In order to facilitate the correlation in the DIC method, the surface of the specimen had been painted random airbrushed black speckles with white background base coat of paint before the specimen was tested. The VIC-3D DIC system offered by Correlated Solutions was used to make the strain measurements. Two DIC cameras took the reference image and deformed images during fatigue testing. The image correlation was made with the subset size of $21 \cdot 21$ pixels and step of 5.

4.5. MODEL VALIDATION

The test data is used to validate the proposed model in this paper. Both the crack growth rates and the delamination shapes from the test and prediction are compared.

First the predicted crack growth rates are compared to the test results of specimen asym-1 (see Tabel. 4.2) in Fig. 4.11. The crack length is measured from the hole centre to the crack tip respectively. As can be seen the prediction correlates well with test data. The initial over prediction is due to the imprecise delamination shape assumed as input for the model. However, this over prediction vanishes after several cycles. Due to the non-symmetry, different crack lengths are obtained after fatigue test, this phenomenon is also captured by the prediction model as can be seen from the final predicted and tested crack lengths in Fig. 4.11.

Then the predicted and measured delamination shapes are compared for asym-1 in Fig. 4.12. The delamination shapes obtained with the DIC method at the end of testing are compared to the results obtained from etching the aluminium layers away to validate the DIC method, and the corresponding prediction results are also presented in Fig. 4.12.

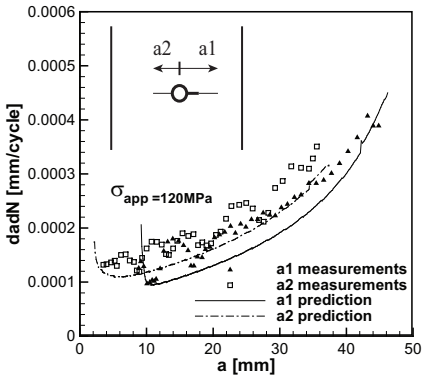

Figure 4.11: comparison of crack growth rates for specimen asym-1

The predicted delamination shapes are compared to the DIC measurements during the growth. Good correlation is observed.

The crack tip of $a1$ in asym-1 started growing at first from the saw-cut tip, another crack initiated at the hole edge after a while. Therefore the delamination shape for $a1$ (b1) is lager than that for $a2$ (b2) in the beginning. The difference in the delamination shapes decreases with fatigue life N until N is around 125500 cycles. Then the crack lengths are long enough so that the boundary condition affects more the crack growth and corresponding delamination growth. b1 is becoming bigger than b2 after this cycle number. This phenomenon is discussed in detail in Section 4.6.

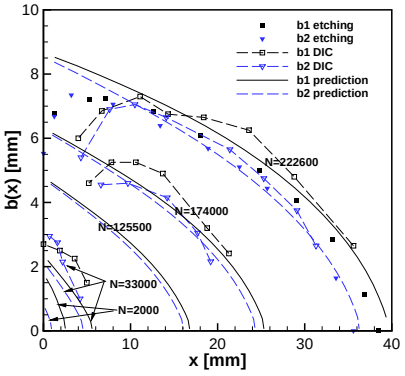

Figure 4.12: Delamination evolution for asym-1

The symmetric crack configuration, sym-1, is a special case of non-symmetric crack scenario. The prediction results together with test data for the symmetric case are given in Fig. 4.13. The corresponding data for asym-2 is also presented to highlight the effects of non-symmetric boundary condition on crack growth in FMLs. The crack length is measured from the hole centre to the crack tip as well. The cracks initiate at the two

saw-cut tips simultaneously for two cases. Symmetric Sym-1 has same crack growth behaviour for the two crack tips. For asym-2, the crack growth rates of the two crack tips are the same for the crack length less than 10 mm where the boundary condition hardly affects the crack growth. Then the effects of boundary condition prevail. The crack tip relatively closer to the free edge grows faster than the other one.

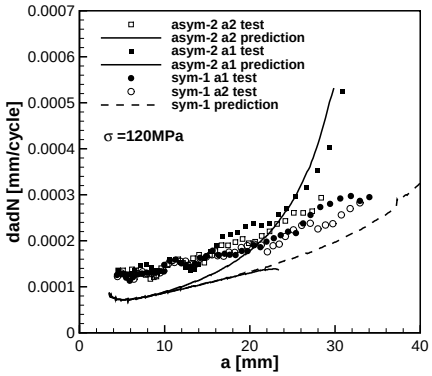

Figure 4.13: Comparison of crack growth rates for sym-1 and asym-2

4.6. DISCUSSION

4.6.1. THE CATCH-UP PHENOMENON FOR NON-SYMMETRIC CRACK GROWTH IN FMLS

From Fig. 4.12 it can be seen that the size of delamination shape b2 catches up with b1 during the short crack growth where the boundary condition effects are limited. This evolution of delamination damage interacts with the crack growth in metal layers. It can also be seen that the crack length bridged by b2 also catches up with the crack length bridged by b1 from Fig. 4.14 where the crack length measured from the saw-cut tip is plotted against the crack growth life N. The predicted crack growth rates presented in the same figure showed higher crack growth rate for $a2^*$ with smaller delamination b2 than $a1^*$ with lager delamination b1 in the beginning phase of the crack growth life.

As can be read from Table 4.3, the calculated far-field stress intensity factors for the two crack tips are very close for the life period from $N = 2000$ to $N = 33000$. This is attributed to the fact that the crack lengths are still small enough so that the boundary condition effects are almost absent. Whereas the stress intensity factor due to bridging for $a2^*$ is smaller, because the smaller delamination shape b2 provides smaller bridging compared to the larger b1 for $a1^*$. This results in a higher total stress intensity factor for $a2^*$ according to Eq. 4.1, resulting in a faster crack growth and accompanying delamination growth.

As can be seen in Fig. 4.14 $a1^*$ grows faster than $a2^*$ after the crack length exceeds 10 mm, where the effects of boundary conditions override the effects of the bridging mechanism on the crack growth behaviour. The calculated stress intensity factors in Table 4.3 further explain this.

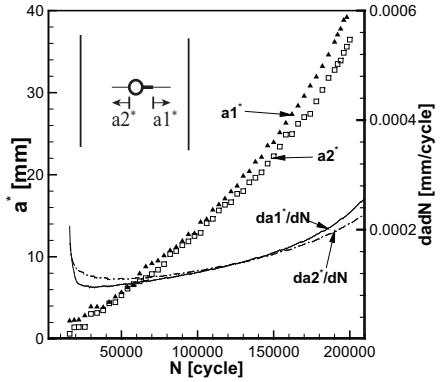

Figure 4.14: Illustration of catch-up phenomenon

Table 4.3: Variation of stress intensity factors

N	$K_{ff,1}$	$K_{ff,2}$	$K_{br,1}$	$K_{br,2}$
2000	702.96	703.24	237.95	227.74
33000	876.33	876.39	459.87	444.23
125500	1324.06	1318.76	848.61	843.67
174000	1622.4	1603.17	1089.86	1082.81
222600	2200.68	2085.52	1506.81	1468.67

4.6.2. IMPLEMENTATION OF THE PROPOSED MODEL FOR PREDICTING MSD IN FMLS

The presented authors of this paper have already detailed a philosophy for predicting multiple-site damage growth behaviour in FMLs in [10]. The philosophy requires the ability to predict the crack interaction effects in terms of the load redistribution mechanism, and the ability to predict the crack growth with asymmetric delamination shapes and asymmetric boundary conditions for two crack tips in metal layers in FMLs. The load redistribution mechanism in FMLs as a result of stiffness variation has been studied with the precursor model proposed in [11], and the prediction model of non-symmetric crack growth in FMLs is proposed in this paper. Since the model proposed in this paper uses the Westergaard stress distributions to characterise the stress distribution ahead of a crack tip, the load redistribution due to stiffness variation caused by the presence of another crack can therefore be modelled [11]. These two models will be integrated to predict the crack growth behaviour in FMLs with MSD scenario.

4.6.3. LIMITATIONS OF THE PROPOSED MODEL

From Fig. 4.13, it is observed that the predicted crack growth rate for the tip very close to the free edge is a little over predicted at the last period of fatigue crack growth in asym-2, while the prediction for the other tip relatively far away from the free edge ahead is underestimated. This inaccuracy originates from the methodology used in Section 4.3

to calculate the far-field stress induced stress intensity factors for two crack tips and the asymmetric crack opening contour of a non-symmetric crack. The methodology is based on the model proposed in [10], which anaylses the deformation behaviour in a 2-dimensional metallic panel damaged by an eccentric crack.

The model in [10] has assumed that the Westergaard stress distribution and associated crack opening solution are applicable to non-symmetric crack tips. And two half crack lengths are defined as the lengths between the maximum crack opening location and the crack tips respectively. These assumptions are valid for most eccentric crack scenarios. For a crack case with very high eccentricity and high ratio of the crack length to the ligament length in front of the critical crack tip, the assumptions lead to inaccuracy in the predicted stress intensity factors. The trend of the inaccuracy is already shown in [10]. This calculation error could result in a cumulative error in terms of fatigue crack growth life.

4.7. CONCLUSION

An analytical model has been developed to analyse the non-symmetric crack growth in FMLs. The non-symmetric crack growth in the metal layers and induced non-symmetric growth of delamination shapes at the composites/metal interfaces in FMLs were investigated in detail. The accuracy of the analytical model has been validated through comparing predictions with experimental data for several non-symmetric crack cases. Good correlation is observed.

Both the stress intensity factor due to the far-field loading (K_{ff}) and the stress intensity factor due to the bridging stress distributions (K_{br}) determine the non-symmetric fatigue crack growth in metal layers of FMLs. Implementation of these two stress intensity factor solutions requires analysis of two sorts of non-symmetries: crack tip non-symmetry and delamination shape non-symmetry. For small cracks, the delamination shape non-symmetry dominates the crack growth behaviour. When the crack length is long enough, the free edge boundary conditions will prevail and the crack growth behaviour is then dominated by the crack tip non-symmetry.

The load redistribution from the cracked metal layers to the intact fibre layers can only be solved on the condition of knowing the far-field loading induced crack opening behaviour of the eccentrically cracked metal layers. The proposed model is capable of analysing the deformation behaviour and calculating the bridging stress distribution of arbitrary delamination shape for non-symmetric fatigue crack growth in FMLs. The proposed model also provides the stress distribution in front of the crack tip, which can be utilised to analyse the effects of load redistribution due to stiffness variation in front of the crack tip on the crack state, such as the presence of other collinear cracks.

REFERENCES

[1] W. Wang, C. Rans, and R. Benedictus, *Analytical prediction model for non-symmetric fatigue crack growth in fibre metal laminates,* to be submitted to International Journal of Fatigue .

[2] A. Vlot and J. W. Gunnink, *Fibre Metal Laminates-An Introduction* (Kluwer Aca-

demic Publisher, Dordrecht, The Netherlands, 2001).

[3] R. C. Alderliesten, *Analytical prediction model for fatigue crack propagation and delamination growth in glare,* International Journal of Fatigue **29**, 628 (2007).

[4] R. C. Alderliesten, *Fatigue crack propagation and delamination growth in GLARE*, Ph.D. thesis, Delft University of Technology, Delft, the Netherlands (2005).

[5] S. Khan, *Fatigue Crack and Delamination Growth in Fibre Metal Laminates under Variable Amplitude Loading*, Ph.D. thesis, Delft University of Technology, Delft, the Netherlands (2013).

[6] S. U. Khan, R. C. Alderliesten, C. D. Rans, and R. Benedictus, *Application of a modified wheeler model to predict fatigue crack growth in fibre metal laminates under variable amplitude loading,* Engineering Fracture Mechanics **77**, 1400 (2010).

[7] S. U. Khan, R. C. Alderliesten, and R. Benedictus, *Delamination in fiber metal laminates (glare) during fatigue crack growth under variable amplitude loading,* International Journal of Fatigue **33**, 1292 (2011).

[8] G. Wilson, *Fatigue Crack Growth Prediction for generalized fiber metal laminates and hybrid materials*, Ph.D. thesis, Delft University of Technology, Delft, the Netherlands (2013).

[9] J. J. Homan, *Fatigue initiation in fibre metal laminates,* International Journal of Fatigue **28**, 366 (2006).

[10] W. Wang, C. Rans, R. Alderliesten, and R. Benedictus, *Philosophy of multiple-site damage analysis for fibre metal laminate structures,* in *Proceedings of 28th Symposium of the International Committee on Aeronautical Fatigue ICAF 2015, Helsinki, Finland* (2015).

[11] W. Wang, C. Rans, R. C. Alderliesten, and R. Benedictus, *Predicting the influence of discretely notched layers on fatigue crack growth in fibre metal laminates,* Engineering Fracture Mechanics **145**, 1 (2015).

[12] M. Isida, *Stress-intensity factors for the tension of an eccentrically cracked strip,* Journal of Applied Mechanics **33**, 674 (1966), 10.1115/1.3625138.

[13] M. Isida, *On the determination of stress intensity factors for some common structural problems,* Engineering Fracture Mechanics **2**, 61 (1970).

[14] D. L. Ball, *The development of mode i, linear-elastic stress intensity factor solutions for cracks in mechanically fastened joints,* Engineering Fracture Mechanics **27**, 653 (1987).

[15] D. L. Chen, B. Weiss, and R. Stickler, *A new approach for the determination of stress intensity factors for finite width plate,* Engineering Fracture Mechanics **48**, 561 (1994).

[16] J. Grandt, A. F., *Stress intensity factors for some through-cracked fastener holes,* International Journal of Fracture **11**, 283 (1975).

[17] X. He, M. Tan, and J. T. Xing, *An investigation on fatigue crack growth rates through a designed nonsymmetric crack growth test,* Engineering Fracture Mechanics **96**, 510 (2012).

[18] W. Qizhi, *The crack-line stress field method for analysing sifs of strips-illustrated with an eccentrically cracked tension strip,* International Journal of Fracture **59**, R39 (1993).

[19] D. Stefanescu, L. Edwards, and M. E. Fitzpatrick, *Stress intensity factor correction for asymmetric through-thickness fatigue cracks at holes,* International Journal of Fatigue **25**, 569 (2003).

[20] S. Spronk, I. Şen, and R. Alderliesten, *Predicting fatigue crack initiation in fibre metal laminates based on metal fatigue test data,* International Journal of Fatigue **70**, 428 (2015).

[21] H. Westergaard, *Bearing pressure and cracks.* Journal of Applied Mechanics **6**, 49 (1939).

[22] H. Tada, P. C. Paris, and G. R. Irwin, *The stress analysis of cracks handbook* (ASME, New York, 2000).

[23] J. Schijve, *Fatigue of structures and materials* (Springer, Dordrecht, The Netherlands, 2008).

[24] E647-00, ASTM, *Standard test method for measurement of fatigue crack growth rates,* (2011).

[25] H. Lemmen, R. C. Alderliesten, R. Benedictus, J. Hofstede, and R. Rodi, *The power of digital image correlation for detailed elastic-plastic strain measurements,* (2008).

[26] R. Rodi, R. C. Alderliesten, and R. Benedictus, *Crack-tip behavior in fiber/metal laminates by means of digital-image correlation,* Journal of Aircraft **47**, 1636 (2010).

[27] Y. Huang, J. Liu, X. Huang, J. Zhang, and G. Yue, *Delamination and fatigue crack growth behavior in fiber metal laminates (glare) under single overloads,* International Journal of Fatigue **78**, 53 (2015).

5

ANALYTICAL PREDICTION MODEL FOR FATIGUE CRACK GROWTH IN FIBRE METAL LAMINATES WITH MSD SCENARIO

This paper presents a theoretical and experimental study on Multiple-site Damage (MSD) crack growth behaviour in Fibre Metal Laminates (FMLs). The prediction model is developed based on a simplified analysis of the effects of load redistribution on a single crack in FMLs containing multiple cracks. Test results show that the crack growth accelerates as cracks grow towards each other. The tests also show non-symmetric crack growth behaviour and non-symmetric interfacial delamination propagation in case of multiple cracks. The prediction model successfully captures the crack growth acceleration and non-symmetric growth behaviour.

This chapter is to be submitted to International Journal of Fatigue [1].

5.1. INTRODUCTION

FMLs are a family of hybrid laminates made of alternating composite layers and thin metal sheets [2]. The FML concept is evolved out of bonded metal laminate structures by adding fatigue resistant fibres in such laminates, to enhance the crack growth resistance of the metal layers and allow a larger critical damage size. These merits of FML materials enable longer inspection intervals and application of less sophisticated inspection techniques to ensure structural integrity, which is very desirable in the context of the damage tolerance philosophy used in the aerospace sector [3].

An identified deficiency of the damage tolerance philosophy, which relies on inspections, is its compatibility with an unbounded structural life. It has been realised that the damage tolerance philosophy is not enough to secure flight safety for an indefinite life as widespread fatigue damage (WFD) within one structural element can occur over time. In 2010, the airworthiness regulations were revised to include the concept of Limit of Validity (LOV): a period of structural life prior to which WFD will not occur [4, 5]. The LOV concept places limits on the damage tolerance philosophy with the intention to combat WFD failure resulting from crack growth at multiple sites, i.e., the MSD scenario.

Consequently it is crucial to examine the MSD crack growth behaviour in FML materials, even though they are very successful in the context of the damage tolerance philosophy. Several robust damage tolerance analyses of isolated crack growth in FMLs can be found in open literature, including an analytical model for constant amplitude loading by Alderliesten [6, 7] which has been refined for variable amplitude loading [8–10], and for part-through crack configurations [11]. However, these well established damage tolerance prediction models fail to characterise the crack growth behaviour in FMLs containing multiple fatigue cracks and accompanying delamination shapes. Extending these models for the MSD problem is also problematic and cumbersome due to the load redistribution mechanism in FMLs, resulting from the simultaneous presence of multiple cracks [3, 12].

Hybrid FMLs exhibit different MSD crack growth behaviour compared to monolithic metal sheets, as shown in Fig. 5.1. Firstly, the growth behaviour of a single crack in an FML is very stable over much longer crack growth life than in a monolithic metallic panel (see Fig. 5.1), which is attributed to the fatigue resistant fibres remaining intact in the wake of fatigue cracks in the metal layers and acting as a second load path. Then the presence of other cracks in the FML causes local reductions in geometric stiffness at each crack location. As a result, loads redistribute from the adjacent cracks to the single crack. This load redistribution mechanism is present for the whole crack growth life and accelerates the crack growth rate, resulting in a significant life reduction. Whereas in metallic panels the load redistribution mechanism makes only a tiny difference in terms of the crack growth life due to the rapid growth behaviour. Therefore, the load redistribution mechanism becomes essential in modelling crack growth behaviour in FMLs containing MSD cracks [3, 12]. A precursor model that analyses the crack growth behaviour in FMLs containing discretely notched layers has been developed by the present authors, with the intention to develop a simplified prediction methodology for modelling the effects of load redistribution on a single crack in an FMLs containing an MSD scenario [3].

The objective of this paper is to integrate two analytical models proposed by the present authors to form another prediction model for analysing the MSD crack growth

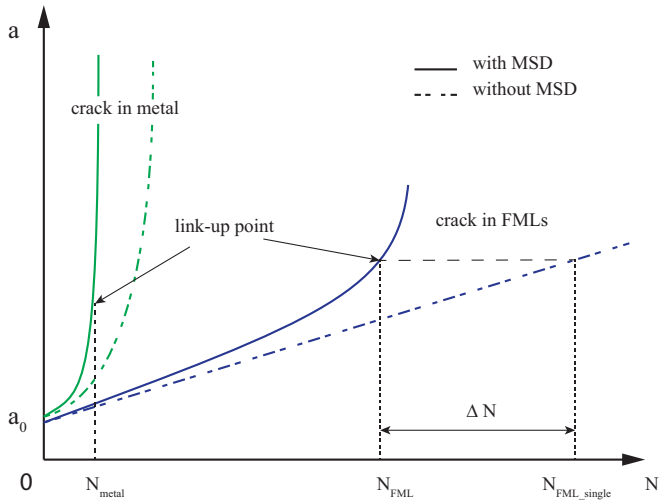

Figure 5.1: Fatigue nature of FMLs

behaviour in FMLs. Based upon the precursor model [3], this paper analyses the load redistribution mechanism as a result of simultaneous presence of multiple cracks in FMLs in a simplified manner. Additionally, the analytical model which addresses non-symmetric crack tip growth and delamination growth in FMLs [13] will be integrated to simultaneously analyse the asymmetric growth behaviour of multiple cracks. A systematical implementation of the two models will be provided in this paper. The validation is completed by comparing prediction results against the test data of three specimens containing MSD cracks.

5.2. BACKGROUND: STATE OF THE ART IN PREDICTING CRACK GROWTH BEHAVIOUR FOR FMLS

5.2.1. FATIGUE CRACK GROWTH MODEL FOR FMLS

Fatigue crack propagation in FMLs consists of crack growth in the metal layers and delamination growth at the metal/composite interfaces. As has been stated in the preceding section, the fatigue resistant fibres remain intact in the wake of fatigue cracks in the metal layers and bridge the cracks, leading to load transfer from the cracked metal layers to the bridging fibres. This load transfer reduces the stresses experienced at the crack tip in the metal layers, and as a result, the stress intensity factor at the crack tip is reduced. Moreover, the load transfer introduces cyclic shear stresses at the interfaces between metal layers and fibre layers, resulting in delamination growth at the interfaces.

Alderliesten has developed an analytical model to calculate the coupled crack growth and delamination propagation using linear elastic fracture mechanics (LEFM) [6, 7]. According to him, the stress intensity factor at the crack tip which is used to characterise crack growth in the metal layers can be decomposed into two components as expressed in Eq. 5.1. The first term, K_{ff}, refers to the stress intensity factor due to stresses in the

metal layers due to far-field applied load. The second term, K_{br}, refers to the stress intensity factor due to the bridging mechanism, which should be superposed upon the first term to derive the total stress intensity factor at the crack tip.

$$K_{total} = K_{ff} + K_{br} \tag{5.1}$$

Whereas the strain energy release rate G is applied to characterise the delamination propagation due to the complexity in calculating K at the interface between two dissimilar materials. As expressed in Eq. 5.2, G varies against x along the crack. Alderliesten subdivides the delamination shape into bar elements perpendicular to the crack and assumes that the delamination grows only in this direction.

$$G = \frac{n_f t_f}{2jE_f}\left(\frac{n_m t_m E_m}{n_m t_m E_m + n_f t_f E_f}\right)(S_f(x) + S_{br}(x))^2 \tag{5.2}$$

It is noteworthy that both K_{total} and G depend on the bridging stress distribution $S_{br}(x)$ along the delamination frontier [6, 7]. Alderliesten calculates $S_{br}(x)$ by implementing the displacement compatibility between the crack opening and the fibre deformation over the delaminated length at each bar element simultaneously. The crack opening in the metal layers (as a result of crack opening due to the far-field load, $v_{ff}(x)$, and crack closing due to the bridging stresses, $v_{br}(x)$,) must be identical to the elongation $\delta_f(x)$ and shear deformation $\delta_{pp}(x)$ of the fibre layers.

$$v_{ff}(x) - v_{br}(x) = \delta_{pp}(x) + \delta_f(x) \tag{5.3}$$

Eq. 5.3 can only be solved numerically with a square matrix whose size is identical to the number of bar elements in the delamination shape [6, 7].

5.2.2. CHALLENGES IN EXTENDING THE MODEL FOR MSD SCENARIO

The description of the crack growth model for FMLs in the preceding subsection highlights the significance of calculating the crack opening in the cracked metal layers and using a square matrix to implement the displacement compatibility in calculation of the bridging stress distribution. In order to simultaneously solve all the crack states in an FML containing MSD scenario with the Alderliesten model, one faces several challenges. To explain these challenges, an example MSD scenario in an FML is illustrated in Fig. 5.2.

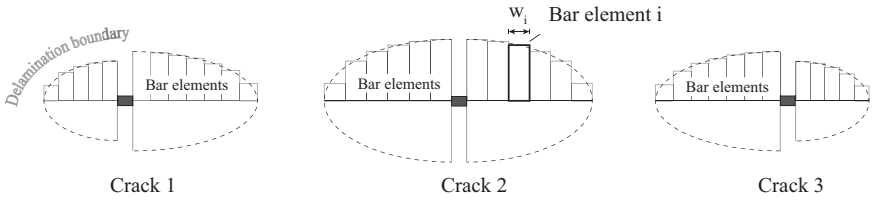

Figure 5.2: Subdivision columns in the delamination shapes for all cracks

The first challenge is to calculate the crack opening displacement at a specific bar element. Crack opening displacements for evenly spaced cracks can be derived [14]. However, the crack opening displacements of non-evenly spaced cracks, which frequently

occur in reality, is vey challenging to derive. In addition, the crack closing term, v_{br}, in Eq. 5.3 at the bar element i is not only effected by the bridging stresses over Crack 2, but also by the the bridging stresses over Crack 1 and Crack 3. Therefore these cracks are coupled in terms of the bridging mechanism, which makes the calculation challenging as well.

Secondly, it is computationally inefficient. Each crack has a matrix to be solved and these cracks are coupled with each other as explained above. A very large matrix then has to be constructed in order to solve the bridging stress distributions for all the cracks. The size of the matrix would depend on the number of the cracks and the length of each crack.

These two challenges make the use of the Alderliesten model for MSD scenario cumbersome. Another limitation of the Alderliesten model is that it cannot predict non-symmetric growth behaviour in FMLs [13]. However, as shown in Fig. 5.2, a non-symmetric crack configuration can arise in case of MSD scenario as a result of crack interaction. This non-symmetry comprises crack tip asymmetry and delamination asymmetry, which has to be dealt with [13].

5.2.3. ALTERNATIVE METHODOLOGY FOR PREDICTING MSD CRACK GROWTH

In response to the challenges and limitation discussed above, an alternative methodology has been proposed by the present authors to predict MSD crack growth behaviour in FMLs. This alternative has two essential elements. The first one is to solve each crack state by modelling the effects of other cracks as local reductions in geometric stiffness [3]. The second one is to predict the non-symmetric growth behaviour [13]. These two elements are briefly summarised here and the implementation of these elements for an MSD scenario is given in the next section.

The effects of other cracks on a single crack in an FML can be separated into crack tip interaction effects and load redistribution effects. Crack tip interaction effects are attributed to the interaction of the stress singularities (plasticities) in front of the two crack tips when they are in the vicinity of each other, which occurs for a small portion of fatigue crack growth life before the link-up of cracks. Load redistribution effects are attributed to the reductions in geometric stiffness caused by the presence of other cracks, which is present over the whole fatigue crack growth life. The nature of slow crack growth behaviour in FMLs leads to modelling load redistribution effects being the key factor for predicting MSD crack growth behaviour since the cumulative effects of load redistribution can result in significant reduction in fatigue crack growth life (see Fig. 5.1) [12]. While the crack tip interaction effects are neglected since the growth rates of two nearby crack tips are so rapid that the error in estimated fatigue life by ignoring these effects is negligible.

This paper adopts the precursor model in [3] to estimate the load redistribution effects in a simplified manner. Other cracks are represented as removals of metal strips when analysing the crack state of a single crack. This representation mimics the reduction in geometric stiffness caused by the crack in the metal layers. The effects of the stiffness reduction is estimated by applying the isostrain condition between the representations of the cracks and the surrounding laminate materials [3]. The reduced stiffness of the laminate at the crack location in front of the single crack causes decrease in

the stress transferred by the laminate as a result of isostrain condition, which could lead to load transfer from the crack to the single crack, exacerbating the stress state of the single crack.

The strain distribution, needed for implementing the isostrain condition, is derived from the Westergaard stress distribution in front of the crack tip [3]. In order to model the non-symmetric growth behaviour in FMLs, two different Westergaard stress distributions are assumed in front of the crack tips of a single crack instead of using the identical Westergaard stress distribution for two crack tips [13]. The non-symmetric crack opening displacement of the single crack arising from the two Westergaard stress functions can also be calculated and used to implement the displacement compatibility expressed in Eq. 5.3. A more generic algorithm for calculating bridging stress distribution proposed in [13] can be used to account for the effects of non-symmetric delamination shapes for the single crack.

With these two elements, the single crack state can be solved without knowing all the crack opening displacements of other cracks, and a relatively small matrix is solved each step with the calculated non-symmetric crack opening displacement of the single crack. The implementation of the elements will be provided in next section. This process can be iterated until all crack states have been calculated.

5.3. MODEL INTEGRATION AND IMPLEMENTATION

5.3.1. MODEL INTEGRATION

Two analytical models have been developed with the intention to address the load redistribution mechanism, and non-symmetric crack growth and delamination propagation behaviour in FMLs containing MSD scenario respectively. A systematic integration and implementation of these two models enables analysis of the state of a single crack at each step.

Consider a generic MSD crack configuration illustrated in Fig. 5.3. Crack i is the single crack to be analysed and the other cracks are idealised as removals of metal strips. The numbering of other cracks is illustrated in Fig. 5.3(a).

In front of the crack tips of the single crack i, two Westergaard stress distributions should be assumed in order to account for the non-symmetry effects [13]. The load redistribution from the other cracks to the single crack is evaluated by implementing the isostrain condition between the representations of the cracks and surrounding laminate material. Consequently, the strain distributions derived from the Westergaard stress distributions in the laminate in front of two crack tips are continuous.

For crack tip $i1$, the strain distribution in front is:

$$\varepsilon_{yy,i1} = \varepsilon_{i1} / \sqrt{1 - (a_{i1}/x_{i1})^2} \tag{5.4}$$

with the subscript $i1$ denoting that every variable in Eq. 5.4 is associated with crack tip $i1$. ε_{i1} is an unknown parameter. x_{i1} starts from the location of the maximum crack opening displacement and the crack length a_{i1} is also measured from the maximum crack opening location to the crack tip (see Fig. 5.3(a)) [13, 15]. This maximum crack opening displacement location is a parameter to be determined.

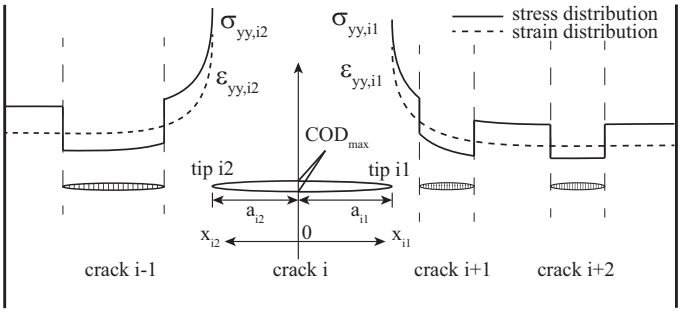

(a) Illustration of stress distributions

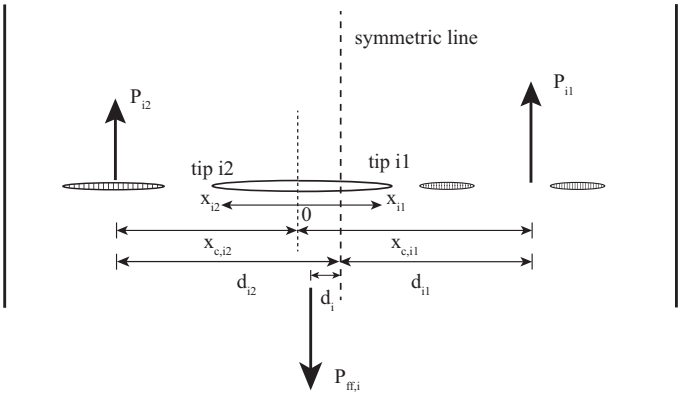

(b) Illustration of balanced equivalent loads

Figure 5.3: Illustration of modelling load redistribution and non-symmetry effects

For crack tip $i2$, the strain distribution in front is expressed as:

$$\varepsilon_{yy,i2} = \varepsilon_{i2} / \sqrt{1 - (a_{i2}/x_{i2})^2} \tag{5.5}$$

with the subscript $i2$ denotes that every variable in Eq. 5.5 is associated with crack tip $i2$. ε_{i2} is a unknown parameter as well. x_{i2} is another local coordinates starting from the location of the maximum crack opening displacement and the crack length a_{i2} another half crack length.

It is worth noting that two half crack lengths a_{i1} and a_{i2} are defined instead of using an equal half crack length, a, in Eqs. 5.4 and 5.5. The definition of two different half crack lengths is attributed to the fact that the Westergaard stress distribution artificially defines a half crack length with the maximum crack opening at the root of the half crack length. In order to obtain a continuous crack opening contour described by two different Westergaard stress distributions, two half crack lengths are defined and the calculated maximum crack opening displacements have to be identical [13].

The stiffness variations in front of the crack tips of the single crack lead to steps in the stress distributions, see Fig. 5.3(a). At the uncracked parts between crack tips, both

the metal layers and fibre layers transfer the load, whereas only fibres at the locations of other cracks transfer the load. In consequence the stress distributions in front of the two crack tips are described through multiplying the strain distributions in Eqs. 5.4 and 5.5 by the stiffness of each part in front of the crack tips respectively.

$$\sigma_{yy,i1} = \begin{cases} E_{lam} \cdot \varepsilon_{i1} / \sqrt{1-(a_{i1}/x_{i1})^2} = \sigma_{i1} / \sqrt{1-(a_{i1}/x_{i1})^2} \\ \text{for uncracked parts} \\ \\ E_{fibre} \cdot \varepsilon_{i1} / \sqrt{1-(a_{i1}/x_{i1})^2} = E_{fibre}/E_{lam} \cdot \sigma_{i1} / \sqrt{1-(a_{i1}/x_{i1})^2} \\ \text{for cracked parts} \end{cases} \tag{5.6}$$

$$\sigma_{yy,i2} = \begin{cases} E_{lam} \cdot \varepsilon_{i2} / \sqrt{1-(a_{i2}/x_{i2})^2} = \sigma_{i2} / \sqrt{1-(a_{i2}/x_{i2})^2} \\ \text{for uncracked parts} \\ \\ E_{fibre} \cdot \varepsilon_{i2} / \sqrt{1-(a_{i2}/x_{i2})^2} = E_{fibre}/E_{lam} \cdot \sigma_{i2} / \sqrt{1-(a_{i2}/x_{i2})^2} \\ \text{for cracked parts} \end{cases} \tag{5.7}$$

E_{lam} in the above equations represents the overall stiffness of the laminate and E_{fibre} represents the stiffness of the fibre layers [3]. The reduced stress distributions at the cracked parts indicate the load redistribution effects caused by the reductions in the geometric stiffness.

In Fig. 5.3(b), P_{i1} and P_{i2} are the integrations of the stress distributions ahead of the crack tips respectively. They are the loads carried by the materials in front of the two crack tips. P_{i1} and P_{i2} and the far-field load $P_{ff,i}$ needs to maintain not only load equilibrium but also moment equilibrium [13]:

$$P_{i1} + P_{i2} = P_{ff,i} \tag{5.8}$$

$$P_{i1} d_{i1} = P_{i2} d_{i2} + P_{ff,i} d_i \tag{5.9}$$

where d_{i1}, d_{i2} and d_i are the distances between the locations of respective loads and the symmetric line of the panel. They can be calculated using their geometrical relations with the centroids of the respective stress distributions ($x_{c,1}$, $x_{c,2}$ in Fig. 5.3(b)) [13].

The model is an integration of the two analytical models proposed in [3, 13]. A system of equations can be derived and solved for all the unknown variables. Detailed calculation of all the unknown variables in the above equations can be found in [3, 13]. Then the stress intensity factors at the two crack tips, $K_{ff,i1}$, $K_{ff,i2}$ can be determined. The effects of load redistribution and non-symmetry are taken into consideration when deriving these stress intensity factors. Meanwhile, a continuous asymmetric crack opening contour $v_{ff,i}$ for the single crack i can also be calculated. For detailed calculation, one can refer to [3, 13].

In addition, two non-symmetric delamination shapes for the two crack tips also contributes to the non-symmetric growth behaviour of the crack tips. The bridging stress

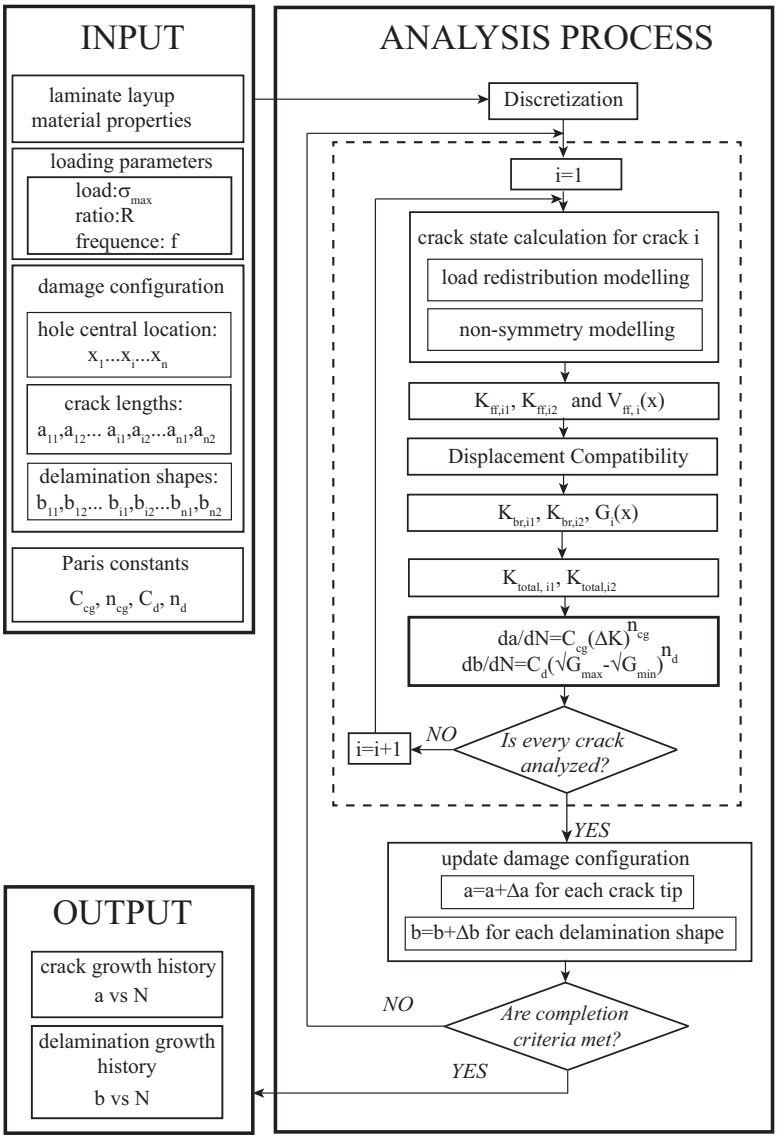

Figure 5.4: Illustration of numerical implementation

distributions, $S_{br,i}(x)$, in the asymmetric delamination shapes over the non-symmetric crack i with asymmetric crack opening contour can also be calculated with the generic algorithm of implementing the displacement compatibility that is detailed in [13]. Then the stress intensity factors due to the bridging mechanism, $K_{br,i1}$, $K_{br,i2}$ can be determined. The strain energy release rate $G_i(x)$ for crack i can also be calculated with the bridging stress distribution for crack i known. For detailed calculation, please refer to

[13].

Eq. 5.1 needs to be applied to calculate the total stress intensity factors at the two crack tips ($K_{total,i1}$, $K_{total,i2}$). The crack growth rates for the two tips can then be determined. So can the delemination growth rate, when $G_i(x)$ is known.

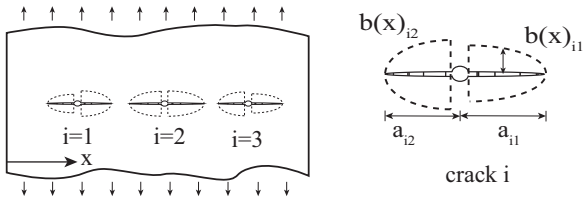

Figure 5.5: MSD configuration definition

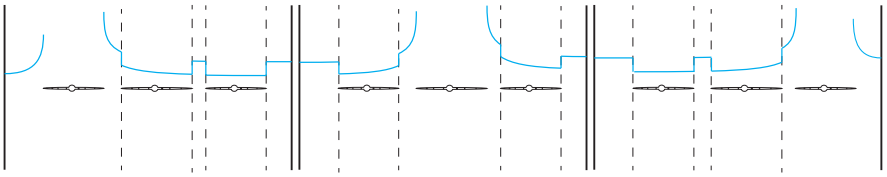

(a) crack state analysis for crack $i = 1$ (b) crack state analysis for crack $i = 2$ (c) crack state analysis for crack $i = 3$

Figure 5.6: Illustration of crack state analysis loop

5.3.2. NUMERICAL IMPLEMENTATION PROCEDURE

Fatigue analysis itself is an iterative process. Fig. 5.4 gives an overview of the iterative process for analysing MSD crack growth in FMLs. The methodology for analysing the crack growth behaviour and delamination propagation behaviour in FMLs with multiple cracks is implemented in a numerical program.

The required input variables are shown in Fig. 5.4. The material properties, loading parameters and Paris constants are standard inputs of fatigue analysis for FMLs. Apart from these inputs, the damage configuration input should be provided. For the case of an MSD scenario, several cracks and their accompanying delamination shapes are present simultaneously. A clear identification system of individual crack and corresponding delamination shape has to be made. In Fig. 5.5, a three-crack configuration is illustrated as an example. The cracks are numbered from left to right. For a single crack i, the associated crack lengths and delamination shapes are identified with the subscripts shown in Fig. 5.5. The crack length is measured from the hole centre to the individual crack tip. The crack location x_i is the distance measured from the left boundary to the hole centre of crack i. The crack lengths and crack locations should be the damage configuration input. The initial delamination shapes for the crack tips are assumed [6, 7].

For a given MSD crack scenario, the state of a single crack can be calculated with the proposed methodology in the preceding subsection. This calculation has to be repeated

in order to calculate each crack state, which is the inner loop enclosed by the dashed box in the analysing process illustrated in Fig. 5.4. A tangible illustration is given in Fig. 5.6 for a case of three cracks.

Knowing the total stress intensity factors of each crack tip and the strain energy release rate at the delamination over each crack, the crack growth rates and delamination growth rates can be determined with the empirical Paris relations. After a small crack increment and delamination increment, the state of each new crack configuration must be reanalysed. This iterative process continues until two crack tips link-up or one crack tip grows to the free edge.

5.4. EXPERIMENTAL TESTING

One variant of FMLs, Glare, was tested to obtain fatigue test data to validate the model. Each specimen has a three-crack configuration, which is illustrated in Fig. 5.7. The middle crack is at the specimen centre with other two symmetrically located on both sides. The symmetric condition for the middle crack results in symmetric crack growth behaviour of the crack. Apart from validating the present model, the test data of the middle crack will be compared to the prediction for an isolated central crack to highlight the effects of load redistribution caused by the presence of other two cracks. The outer two cracks depicted in Fig. 5.7 should possess non-symmetric crack growth behaviour. The multiple cracks interact with each other under fatigue loading.

The used Glare comprised of 2024-T3 aluminium sheets and prepregs made of S-2 glass fibre reinforced FM 94 adhesive. Prepregs with different fibre orientations were stacked together to make a fibre layer, Al layers and fibre layers were then piled up alternately. Standard Glare3 and Glare4B were used [2], the lay-up of each laminate is given in Table 5.1. The stacked laminates were cured in an autoclave with curing temperature of 120 °C and pressure of 6 bar. The cured laminate panels were milled into the specimen dimensions given in Fig. 5.7. Three holes with a diameter of 3 mm were applied to each panel. Two notches were cut on both side of each hole with hand saw in order to obtain roughly simultaneous crack growth starting from the tips.

Table 5.1: Test matrix

specimen	Glare grade	Al layer number	fibre layer number	prepreg orientation in each fibre layer	applied load
1	Glare3	3	2	0/90	120 MPa
2	Glare4B	3	2	90/0/90	100 MPa
3	Glare4B	4	3	90/0/90	100 MPa

The test matrix comprises 3 panels whose configurations are given in Table 5.1. Specimen 2 and 3 were under same loading but the metal volume fraction (MVF) of specimen 3 is lower than specimen 2 [2]. Due to the fact that the stiffness of Al is higher than that of S-2 fibres, the presence of cracks in the metal layers of an FML with higher MVF results in more reduction in stiffness.

Testing was carried out on an MTS 810 servo hydraulic test frame containing a pin-hole clevis and a 250 kN load-cell (model 661. 22D-01). All the fatigue tests were con-

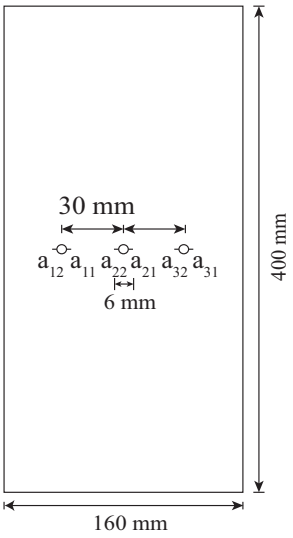

Figure 5.7: MSD crack configuration

ducted under constant amplitude fatigue loading with a stress ratio of $R = 0.05$ and a frequency of 10 Hz. The respective maximum applied stresses are given in Table. 5.1. The crack lengths were measured using a monocular microscope with a precision of 0.1 mm while the fatigue test was suspended and maximum stress was applied, the corresponding fatigue life was also recorded. The test resumed after the crack length measurement. The fatigue test stopped when two crack tips linked up.

After fatigue tests, chemical etching was employed to remove the outer aluminium layers to reveal the final delamination shapes. All crack lengths were processed with a 7-point incremental polynomial method recommended in the ASTM E647-00 [16] to obtain the crack growth rate.

5.5. RESULTS AND DISCUSSION

5.5.1. CRACK GROWTH BEHAVIOUR COMPARISON

The crack growth behaviour of all three tested specimens are used to compare against the prediction results. Both crack growth rate comparisons and a-N comparisons are given in Fig. 5.8, Fig. 5.9 and Fig. 5.10 for each specimen respectively.

For each specimen configuration, the predictions for an isolated central crack using the Alderliesten model [6, 7] are also provided as dashed lines. The comparison between the predicted growth rate of the isolated crack and that of the middle crack (a_{21}, a_{22}) in the case of MSD highlights the increase in the crack growth rate due to the stiffness reductions caused by multiple crack growths. The predicted growth rate without considering the effects of load redistribution for MSD scenario is highly inaccurate and the cumulative error leads to over prediction of the fatigue life by a factor of about 1.8 (see Fig. 5.8(b), Fig. 5.9(b), Fig. 5.10(b)).

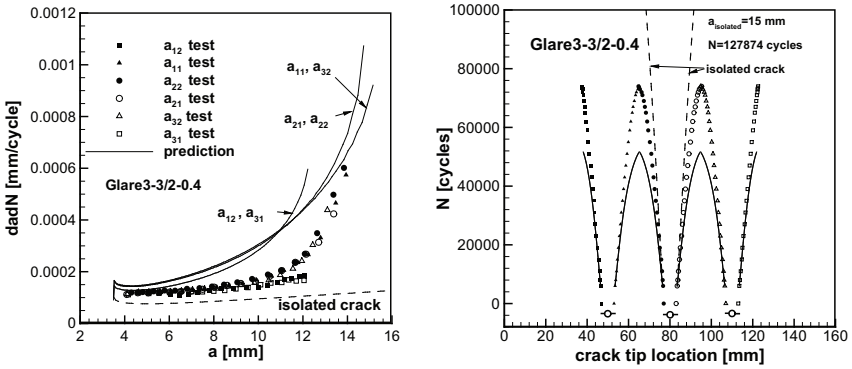

(a) da/dN comparison (b) a-N comparison

Figure 5.8: Comparison between prediction and measurements of Glare3-3/2-0.4 specimen

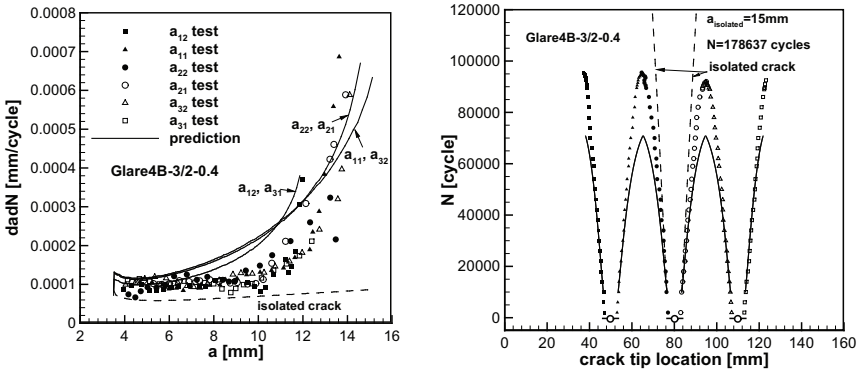

(a) da/dN comparison (b) a-N comparison

Figure 5.9: Comparison between prediction and measurements of Glare4B-3/2-0.4 specimen

In the present prediction methodology, the load redistribution effects are accounted for throughout the entire crack growth period. The predicted crack growth rates capture the crack acceleration feature of interacting crack tips in FMLs (see Figs. 5.8(a), 5.9(a) and 5.10(a)). However, the idealization of the cracks in modelling load redistribution leads to over predicted results.

For the major portion of the crack growth and the major portion of the growth life, two crack tips that grow towards each other are not close enough for the stress singularities (plasticities) in front to interact. It is the load redistribution mechanism that increases the crack growth rate. Whereas the effects of plasticity interaction present when one crack tip is in the vicinity of another, resulting in dramatic increase in the crack growth rate, shown in Fig. 5.9 and Fig. 5.10. The load redistribution effects are modelled

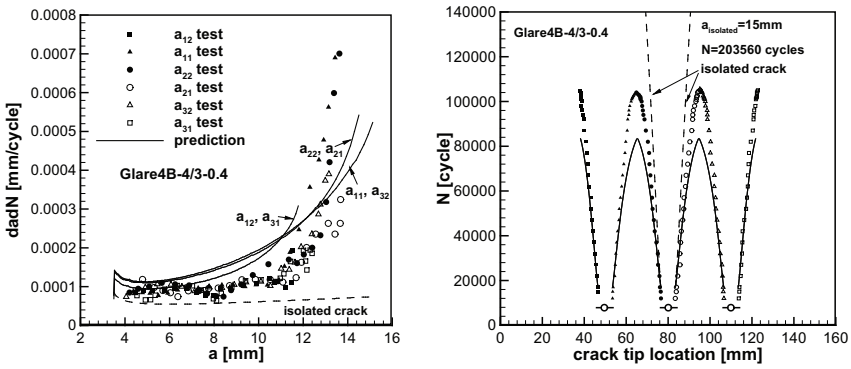

(a) da/dN comparison (b) a-N comparison

Figure 5.10: Comparison between prediction and measurements of Glare4B-4/3-0.4 specimen

5

throughout the whole crack growth even in the presence of the plasticity interaction, however the stress singularity interaction effects in the vicinity of two crack tips are ignored.

The calculation of the size of plasticity in front of the crack tip and the stress singularity interaction is beyond the scope of this paper. Eq. 5.10 is merely used to provide an indication of the plastic zone size r_p. The total stress intensity factor K_{total} for $a_{22} = 13\ mm$ in specimen $Glare4B-4/3-0.4$ and the yield strength $\sigma_{ys} = 347\ MPa$ for the used aluminium are substituted into Eq. 5.10. The obtained plastic zone size is $1.1\ mm$. Neglecting the plasticity interaction effects therefore leads to underestimation of the crack growth rate only over an estimated crack length of roughly 1 to 2 mm before link-up of the crack tips (see Fig. 5.10(a)). It is worth noting that this plasticity interaction only occurs over a rather small portion of crack length with rapid growth rate, resulting in a minimum error in fatigue life prediction without considering this in the model.

$$r_p = \frac{K_{total}^2}{\pi \sigma_{ys}^2} \tag{5.10}$$

The deviations in predicted fatigue crack growth life and measured crack growth life in a-N comparison figures are attributed to the over predicted crack growth rates. The over prediction is a result of the idealisation of adjacent cracks as removal of strips of metal layers when analysing the crack state of a single crack in the prediction model. The idealisation is not a true physical representation of cracks in the proposed model, which introduces more stiffness reduction and thus more load redistribution in modelling than actual cracks do in a laminate. However, the load redistribution is adequately captured by the non-physical representation. The over predicted crack growth rates lead to conservative calculation results. Otherwise the fatigue growth life prediction could be very non-conservative if the load redistribution effects are not considered, illustrated by the predicted life of an isolated crack growing to the length where the link-up occurs for

the tested MSD cracks (Fig. 5.8(b), Fig. 5.9(b), Fig. 5.10(b)).

The predicted crack growth life and the measured crack growth life for each specimen are given in Table 5.2. The MVF, the ratio between the total thickness of metal layers and the total thickness of the laminate, of each specimen, and the relative error between the prediction and the measurement are also given. A consistent trend between the MVF and the relative error can be observed: the relative error is smaller with lower MVF. This can be attributed to the idealisation in the prediction model. The influence of other cracks on a single crack is estimated by idealizing the cracks as negative stiffeners, which artificially enlarges the reduction in stiffness caused by real cracks in the model. The model tends to enhance the enlargement for FMLs with higher MVF, leading to more conservative crack growth rate prediction and thus more error.

Table 5.2: Prediction accuracy vs MVF

specimen	Glare grade	MVF	measured life	predicted life	relative error
1	Glare3-3/2-0.4	0.69	74000	51600	-30.3%
2	Glare4B-3/2-0.4	0.60	95500	70800	-25.9%
3	Glare4B-4/3-0.4	0.57	104000	83400	-19.8%

5.5.2. DELAMINATION COMPARISON

The proposed model also predicts the individual delamination shape evolution in an FML containing MSD cracks. The comparison between prediction and measurement is made for specimen 1 (see Table 5.1) in Fig. 5.11. The delamination measurements were made after etching the outer aluminium layers of specimen 1 away. Due to the symmetry, delaminations of crack tip 1, 2 and 3 are shown only. An very good correlation can be observed in the comparison.

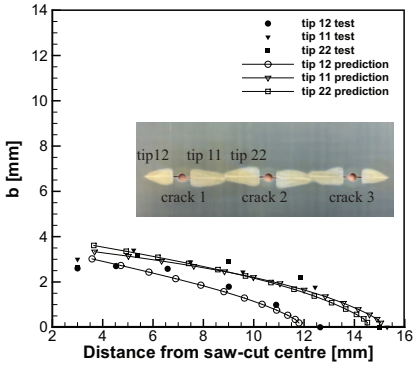

Figure 5.11: Delamination comparison for specimen 1

Due to the interaction effects of crack tip 2 and crack tip 3, their delamination shapes are larger than the delamination for crack tip 1. The good correlation between calculated and measured non-symmetric delamination shapes for crack tip 1 and crack tip 2 of

the single crack indicates high accuracy of the predicted non-symmetry effects by the proposed model.

5.6. CONCLUSION

A new prediction methodology for MSD growth in FMLs has been developed based on other two models proposed by the present authors. The proposed model in this paper analyses both crack interaction in terms of load redistribution mechanism and non-symmetric growth behaviour of multiple cracks in FMLs. The load redistribution resulting from the presence of multiple cracks is modelled by idealising the cracks as removals of metal strips and applying the isostrain condition at the crack locations. The non-symmetry effects are modelled by applying two different Westergaard stress distributions in front of two tips of a single crack that is being analysed. These two mechanisms have to be simultaneously solved to obtain the state of a single crack, which is iterated to determine all crack states sequentially.

Based on the analysis and results obtained in this paper, the following remarks can be made:

1. The nature of fatigue crack growth in FMLs leads to the significance of modelling load redistribution in analysing MSD scenarios in FMLs. Neglecting the interaction of stress singularities in the vicinity of two crack tips results in a negligible error in terms of fatigue growth life. However, not considering the load redistribution mechanism for MSD scenario could result in a very non-conservative predicted fatigue life.

2. The non-physical representation of cracks leads to conservative prediction results. However, it adequately captures the crack growth acceleration in the case of MSD cracks in FMLs.

3. The non-physical idealisation of cracks as removal of metal strips in modelling the load redistribution mechanism exaggerates the stiffness reduction caused by the actual cracks. Therefore the predicted results are more accurate for FMLs with lower MVF since the exaggeration is less (Table 5.2).

4. In addition to the non-symmetric free boundary edges and crack configurations in front of two tips of a crack, the asymmetric delamination shapes for two crack tips also contribute to the non-symmetric crack growth behaviour.

5. The non-symmetric crack lengths and delamination shapes are well predicted by the proposed model.

6. The presence of fatigue resistant fibres in FMLs alleviates the stiffness reduction due to the co-existence of multiple cracks compared to monolithic metals.

REFERENCES

[1] W. Wang, C. Rans, and R. Benedictus, *Analytical prediction model for fatigue crack growth in fibre metal laminates with msd scenario,* to be submitted to International Journal of Fatigue ().

[2] A. Vlot and J. W. Gunnink, *Fibre Metal Laminates-An Introduction* (Kluwer Academic Publisher, Dordrecht, The Netherlands, 2001).

[3] W. Wang, C. Rans, R. C. Alderliesten, and R. Benedictus, *Predicting the influence of discretely notched layers on fatigue crack growth in fibre metal laminates,* Engineering Fracture Mechanics **145**, 1 (2015).

[4] R. Eastin, *'wfd'-what is it and what's 'lov' got to do with it?* International Journal of Fatigue **31**, 1012 (2009).

[5] *Federal register/vol. 77, no. 101, thursday may 24, 2012/ rules and regulations,* .

[6] R. C. Alderliesten, *Fatigue crack propagation and delamination growth in GLARE*, Ph.D. thesis, Delft University of Technology, Delft, the Netherlands (2005).

[7] R. C. Alderliesten, *Analytical prediction model for fatigue crack propagation and delamination growth in glare,* International Journal of Fatigue **29**, 628 (2007).

[8] S. Khan, *Fatigue Crack and Delamination Growth in Fibre Metal Laminates under Variable Amplitude Loading*, Ph.D. thesis, Delft University of Technology, Delft, the Netherlands (2013).

[9] S. U. Khan, R. C. Alderliesten, C. D. Rans, and R. Benedictus, *Application of a modified wheeler model to predict fatigue crack growth in fibre metal laminates under variable amplitude loading,* Engineering Fracture Mechanics **77**, 1400 (2010).

[10] S. U. Khan, R. C. Alderliesten, and R. Benedictus, *Delamination in fiber metal laminates (glare) during fatigue crack growth under variable amplitude loading,* International Journal of Fatigue **33**, 1292 (2011).

[11] G. Wilson, *Fatigue Crack Growth Prediction for generalized fiber metal laminates and hybrid materials*, Ph.D. thesis, Delft University of Technology, Delft, the Netherlands (2013).

[12] W. Wang, C. Rans, R. Alderliesten, and R. Benedictus, *Philosophy of multiple-site damage analysis for fibre metal laminate structures,* in *Proceedings of 28th Symposium of the International Committee on Aeronautical Fatigue ICAF 2015, Helsinki, Finland* (2015).

[13] W. Wang, C. Rans, and R. Benedictus, *Analytical prediction model for non-symmetric fatigue crack growth in fibre metal laminates,* to be submitted to International Journal of Fatigue ().

[14] H. Tada, P. C. Paris, and G. R. Irwin, *The stress analysis of cracks handbook* (ASME, New York, 2000).

[15] W. Wang, C. Rans, and R. Benedictus, *Towards the analysis of built-up structures containing eccentric cracks: Analytical solutions for crack opening displacements of eccentric cracks,* to be submitted to European Journal of Mechanics - A/Solids ().

[16] E647-00, ASTM, *Standard test method for measurement of fatigue crack growth rates,* (2011).

6

PREDICTION METHODOLOGY FOR FATIGUE CRACK GROWTH BEHAVIOUR IN FIBRE METAL LAMINATES SUBJECTED TO TENSION AND PIN LOADING

Fibre Metal Laminates (FMLs) are a hybrid metal-composite laminate technology known for their superior resistance to fatigue crack growth compared to monolithic metals. This crack growth behaviour has been the subject of many studies, resulting in numerous empirical and analytical models to describe the complex damage growth phenomenon in the material. This study builds upon the analytical Alderliesten crack growth prediction methodology for FMLs, extending it from a tension loaded plate to a case of a combined tension-pin loaded plate. This new loading case is a more representative case to utilise for predicting fatigue crack growth behaviour in mechanically fastened joints. Development of the model extension and validation through experimental testing are detailed within this paper.

This chapter is under review at the Composite Structures [1].

6.1. INTRODUCTION

Fibre Metal Laminates (FMLs) are a material technology known for their superior fatigue crack growth behaviour. This favourable behaviour is a result of the fibre bridging mechanism whereby the intact fibre layers provide an alternative load path around the cracked metal layers, reducing stress in front of the crack tip (see Fig. 6.1).

Although the basic concept of fibre bridging is simple to understand, it proved to be a complex phenomenon to capture effectively in crack growth prediction models for FMLs. Early attempts at predicting fatigue crack growth took a phenomenological approach, treating an FML as a bulk material and developing empirical β correction factors to represent the contribution of the fibre bridging mechanism. These β corrections were then used to correct the standard stress intensity factor solutions used in the Linear Elastic Fracture Mechanics approaches for crack growth prediction in monolithic materials [2–4]. Additional phenomenological approaches based on treating FMLs as a bulk material include the compliance method of Takamatsu [5], bridging stress linearization approach of Cox [6], and the equivalent crack length approach of Guo and Wu [7]. Although these models achieved some limited success, the bridging mechanism could not be adequately captured with this bulk material approach [8].

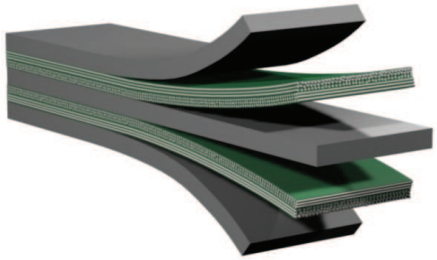

Figure 6.1: Illustration of typical FML concept

Greater success was achieved by embracing the composite nature of FMLs and attempting to analytically describe the interplay between the metal and fibre layers. Marissen [9] investigated the influence of bridging stress on the growth of the interface delamination between cracked metal layers and intact fibre layers. The opening of the crack in the metal layers is dependent on the compliance, and thus size, of this delaminated region. Alderliesten [10, 11] further built on this work by formulating an analytical fracture mechanics model that captured the load redistribution of the fibre bridging mechanism by enforcing compatibility between the crack opening displacement in the metal layers and elongation of the delaminated region of the fibre layers. With the bridging stress determined, growth of the interface delamination under the driving force of the bridging stress could be predicted, and growth of the crack through superposition of the far-field and bridging stress intensity factors in the metal could be achieved. This analytical approach, referred to in this paper as the Alderliesten model, has been the backbone of continued effort in extending crack growth prediction capabilities in FMLs with exten-

sions to account for residual strength [12], variable amplitude loading [13–15], generalized laminate configurations [16, 17], and more recently multiple site damage [18, 19].

It is worth noting that mechanically fastened joints are potentially vulnerable structures in consequence of secondary bending, stress concentration at fastener holes and pin bearing effects as load transfers from one substance to another via the joint. The structural behaviour of mechanically fastened FML joints has therefore drawn particular attention. In open literature, the neutral line model developed by Schijve [20] has been extended by de Rijk for calculating the load transfer and secondary bending stresses in FML joints [21]. The progressive damage behaviour in pin loaded FMLs has been investigated by Frizzell et al. [22, 23] and the bearing strength of FMLs has also been extensively studied [24–26].

Apart from the static behaviour of FML joints, another issue associated with mechanically fastened FML joints is the fatigue crack growth in the metal layers and the delamination propagation at metal-composite interfaces under fatigue loading. Even though extensive analytical models have been developed for predicting the crack growth behaviour in flat FML panels subjected to tensile loading [10, 11, 15, 16], the influence of pin loading on the crack growth behaviour in FMLs has not been fully studied. There is a risk that multiple cracks are present simultaneously in the critical row of an FML joint, which is crucial to examine in light of the introduction of Limit of Validity (LOV) to the airworthiness regulations that defines a fatigue life free of Widespread Fatigue Damage [19, 27, 28]. The analysis of pin loading effects on the crack growth behaviour in FMLs becomes indispensable for the analysis of MSD crack growth behaviour in FML joints.

This paper aims to develop an analytical model capable of predicting the growth behaviour of an isolated crack in a mechanically fastened FML joint where the pin loading effects are present. This model is developed with the intention to further incorporate it into an analysis frame which can eventually analyse the MSD growth behaviour in FML joints. The development of this model is based on the findings of an experimental investigation of pin loading effects on the crack growth behaviour in FMLs [29] and the success of an analytical model by Alderliesten for analysing the damage growth in FMLs subjected to pure far-field loading. Firstly the test procedure and test results are briefly summarized in Section 6.2, and then the model development is detailed in Section 6.3. The analytical model will be validated against the test data in Section 6.4.

6.2. REMARKS REGARDING TEST RESULTS

The principle of superposition is normally applied to calculate the stress intensity factor for a crack in a metallic panel subjected to tension-pin loading by splitting the loading case into simpler loading cases and summing the stress intensity factors for simpler split loading cases together [30]. The crack growth mechanism in FMLs, however, differs from that of monolithic metallic panels because of the fibre bridging. The bridging mechanism is accounted for using the principle of superposition in the Alderliesten model. The total stress intensity factor at the crack tip in an FML is a superposition of the far-field stress intensity factor and the bridging stress intensity factor [10, 11]. The calculation of the stress intensity factor, K_{joint}, at the crack tip in an FML subjected to tension-pin loading therefore have more complications.

An experimental investigation into the effects of pin loading on the fatigue crack

growth behaviour in FMLs has been carried out by the current authors [29]. These experiments were conducted to achieve two objectives. The first objective was to observe the fatigue damage mechanism in FMLs subjected to tension-pin loading. The second objective was to verify that the principle of superposition can be used to calculate the stress intensity factor, K_{joint}, at a crack tip in an FML plate subjected to tension-pin loading. This calculation can be conducted by decomposing the complex tension-pin loading acting on a cracked FML into simpler loading states for which total stress intensity factors can be determined, superposing the calculated total stress intensity factors. The calculation of the total stress intensity factor at a crack tip in an FML plate subjected to a simpler loading case follows the same basic approach as the Alderliesten model [10, 11].

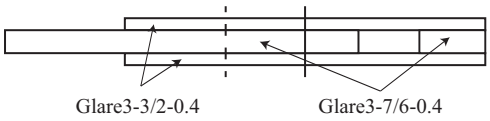

(a) Lateral view of the joint

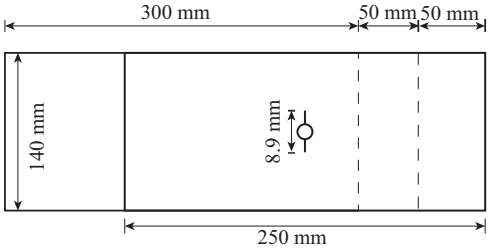

(b) Type 1 joint with one pin

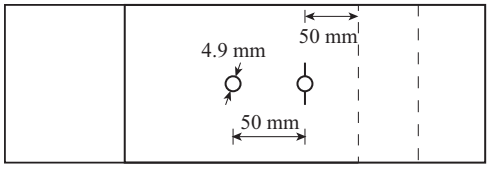

(c) Type 2 joint with two pins

Figure 6.2: Symmetric FML joint configurations

The joint configuration chosen for this study is a symmetric double shear joint illustrated in Fig. 6.2. This configuration avoids secondary bending effects in the joint that were not taken into account in the present model development. The test configuration thus permits a more accurate validation of the performance of the model.

The basic joint configuration tested comprised of outer plates of Glare3-3/2-0.4 and an inner plate of Glare3-7/6-0.4 (Fig. 6.2(a)). Two variations of this configuration were adopted: a type with one pin (Fig. 6.2(b)), and another type with two pins (Fig. 6.2(c)).

In the joint with one pin illustrated in Fig. 6.2(b), the load transfers from the middle plate to the specimens through the only pin. The crack in the specimen therefore subjects to pin loading and far-field loading. In addition to the loading cases for the cracked

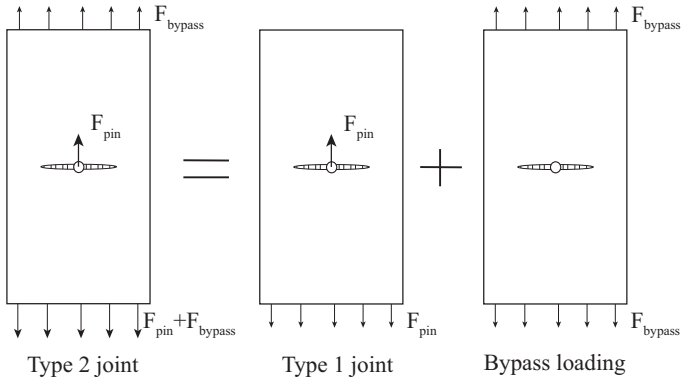

Figure 6.3: Relation of the loading cases for the two types of joints

specimen in this type of joint, the additional pin in another joint shown in Fig. 6.2(c) introduces bypass loading to the crack. A small degree of plastic deformation at the fastener holes of both pins was found following fatigue testing. This deformation was due to the high pin bearing load in Type 2 joint. The plastic deformation and fatigue crack growth from the additional pin hole in the specimens in Type 2 joint indicate an approximately equal load transfer by the two pins [29, 31].

A comparison of the loading cases for the cracks of interest in each of the specimens in the two types of joints is given in Fig. 6.3. The maximum bypass loading F_{bypass} and pin loading F_{pin} are equal to 5 kN with an applied stress ratio of 0.05 and a frequency of 10 Hz. A detailed description of the test is given in [29].

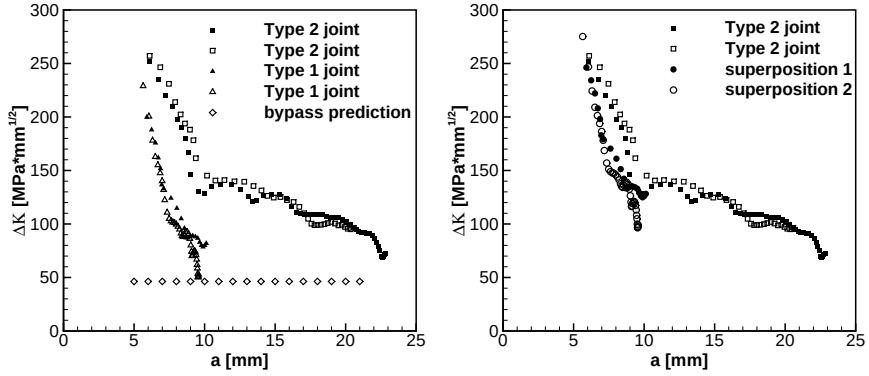

(a) calculated stress intensity factor ranges for each loading case

(b) comparison between superposed results and results for Type 2 joint

Figure 6.4: Illustration of superposition

The stress intensity factor ranges for the loading cases illustrated in Fig. 6.3 have been calculated based on the measured crack growth rates of the cracks in the two joint types.

The calculation was accomplished using the empirical Paris relation for the metal sheet used and the stress intensity factor ranges have been plotted versus crack length, a, in Fig. 6.4(a). For the given bypass load, the stress intensity factor ranges for only a small crack increment were calculated with the Alderliesten model [10, 11]. The stable crack growth behaviour of FMLs was then exploited to extrapolate the data for a larger crack length range.

The superposition data in Fig. 6.4(b) is obtained by superposing the stress intensity factor range for the loading case of the specimen in Type 1 joint upon the stress intensity factor range for the bypass loading. Good correlation between the superposed results and results for Type 2 joint in Fig. 6.4(b) can be observed. Therefore, the superposition relation of the stress intensity factor ranges for the loading cases illustrated in Fig. 6.3 is also valid, which is expressed by the following equation:

$$\Delta K_{pin+bypass} = \Delta K_{pin} + \Delta K_{bypass} \tag{6.1}$$

Since the stress ratios for all the tested configurations are the same and the maximum stress intensity factor and the stress intensity factor range have a linear relation, Eq. 6.1 can be reformulated, in terms of maximum stress intensity factors, as follows:

$$K_{pin+bypass} = K_{pin} + K_{bypass} \tag{6.2}$$

The test data verifies that the total stress intensity factors for each of the simpler loading cases acting on a cracked FML can be superposed to get the stress intensity factor of the crack in the FML subjected to a complexly compound loading system comprising the simpler loading cases. Then the key to the problem is how to derive the total stress intensity factor for each simpler loading case acting on a cracked FML, i.e., calculation of K_{pin} and K_{bypass} in Eq. 6.2.

6.3. MODEL DEVELOPMENT

6.3.1. STATE OF THE ART IN FML CRACK GROWTH PREDICTION

Fatigue crack growth of the metal layers in an FML is accompanied by delamination propagation at the metal/composite interfaces. The fibres in the wake of fatigue cracks within the metal layers remain intact and bridge the crack opening. This bridging mechanism reduces the stress transferred at the crack tip, which could improve crack growth resistance in the metal layers. Meanwhile, the bridging mechanism introduces cyclic shear stresses at the metal/composites interfaces, which could result in delamination growth [10, 11].

Alderliesten has developed an analytical model to predict the coupled crack growth and delamination propagation in FMLs under far-field applied fatigue loading [10, 11]. Both the crack growth and delamination growth are characterized using classical LEFM approaches. A summary of the methodology of his model is provided in this work. The reader is referred to [10, 11] for a more detailed review.

In the context of LEFM, the stress state at the crack tip in the metal layers is characterized by stress intensity factors. The total stress intensity factor, K_{total}, at the crack tip in the metal layers in FMLs for a given load can be decomposed into two terms using

superposition:

$$K_{total} = K_{ff} + K_{br} \tag{6.3}$$

where K_{ff} is due to the stresses in the metal layers resulting from the far-field applied load and K_{br} is due to the bridging mechanism.

The strain energy release rate, G, is employed to characterize the complex stress state at a metal/composites interface, which is given as:

$$G = \frac{n_f t_f}{2jE_f}\left(\frac{n_m t_m E_m}{n_m t_m E_m + n_f t_f E_f}\right)(S_f + S_{br}(x))^2 \tag{6.4}$$

For the metallic material used, K_{total} and an empirical Paris relation can be employed to calculate the crack extension in the metal layers. Similarly, G and an empirical Paris relation for the resistance of the delamination growth can be employed to calculate the delamination propagation. However, the calculation of K_{br} and G can only be implemented once the bridging stress distribution, $S_{br}(x)$, is determined [10, 11].

Alderliesten calculates $S_{br}(x)$ by employing the displacement compatibility between the metal layers and fibre layers over the delaminated length, which is expressed in Eq. 6.5. The crack opening displacement in the metal layers which comprises a crack opening term $v_{ff}(x)$ due to applied load and a crack closing term $v_{br}(x)$ due to bridging mechanism should be equal to the elongation of the delaminated fibre layers $\delta_f(x)$ and deformation due to shear $\delta_{pp}(x)$.

$$v_{ff}(x) - v_{br}(x) = \delta_f(x) + \delta_{pp}(x) \tag{6.5}$$

Each term in Eq. 6.5 varies along the delamination front. Alderliesten divides the delamination shape into bar elements. At x of each bar element location, Eq. 6.5 needs to be implemented. A numerical matrix therefore has to be applied to simultaneously solve for the displacement compatibility at every discretized element along the delamination shape.

6.3.2. PREDICTION MODEL INCORPORATES PIN LOADING EFFECTS

The Alderliesten model has already provided the solution for calculating K_{bypass} since the bypass loading can be treated as far-field load. Based on the experimental findings, it can be argued that the overall stress intensity factor K_{pin} for a crack in an FML subjected to both pin loading and far-field loading, a non-symmetric loading case, can be estimated by decomposing the loading cases, calculating the total stress intensity factor for each loading case, and summing the total stress intensity factor of each loading case as illustrated in Fig. 6.5.

Therefore the estimation of K_{pin} can be expressed by the following:

$$K_{pin} = 0.5(K_{pin,bearing} + K_{pin,ff}) \tag{6.6}$$

Again $K_{pin,ff}$ can be calculated with the Alderliesten model. At this point, there is only one unknown variable $K_{pin,bearing}$. It is noteworthy that the calculation of $K_{pin,bearing}$ should also involve calculating the stress intensity factor resulting from the bridging

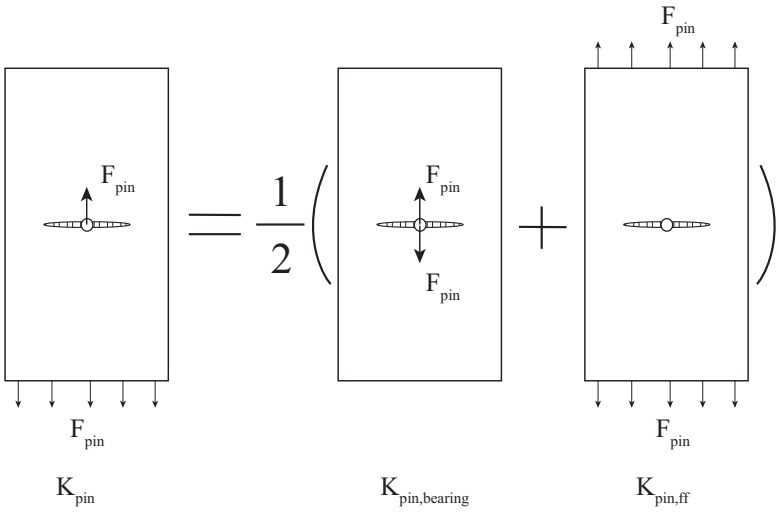

Figure 6.5: Estimation of total stress intensity factor for asymmetric pin loading case in FMLs

mechanism. In view of the computational cost when individually implementing displacement compatibility for each simpler loading case of a given crack and delamination configuration, a succinct approach incorporating the analysis of pin loading effects needs to be developed for FMLs.

Analogous to the approach adopted by Alderliesten, the overall stress intensity factor K_{joint} for a cracked FML subjected a tension-pin loading system as illustrated on the left in Fig. 6.3 can be decomposed into two terms using the principle of superposition. As expressed in Eq. 6.7, K_{app} refers to the stress intensity factor due to the applied loads such as the far-field applied load, pin bearing load and the bypass load. K_{br} refers to the stress intensity factor due to the bridging mechanism. When calculating the bridging stress distribution by implementing displacement compatibility, the crack opening displacement should be comprise of all of the opening terms resulting from the applied loads.

$$K_{joint} = K_{app} + K_{br} \tag{6.7}$$

The superposition relation for the complex loading cases illustrated in Fig. 6.3 and Fig. 6.5 can be still used. K_{app} can also be decomposed into terms due to the corresponding simpler loading cases, as expressed in Eq. 6.8. $K^*_{pin,bearing}$ denotes the stress intensity factor in the metal layers resulting from a pair of pin loads, F_{pin}, acting on the crack flanks and $K^*_{pin,ff}$ denotes the stress intensity factor in the metal layers due to the far-field load, F_{pin}, see Fig. 6.5. K^*_{bypass} refers to the stress intensity factor due to far-field bypass loading which is illustrated in Fig. 6.3. The calculation of $K^*_{pin,ff}$ and K^*_{bypass} can be carried out according to the approach adopted by Alderliesten [10, 11].

$$K_{app} = 0.5 \cdot K^*_{pin,bearing} + 0.5 \cdot K^*_{pin,ff} + K^*_{bypass} \tag{6.8}$$

6.3.3. $K^*_{pin,bearing}$ DUE TO PIN LOADING

The load applied by a fastener to the jointed panels occurs through a pin bearing scenario. Since the metal layers in FMLs are thicker and stiffer than fibre layers, it is assumed for this work that the metal layers bear all of the load applied by the fastener and that the cut fibres along the fastener hole do not carry any load. The intact fibres in the wake of the fatigue cracks in the metal layers restrict the crack opening induced by the pin loading.

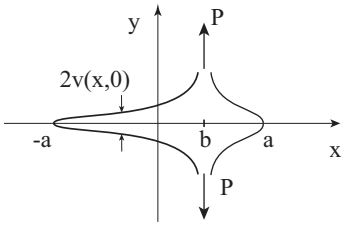

Figure 6.6: A pair of point loads acting on crack flanks

The pin loads applied by the fastener to the hole edges in the metal layers are regarded as point loads in this paper [32]. Fig. 6.6 illustrates a pair of point loads acting on the edges of a crack in a metal panel with P as a point load per unit thickness. For a given pin load in the laminate, F_{pin}, the value of the point load for a metal layer can be calculated with the following equation:

$$P = \frac{F_{pin}}{n_m t_m} \tag{6.9}$$

where n_m is the number of metal layers and t_m is the thickness of each metal layer.

The stress intensity factors for the two crack tips subjected to the loading case illustrated in Fig. 6.6 can be written as [32]:

$$K_a = \frac{P}{\sqrt{\pi a}} \frac{\sqrt{a^2 - b^2}}{a - b} \tag{6.10}$$

$$K_{-a} = \frac{P}{\sqrt{\pi a}} \frac{\sqrt{a^2 - b^2}}{a + b} \tag{6.11}$$

and the corresponding crack opening is given as:

$$2 \cdot v(x,0) = \frac{4P}{\pi E} cosh^{-1} \frac{a^2 - bx}{a|x - b|} \tag{6.12}$$

For the case in which the point loads act at the centre of the crack, Eq. 6.10, Eq. 6.11 and Eq. 6.12 can be rewritten concisely with $b = 0$. The stress intensity factors for the two crack tips are equal and the crack opening contour is symmetric with respect to the centre of the crack.

Then $K^*_{pin,bearing}$ due to a pair of bearing loads can be calculated by substituting Eq. 6.9 and $b = 0$ into either Eq. 6.10 or Eq. 6.11:

$$K^*_{pin,bearing} = \frac{F_{pin}}{n_m t_m \sqrt{\pi a}} \tag{6.13}$$

and the corresponding crack opening displacement is given as:

$$2 \cdot v_{pin,bearing}(x) = \frac{4P}{\pi E} cosh^{-1} \frac{a}{x} \tag{6.14}$$

6.3.4. IMPLEMENTATION OF DISPLACEMENT COMPATIBILITY

In view of the computational cost when individually implementing displacement compatibility for each loading case, the total crack opening displacement resulting from different loading cases can be calculated and the displacement compatibility between cracked metal layers and bridging fibres over delaminated length can only be implemented once.

The displacement compatibility is expressed by Eq. 6.15. The sum of $0.5 v_{pin,bearing}(x)$ and $0.5 v_{pin,ff}(x)$ is an equivalent crack opening as a result of the asymmetric loading illustrated in Fig. 6.5 in the metal layers. $v_{bypass}(x)$ denotes the crack opening due to bypass loading. The crack opening in the metal layers as a result of the applied loads and crack closing, v_{br}, due to the bridging stress distribution in the bridging fibres must equal the elongation of the fibre layers over the delaminated length, $\delta_f(x)$, plus the deformation in the fibre layers due to shear at the delamination front $\delta_{pp}(x)$.

$$0.5 v_{pin,bearing}(x) + 0.5 v_{pin,ff}(x) + v_{bypass}(x) - v_{br}(x) = \delta_f(x) + \delta_{pp}(x) \tag{6.15}$$

$v_{pin,ff}(x)$ and $v_{bypass}(x)$ can be derived by treating the loads as far-field loads. The stresses in the metal layers resulting from these far-field loads can be calculated using Classic Laminate Theory [33, 34]. For the detailed calculation of these variables in Eq. 6.15, please refer to the work of Alderliesten [10, 11].

Solving for the displacement compatibility expressed in Eq. 6.15 simultaneously for all of the bar elements provides the bridging stress distribution, $S_{br}(x)$. Once this bridging stress distribution is known, K_{br} and the strain energy release rate G along the delamination front can be calculated [10, 11].

6.3.5. CRACK GROWTH MODEL AND DELAMINATION GROWTH MODEL

Once the overall stress intensity factor at the crack tip for a crack subjected to pin loading and far-field loading is estimated, the crack growth rate can be calculated using an empirical Paris relation for the metallic material employed in an FML.

$$da/dN = C_{cg}(\Delta K_{eff})^{n_{cg}} \tag{6.16}$$

where C_{cg} and n_{cg} are Paris constants. For the tested FML Glare, $C_{cg} = 2.17 * 10^{-12}$ and $n_{cg} = 2.94$.

Knowing the bridging stress distribution $S_{br}(x)$ along the delamination shape, the strain energy release rate at the composite/metal interface can be calculated with Eq. 6.4.

And the delamination growth rate at each discretized element can be similarly calculated using a Paris relation:

$$db/dN = C_d(\sqrt{G_{max}} - \sqrt{G_{min}})^{n_d} \tag{6.17}$$

where C_d and n_d are Paris constants. For Glare, $C_d = 0.05$ and $n_d = 7.5$.

6.4. VALIDATION AND DISCUSSION

This model is validated through comparing the predicted crack growth results with the measurements of the two tested joint types. The crack growth rates are plotted against the crack length in Fig. 6.7 for both loading cases. It can be observed that the prediction results correlate with the measurements very well.

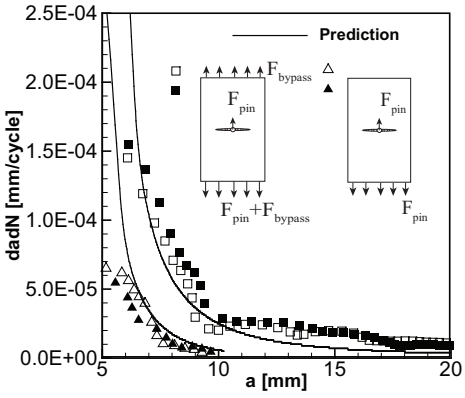

Figure 6.7: Crack growth rates comparison for two loading cases

As can be seen in Fig.6.7, the crack growth rates of both loading cases decrease dramatically with increasing crack length in the vicinity of the fastener hole. This is because the driving force induced by pin loading decreases exponentially as the crack length increases (Eq. 6.13). Without bypass loading, the crack growth driven by pin loading stops around 10 mm. For another loading case, the crack growth becomes very stable when the crack tip is away from the fastener hole, which is consistent with the stable crack growth results of FMLs under uniform far-field loading [10, 11].

The delamination shape of the specimen in Type 1 joint is obtained by etching the outer aluminium layers away following fatigue testing and is shown in Fig. 6.8(a). Minimal delamination is noted at the hole perimeter due to the small scale plastic deformation of the metal layers resulting from the high bearing load. As shown in Fig. 6.8(a), the delamination shape inclines to the direction of pin loading and so does the crack path. This non-symmetry, compared to a Mode I cracking scenario in an FML under uniform far-field loading, is neglected in this paper. The crack length, a, and the delamination length, b, are measured as depicted in Fig. 6.8(a).

In order to get a closed analytical solution in the prediction model, the non-symmetric loading of a pin load and its corresponding far-field load is treated as half of the superposition of two symmetric loading cases, which is illustrated in Fig. 6.5. Therefore the

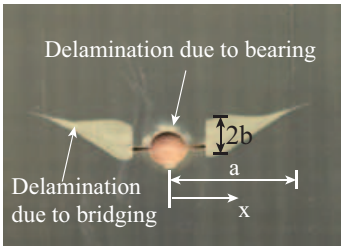

(a) Delamination shape after etching

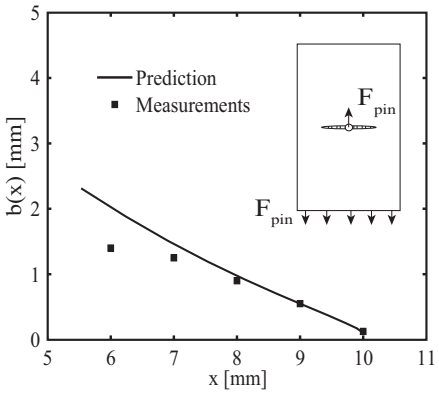

(b) Predicted delamination shape

Figure 6.8: Delamination comparison for the specimen in Type 1 joint

prediction model analyses a Mode I crack growth with symmetric delamination shapes with respect to the crack path. The predicted delamination length is plotted against the measured delamination length along the crack flank in Fig. 6.8(b). The overall prediction correlates very well with the measurements with the exception of the delamination length in the vicinity of the pin hole which was over-predicted. Based on Eq. 6.15 for displacement compatibility, the delaminated length of the bridging fibres is of significance. Consequently, the analytical model in this paper predicts a symmetric delamination shape which is equivalent to the measured delamination shape in terms of the bridging mechanism.

6.5. CONCLUSION

An analytical model incorporating the analysis of the effects that pin loading has on the fatigue crack growth behaviour in FMLs has been presented and validated in this paper. It has been demonstrated that the total stress intensity factor in the metal layers of an FML due to external applied loading cases can be calculated by summing the stress intensity factors for each of the simpler loading cases together. Furthermore, the total crack opening displacement due to external loading cases can be derived in the same manner. The displacement compatibility between the crack opening and the deforma-

tion of the delaminated fibre layer can then be used to calculate the load transferred between the cracked metal layers and the intact bridging fibres and thus the stress intensity factor induced by bridging mechanism.

Despite the fact that the pin loading in the FML joints results in a non-symmetric loading scenario for the crack, the model using the superposition of the two symmetric loading cases successfully estimates the driving force for the crack. The model captures the rapid crack growth in the vicinity of the fastener hole. The pin loading effects on the crack growth behaviour diminish as the crack tip grows away from the location of pin loading, which is also successfully predicted by the analytical model.

The non-symmetric loading scenario slightly deviates the crack growth from the transverse direction perpendicular to the far-field loading direction. Non-symmetric delamination shapes with respect to the crack flank also develop. These effects are neglected in the prediction model. However, the model still provides a reasonable prediction of an equivalent delamination shape in terms of the bridging mechanism.

REFERENCES

[1] W. Wang, C. Rans, Z. Zhang, and R. Benedictus, *Prediction methodology for fatigue crack growth behaviour in fibre metal laminates subjected to tension and pin loading,* Under review at the Composite Structures .

[2] R. Toi, *An empirical crack growth model for fiber/metal laminates,* in *Proceedings of the 18th symposium of the international committee on aeronautical fatigue* (Melbourne,Australia, 1995) pp. 899–909.

[3] T. Takamatsu, T. Matsumura, N. Ogura, T. Shimokawa, and Y. Kakuta, *Fatigue crack growth properties of a glare3-5/4 fiber/metal laminate,* Engineering Fracture Mechanics **63**, 253 (1999).

[4] T. Takamatsu, T. Matsumura, N. Ogura, T. Shimokawa, and Y. Kakuta, *Fatigue crack growth of a glare3-5/4 fiber/metal laminate and validity of methods for analysing results,* in *20th symposium international committee on aeronautical fatigue* (Bellevue Washington, USA, 1999).

[5] T. Takamatsu, T. Shimokawa, T. Matsumura, Y. Miyoshi, and Y. Tanabe, *Evaluation of fatigue crack growth behavior of glare3 fiber/metal laminates using a compliance method,* Engineering Fracture Mechanics **70**, 2603 (2003).

[6] B. Cox, *Life prediction for bridged fatigue cracks,* in *Life prediction methodology for titanium matrix composites*, ASTM STP 1253, edited by L. J. Johnson, W.S. and B. Cox (ASTM, 1996) pp. 552–572.

[7] Y.-J. Guo and X.-R. Wu, *A phenomenological model for predicting crack growth in fiber-reinforced metal laminates under constant-amplitude loading,* Composites Science and Technology **59**, 1825 (1999).

[8] R. C. Alderliesten, *Development of an empirical fatigue crack growth prediction model for the fibre metal laminate glare*, Master thesis, Delft University of Technology, Delft, the Netherlands (1999).

[9] R. Marissen, *Fatigue crack growth in ARALL. A hybrid aluminium-aramid composite material: Crack growth mechanisms and quantitative predictions of the crack growth rates*, Ph.D. thesis, Delft University of Technology, Delft, the Netherlands (1988).

[10] R. C. Alderliesten, *Fatigue crack propagation and delamination growth in GLARE*, Ph.D. thesis, Delft University of Technology, Delft, the Netherlands (2005).

[11] R. C. Alderliesten, *Analytical prediction model for fatigue crack propagation and delamination growth in glare,* International Journal of Fatigue **29**, 628 (2007).

[12] R. Rodi, *The Residual Strength Failure Sequence in Fibre Metal Laminates*, Ph.D. thesis, Delft University of Technology, Delft, the Netherlands (2012).

[13] S. U. Khan, R. C. Alderliesten, C. D. Rans, and R. Benedictus, *Application of a modified wheeler model to predict fatigue crack growth in fibre metal laminates under variable amplitude loading,* Engineering Fracture Mechanics **77**, 1400 (2010).

[14] S. U. Khan, R. C. Alderliesten, and R. Benedictus, *Delamination in fiber metal laminates (glare) during fatigue crack growth under variable amplitude loading,* International Journal of Fatigue **33**, 1292 (2011).

[15] S. Khan, *Fatigue Crack and Delamination Growth in Fibre Metal Laminates under Variable Amplitude Loading*, Ph.D. thesis, Delft University of Technology, Delft, the Netherlands (2013).

[16] G. Wilson, *Fatigue Crack Growth Prediction for generalized fiber metal laminates and hybrid materials*, Ph.D. thesis, Delft University of Technology, Delft, the Netherlands (2013).

[17] G. S. Wilson, R. C. Alderliesten, and R. Benedictus, *A generalized solution to the crack bridging problem of fiber metal laminates,* Engineering Fracture Mechanics **105**, 65 (2013).

[18] W. Wang, C. Rans, R. C. Alderliesten, and R. Benedictus, *Predicting the influence of discretely notched layers on fatigue crack growth in fibre metal laminates,* Engineering Fracture Mechanics **145**, 1 (2015).

[19] W. Wang, C. Rans, R. Alderliesten, and R. Benedictus, *Philosophy of multiple-site damage analysis for fibre metal laminate structures,* in *Proceedings of 28th Symposium of the International Committee on Aeronautical Fatigue ICAF 2015, Helsinki, Finland* (2015).

[20] J. Schijve, *Some elementary calculations on secondary bending in simple lap joints,* (1977).

[21] J. J. M. De Rijck, *Stress analysis of fatigue cracks in mechanically fastened joints: an analytical and experimental investigation*, Ph.D. thesis, Delft University of Technology, Delft, the Netherlands (2005).

[22] R. M. Frizzell, C. T. McCarthy, and M. A. McCarthy, *An experimental investigation into the progression of damage in pin-loaded fibre metal laminates,* Composites Part B: Engineering **39**, 907 (2008).

[23] R. M. Frizzell, C. T. McCarthy, and M. A. McCarthy, *A comparative study of the pin-bearing responses of two glass-based fibre metal laminates,* Composites Science and Technology **68**, 3314 (2008).

[24] G. Caprino, A. Squillace, G. Giorleo, L. Nele, and L. Rossi, *Pin and bolt bearing strength of fibreglass/aluminium laminates,* Composites Part A: Applied Science and Manufacturing **36**, 1307 (2005).

[25] P.-C. Yeh, P.-Y. Chang, J. Wang, J.-M. Yang, P. H. Wu, and M. C. Liu, *Bearing strength of commingled boron/glass fiber reinforced aluminum laminates,* Composite Structures **94**, 3160 (2012).

[26] R. Van Rooijen, J. Sinke, T. De Vries, and S. Van Der Zwaag, *The bearing strength of fiber metal laminates,* Journal of Composite Materials **40**, 5 (2006).

[27] R. Eastin, *'wfd'-what is it and what's 'lov' got to do with it?* International Journal of Fatigue **31**, 1012 (2009).

[28] *Federal register/vol. 77, no. 101, thursday may 24, 2012/ rules and regulations,* .

[29] Z. Zhang, W. Wang, C. Rans, and R. Benedictus, *An experimental investigation into pin loading effects on fatigue crack growth in fibre metal laminates,* Procedia Structural Integrity **2**, 3361 (2016).

[30] J. Schijve, *Fatigue of structures and materials* (Springer, Dordrecht, The Netherlands, 2008).

[31] R. Müller, *An experimental and analytical investigation on the fatigue behaviour of fuselage riveted lap joints : the significance of the rivet squeeze force, and a comparison of 2024-T3 and glare 3*, Ph.D. thesis, Delft University of Technology, Delft, the Netherlands (1995).

[32] H. Tada, P. C. Paris, and G. R. Irwin, *The stress analysis of cracks handbook* (ASME, New York, 2000).

[33] J. J. Homan, *Fatigue initiation in fibre metal laminates,* International Journal of Fatigue **28**, 366 (2006).

[34] S. Spronk, I. Şen, and R. Alderliesten, *Predicting fatigue crack initiation in fibre metal laminates based on metal fatigue test data,* International Journal of Fatigue **70**, 428 (2015).

7

ANALYSIS OF MSD CRACK GROWTH IN MECHANICALLY FASTENED FIBRE METAL LAMINATE JOINTS

In the previous two chapters, models for MSD crack growth in FMLs under far-field tension and crack growth in FMLs subjected to tension and pin loading were developed and validated. Within this chapter, the relevance and applicability of theses models for predicting the MSD behaviour in mechanically fastened FML joints is examined. The crack growth in FML joints is affected by many stress components that are present due to the complexity of load transfer from one jointed FML panel to another via fastened joints. This chapter therefore starts with an introduction of the stress components in mechanically fastened joints and their complications in developing an analytical model for predicting the MSD crack growth behaviour in such joints. The development of the prediction model is presented in Section 7.2 and respective model validations for a joint without secondary bending and a joint with secondary bending are given in Section 7.3 and Section 7.4.

7.1. BACKGROUND: STRESSES IN A MECHANICALLY FASTENED FML JOINT AND THEIR INFLUENCES ON CRACK GROWTH BEHAVIOUR

In order to evaluate the fatigue crack growth behaviour in a mechanically fastened FML joint, the stress distribution in the joint and the interplay between the stress distribution and crack growth have to be understood. To aid in the explanation of the interplay, the nomenclature for a typical mechanically fastened joint containing three rows of fasteners is shown in Fig. 7.1. The three-row joint configuration is chosen since this configuration is widely applied in aircraft structures due to the trade-off between structural efficiency and structural weight. The first fastener row and third fastener row are also denoted as the outer fastener rows.

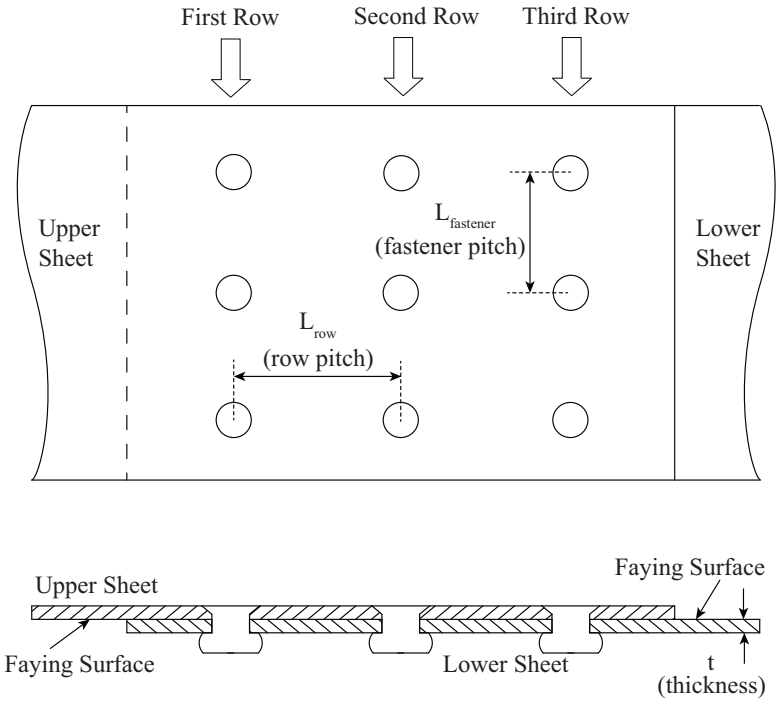

Figure 7.1: Nomenclature for a three-row lap joint

As illustrated in Fig. 7.2, the stress distribution in a joint can be decomposed into stress components related to bearing, friction and bypass loading components resulting from load transfer. In addition, the stress distribution can comprise secondary bending stresses in mechanically fastened joints where eccentricities in load path exist, and local compressive residual stresses around the periphery of each fastener hole to which an interference fit fastener or cold expansion processes are applied [1]. The impact of stress components resulting from load transfer on the crack growth behaviour in mechanically fastened FML joints containing MSD scenario will be the focuses of this chapter. The

impact of secondary bending stresses and favourable residual compressive stresses will be qualitatively analysed.

7.1.1. LOAD TRANSFER

Load is transferred in a mechanically fastened joint by means of bearing between fasteners and jointed substances and friction between the jointed plates. A significant portion of overall load is transferred by bearing. Friction only accounts for a small portion and is therefore often neglected; however, friction results in fretting damage which is a contributor to the crack nucleation starting from the faying surface. For a multiple-row joint, each row of fasteners transfers a portion of the applied load while the remainder known as the bypass load remains in the loaded plate. Based on the displacement compatibility between jointed plates and fasteners, closed form solutions have been derived to calculate the load transferred by each fastener row.

In a mechanically fastened joint containing two fastener rows, each fastener row transfers 50 percent of the applied load as a result of the symmetry of the joint. For a joint containing three rows of fasteners, as illustrated in Fig. 7.1, the load transferred by each row of fasteners can be calculated, neglecting the load transfer by means of friction, with the following equations [2]:

$$T1 = \frac{f_{fastener} + f_{plate}}{3 \cdot f_{fastener} + 2 \cdot f_{plate}} \cdot F_{app} \tag{7.1}$$

$$T2 = \frac{f_{fastener}}{3 \cdot f_{fastener} + 2 \cdot f_{plate}} \cdot F_{app} \tag{7.2}$$

$$T3 = T1 \tag{7.3}$$

where F_{app} refers to the applied load. $T1$, $T2$ and $T3$ denote the loads transferred by the first row, second row and third row respectively. $f_{fastener}$ and f_{plate} refer to the fastener flexibility and the plate flexibility respectively. As expressed in Eq. 7.4, plate flexibility is related to the joint geometry (row pitch L_{row}, fastener pitch $L_{fastener}$ and plate thickness t) and plate stiffness (Young's modulus E). Laminate-level material properties of FMLs have to be substituted into the equation to calculate the plate flexibility [3]. Whereas fastener flexibility is normally empirically determined, several empirical equations have been reported [4–6].

$$f_{plate} = \frac{L_{row}}{L_{fastener} \cdot t \cdot E} \tag{7.4}$$

Eqs. 7.1-7.3 indicate that the outer rows alway transfer more load than the middle row as negative f_{plate} is not possible. It is obvious that the first fastener row in the upper sheet and the third fastener row in the lower sheet (Fig. 7.1) are the critical rows where the fastener holes subject to the highest bypass load and the highest bearing load among all fastener holes. In consequence, cracks tend to initiate at fastener hole edges in the critical fastener rows. Another significant contributor to the crack initiation in the critical fastener rows is the secondary bending stresses, which will be explained in the next subsection.

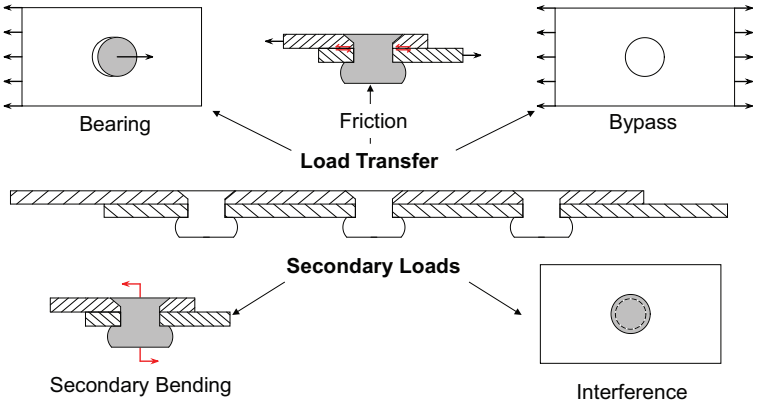

Figure 7.2: Loading components in a mechanically fastened joint [1]

For the critical fastener row without any cracks, the bearing load is equal to T3, and the bypass load equals the total load transferred by other fastener rows, i.e., $T1+T2$. It is important to understand that crack growth in the joint can change the bypass load and bearing load for the critical fastener row. The cracks initiating from fastener holes permit fasteners to have more freedom of rotation, indicating a higher fastener flexibility at the cracked fastener hole. Moreover, the crack growth in the critical row results in the jointed plate becoming less stiff, indicating a higher plate flexibility.

Analytically estimating the sophisticated changes in the fastener flexibility and plate flexibility as a result of the crack growth in the critical row is extremely challenging and can be an extensive research topic on it own. Finite element modelling or experimental measuring techniques can be implemented to evaluate the load transfer in a mechanically fastened joint containing MSD cracks in the critical row of fasteners.

7.1.2. SECONDARY BENDING

Eccentricities in the load path of a mechanically fastened joint can lead to out-of-plane displacements and bending stresses known as secondary bending. The bending stresses caused by load path eccentricities inherent to mechanically fastened joints can be estimated using the neutral line model [7, 8]. For the typical three-row joint configuration illustrated in Fig. 7.1, the outer fastener rows encounter the highest secondary bending stresses.

Secondary bending stresses vary through the thickness of the jointed plate. Superposed upon the tensile stress resulting from the load transfer in the critical row, the bending stress leads to the faying surface experiencing the highest tensile stress. As a consequence the faying surface in the critical row is susceptible to fatigue crack nucleation and crack growth. For FMLs, the stiffness variation trough the laminate thickness has to be considered when calculating the bending stresses in FML joints [3]. An example of stress distribution through the laminate thickness in the critical row of a three-row riveted Glare3-3/2-0.3 lap joint is given in Fig. 7.3.

Secondary bending stresses could induce complex crack configuration in FML joints.

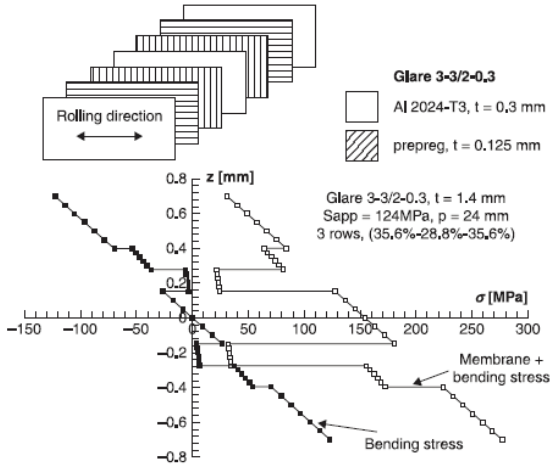

Figure 7.3: Illustration of the stress distribution through thickness predicted by the neutral line model for a critical rivet row of a three-row riveted Glare joint [3]

The cracks in the metal layers originating from the same fastener hole could possess different crack lengths through the laminate thickness and different delamination shapes at the metal/composite interfaces as a consequence of the stress variation through the laminate thickness [9], as illustrated in Fig. 7.3.

This effect of bending stresses poses two complications in calculating the crack growth behaviour of multiple cracks in the same fastener row. The first one is that the variation in crack lengths through the laminate thickness requires local discretization of the crack configurations in the metal sheets originating from the same fastener hole. The uncracked metal sheets in the wake of cracks in other metal sheets act as bridging materials and the local load path eccentricity induces local bending stresses [9]. Special care needs to be taken to account for these effects [9]. Another complication is induced from the calculation of crack interaction in terms of the load redistribution mechanism explained in detail in Chapter 5. The presence of other cracks reduces the local geometric stiffness, resulting in load redistribution from the cracks to a single crack for a given loading case when analysing the state of the single crack. The strain distribution derived from the Westergaard stress distribution is assumed the same through the laminate thickness in front of the crack tip of the single crack in order to evaluate the load redistribution [10]. At the location of a crack of the same length in the metal layers, the isostrain condition is applied to calculate the stress reduction, thus the load reduction, caused by the cracked metal layers. However, the complex crack configuration induced by the secondary bending stresses requires great modification of the method to evaluate the load redistribution and the effects on a single crack with different crack lengths in the metal layers.

It is important to make a distinction between the load redistribution among multiple cracks and the load redistribution over multiple fastener rows. The later is due to the

changes in the plate flexibility and fastener flexibility caused by the multiple cracks. For a given load transfer over multiple fastener rows, the load redistribution from other cracks to a single crack needs to be evaluated in order to calculate the state of the single crack.

7.2. MODEL IMPLEMENTATION

From the previous section, it can be concluded that developing an analytical model to consider the influences of the load redistribution over multiple rows and secondary bending on MSD crack growth in an FML joint is burdensome and impractical. Therefore a simplified model based on the prediction models in Chapter 5 and Chapter 6 is proposed with some assumptions and simplifications.

7.2.1. ASSUMPTIONS AND SIMPLIFICATIONS

Due to the complexity in calculating the load redistribution over multiple rows in a mechanically fastened joint containing MSD cracks, the load redistribution is simplified not to be simultaneously considered when calculating the crack states in the critical fastener row in this proposed model. In other words, the changes in $f_{fastener}$ and f_{plate} due to the crack growth are not taken into account. The load transfer over multiple rows can be calculated using Eqs. 7.1-7.3. The calculated load transfer in each row can then be used to obtain the bypass load and bearing load for the critical fastener row, which are the input loading parameters for calculating the crack growth behaviour in the critical fastener row.

As discussed in Section 7.1.2, the secondary bending effects can result in a complex fatigue crack configuration through the laminate thickness. Calculating the state of a complex fatigue crack configuration in an FML requires the implementation of the Wilson's model [9] at the cost of great computational inefficiency. In order to derive a computationally efficient model to evaluate the MSD crack growth behaviour in FML joints, the effects of secondary bending are neglected in this proposed model, but will be qualitatively analysed in Section 7.4.

In consequence of the assumptions and simplifications, cracks in the critical fastener row are subjected to the calculated pin bearing load and bypass load. The methodology in the previous chapter will be followed here: LEFM and the principle of superposition are applied to calculate the crack growth in the metal layers and the delamination growth at the interfaces between metal layers and composite layers. The method for a single symmetric crack in an FML under pin loading and far-field loading is summarized at first, then the method is extended for a non-symmetric crack, and for MSD cracks.

7.2.2. SINGLE SYMMETRIC CRACK

In the previous chapter, an analytical model has been developed for calculating the crack state of a single symmetric crack in an FML subjected to pin loading and far-field tension (see Fig. 7.4). The overall stress intensity factor, K_{joint}, at the crack tip in the metal layers is expressed by the following equation:

$$K_{joint} = K_{bypass} + 0.5K_{pin,ff} + 0.5K_{pin,bearing} \tag{7.5}$$

The superposition of the stress intensity factors is illustrated in Fig. 7.4. It is impor-

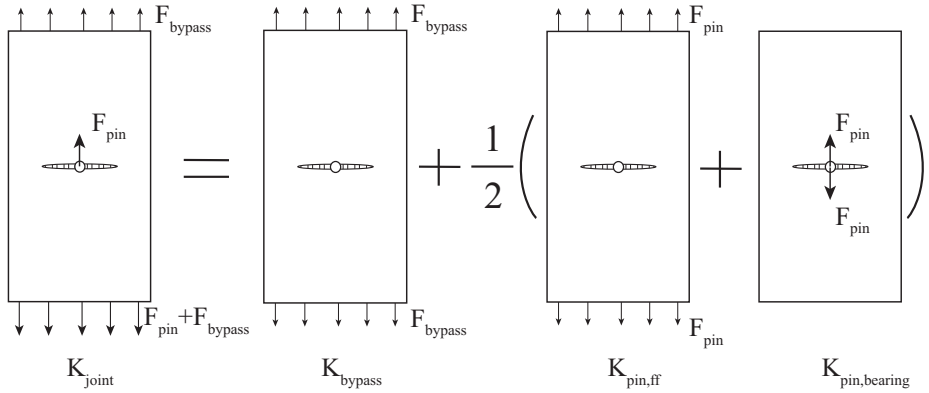

Figure 7.4: Superposition scheme of the overall stress intensity factor for a single symmetric crack in an FML

tant to understand that each of the stress intensity factors on the right side of Eq. 7.5 can be decomposed into two items. The first item is the stress intensity factor due to the stress in the metal layers resulting from one corresponding loading case. The second item is the stress intensity factor due to the fibre bridging mechanism. In order to avoid repetitively calculating the bridging mechanism and thus the stress intensity factors due to the bridging mechanism for each loading case, an alternative method has been proposed in the previous chapter: K_{joint} can be alternatively expressed as:

$$K_{joint} = K_{app} + K_{br} \tag{7.6}$$

where K_{app} denotes the sum of stress intensity factors due to the loading cases acting on the single crack, which is given by Eq. 7.7. The stress intensity factors on the right side of Eq. 7.7 are associated with the stresses in the metal layers resulting from the respective loading components illustrated in Fig. 7.4. The superscript * is added to make a distinction between these stress intensity factors and the total stress intensity factors in Eq. 7.5.

$$K_{app} = K^*_{bypass} + 0.5K^*_{pin,ff} + 0.5K^*_{pin,bearing} \tag{7.7}$$

The calculation of K_{br} is dependent on the total crack opening displacement of the crack due to the loading cases illustrated in Fig. 7.4. Similar to the decomposition of K_{app}, the total crack opening displacement, v_{app}, is also broken down into contributing factors related to the corresponding loading cases illustrated in Fig. 7.4.

$$v_{app}(x) = v^*_{bypass}(x) + 0.5v^*_{pin,ff}(x) + 0.5v^*_{pin,bearing}(x) \tag{7.8}$$

The displacement compatibility between the crack opening and the deformation of the bridging fibres can be applied to calculate the bridging stress distribution, $S_{br}(x)$, in the bridging fibres.

$$v_{app}(x) - v_{br}(x) = \delta_f(x) + \delta_{pp}(x) \tag{7.9}$$

Once the bridging stress distribution, $S_{br}(x)$, is determined, K_{br} and the strain energy release rate, G, can be calculated. The detailed calculation of the unknown variables in Eqs. 7.7-7.9 can be found in the previous chapter.

7.2.3. SINGLE NON-SYMMETRIC CRACK

For a non-symmetric crack in an FML subjected to pin loading and far-field tension, as illustrated in Fig. 7.5, the same approach in the previous subsection can be followed to calculate the crack state. Nevertheless, it is noted that the states of the two tips of the non-symmetric crack are not identical as a result of the crack tip non-symmetry, the delamination non-symmetry and the non-symmetric pin loading effects for the two crack tips (see Fig. 7.5).

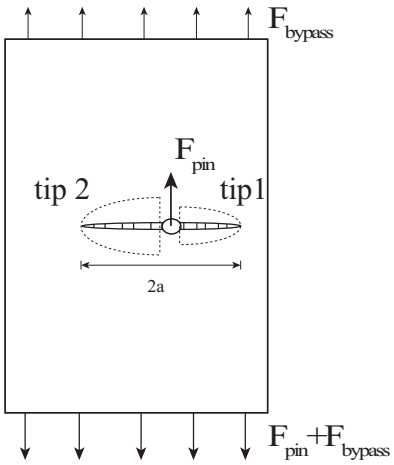

Figure 7.5: A non-symmetric crack in an FML subjected to pin loading and far-field tension

In Chapter 4, a detailed calculation of the stress intensity factors at two crack tips of a non-symmetric crack due to the stresses in the metal layers resulting from far-field tension, and the non-symmetric crack opening displacement, has been described. The calculation method can be adopted to determine $(K^*_{bypass} + 0.5K^*_{pin,ff})_1$ for crack tip 1, $(K^*_{bypass} + 0.5K^*_{pin,ff})_2$ for crack tip 2 and the crack opening displacements $v^*_{bypass}(x) + 0.5v^*_{pin,ff}(x)$.

The effects of pin loading on the two crack tips of the non-symmetric crack should be different since the crack tips are not symmetric with respect to the pin hole (see Fig. 7.5). Based on the work pertaining to the analysis of the pin loading effects on the crack state of a symmetric crack in an FML in the previous chapter, a pair of pin bearing loads acting on the crack flanks of a through thickness crack in an FML can be modelled as a pair of point loads and are assumed to be borne by the metal layers only. A generic illustration of a pair of point loads acting on the crack flanks of a crack is depicted in Fig. 7.6.

The stress intensity factors for the two crack tips illustrated in Fig. 7.6 can be ex-

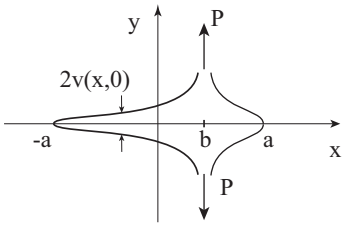

Figure 7.6: Illustration of a pair of point loads acting on crack flanks [11]

pressed with the following equation:

$$K_{P\pm a} = \frac{P}{\sqrt{\pi a}} \frac{\sqrt{a^2 - b^2}}{a \mp b} \tag{7.10}$$

The crack opening displacement of the crack is written as:

$$2v(x,0) = \frac{4P}{\pi E} cosh^{-1} \frac{a^2 - bx}{a|x-b|} \tag{7.11}$$

with E being the Young's modulus of the metallic panel.

For the non-symmetric crack illustrated in Fig. 7.5, the location of the pair of point loads, b, can be determined according to the geometric relation between the pin hole and the two crack tips. The point load, P, for each metal layer can be given by:

$$P = \frac{F_{pin}}{n_m t_m} \tag{7.12}$$

where n_m denotes the number of the metal layers and t_m denotes the thickness of each metal layer.

Then $(K^*_{pin,bearing})_1$ for crack tip 1 and $(K^*_{pin,bearing})_2$ for crack tip 2 can be obtained by substituting Eq. 7.12 into Eq. 7.10. $v^*_{pin,bearing}$ can also be derived by substituting Eq. 7.12 into Eq. 7.11. The generic algorithm for calculating the bridging stress distribution, $S_{br}(x)$, of a non-symmetric crack in Chapter 4 has to be applied. A non-symmetric bridging stress distribution can be derived. In consequence, two bridging stress intensity factors can be obtained: $(K_{br})_1$ for crack tip 1 and $(K_{br})_2$ for crack tip 2.

To summarize, the overall stress intensity factor, $(K_{joint})_1$, for crack tip 1 can be expressed as:

$$(K_{joint})_1 = (K_{app})_1 + (K_{br})_1 = (K^*_{bypass} + 0.5K^*_{pin,ff})_1 + 0.5(K^*_{pin,bearing})_1 + (K_{br})_1 \tag{7.13}$$

and the overall stress intensity factor, $(K_{joint})_2$, for crack tip 2 can be expressed as:

$$(K_{joint})_2 = (K_{app})_2 + (K_{br})_2 = (K^*_{bypass} + 0.5K^*_{pin,ff})_2 + 0.5(K^*_{pin,bearing})_2 + (K_{br})_2 \tag{7.14}$$

The subscripts $_1$ and $_2$ are employed to denote the associated variables in this subsection are related to crack tip 1 and crack tip 2 respectively. The non-symmetric crack configuration in this subsection is a more generic configuration in comparison with the symmetric crack configuration in the previous subsection.

7.2.4. MSD CRACKS

Fig. 7.7 illustrates the decomposition of the pin loading and far-field tension acting on MSD cracks in an FML into simpler symmetric loading cases. For each crack tip, a set of stress intensity factors can be derived for the corresponding loading cases and superposed to get the overall stress intensity factor, following the same basic approach discussed in subsection 7.2.2. Since several cracks are present, the identification system as illustrated in Fig. 5.5 in Chapter 5 is followed to aid in clarifying the discussion. The derivation of the stress intensity factors for the tip on the right side of crack i, denoted with the subscript $_{i1}$, is described in this subsection as an example.

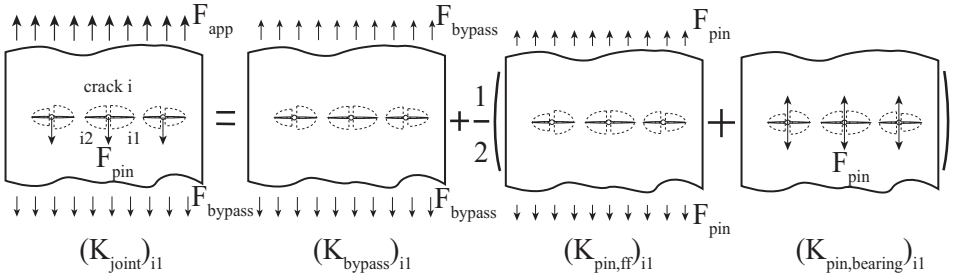

Figure 7.7: Superposition scheme of loading cases for MSD cracks in an FML

The decomposition of the stress intensity factor, $(K_{joint})_{i1}$, for crack tip $i1$, as illustrated in Fig. 7.7, can be written as:

$$(K_{joint})_{i1} = (K_{bypass} + 0.5K_{pin,ff})_{i1} + 0.5(K_{pin,bearing})_{i1} \tag{7.15}$$

In order to avoid repetitively calculating the bridging stress distribution for the same crack configuration under different loading cases, the above equation is alternatively given as:

$$(K_{joint})_{i1} = (K_{app})_{i1} + (K_{br})_{i1} \tag{7.16}$$

with

$$(K_{app})_{i1} = (K^*_{bypass} + 0.5K^*_{pin,ff})_{i1} + 0.5(K^*_{pin,bearing})_{i1} \tag{7.17}$$

The corresponding crack opening displacement of the single crack i, $(v^*_{app}(x))_i$, is expressed as:

$$(v_{app}(x))_i = (v^*_{bypass}(x) + 0.5v^*_{pin,ff}(x))_i + 0.5(v^*_{pin,bearing}(x))_i \tag{7.18}$$

When analysing the crack state of the single crack i, the adjacent cracks are treated as local stiffness reductions in this research. The reductions in local stiffness lead to load redistribution from the adjacent cracks to the single crack, enlarging the stress intensity factor and the corresponding crack opening of the single crack in comparison with the isolated crack scenario.

The calculation of $(K^*_{bypass} + 0.5K^*_{pin,ff})_{i1}$ involves considering the load redistribution mechanism, which is described in detail in Chapter 5. Two different Westergaard

stress distributions in front of the single crack can be applied to evaluate the load redistribution as a result of the reductions in local stiffness cased by the presence of the adjacent cracks. Simultaneously the non-symmetry of the single crack needs to be modelled to get $(K^*_{bypass} + 0.5K^*_{pin,ff})_{i1}$ and $(v^*_{bypass}(x) + 0.5v^*_{pin,ff}(x))_i$.

The significance of modelling the load redistribution mechanism under far-field tension has been demonstrated in Chapter 5. Nevertheless, the significance of modelling it in calculating $K^*_{pin,bearing}$ for the case of MSD cracks subjected to pairs of point loads needs to be re-evaluated.

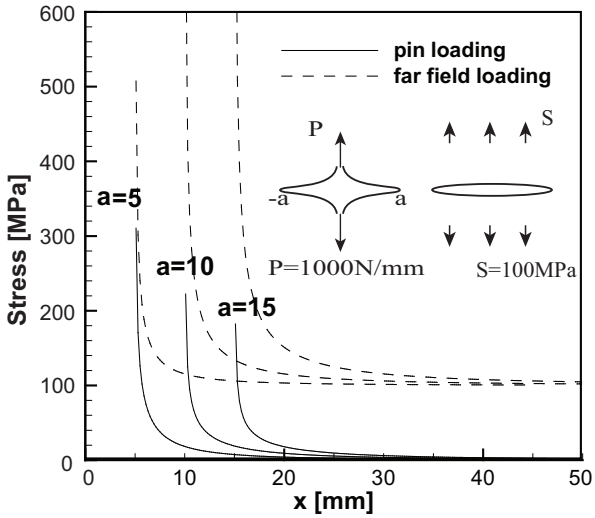

Figure 7.8: Comparison of stress distributions ahead of a crack tip for a far-field tension of $S = 100\ MPa$ and for a pair of point loads with $P = 1000\ N/mm$ for different crack lengths

The stress distribution in front of the tip of a crack loaded by a pair of point loads, illustrated in Fig. 7.6, can be given as:

$$\sigma_{yy} = \frac{P}{\pi} \frac{\sqrt{a^2 - b^2}}{(x-b)\sqrt{x^2 - a^2}} \tag{7.19}$$

In Fig. 7.8, the stress distributions in front of a crack in an infinite panel subjected to a pair of point loads acting at the center of the crack ($b = 0$) are compared to the stress distributions of the crack subjected to far-field tensile stress for different crack lengths. Typical quantities for the pin load and far-field stress are chosen respectively. As can be seen, the magnitude of the stress distribution in front of the crack subjected to a pair of point loads is much lower than that of the same crack subjected to far-field loading, the stress roughly 15 mm away from the crack tip gets close to 0 MPa. The scale of the stress distribution for the case of far-field loading escalates with increasing crack length. On the contrary, in case of a pair of point loads, the stress distribution magnitude decreases with increasing crack length.

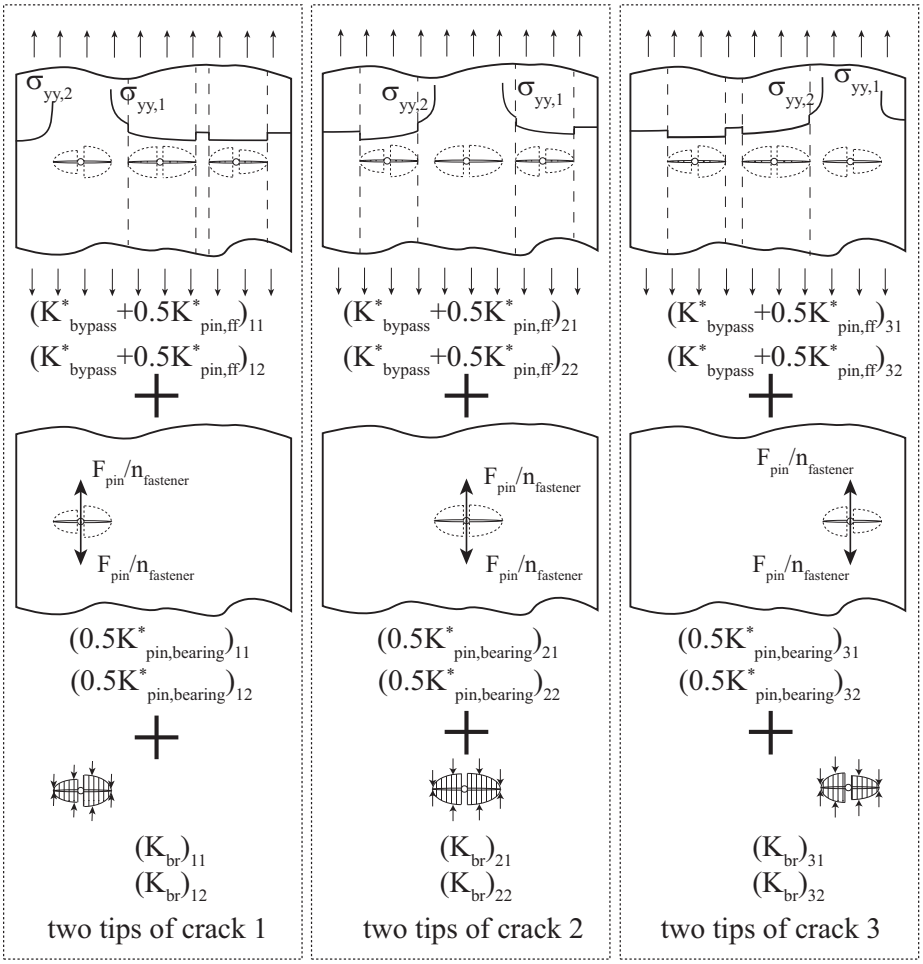

Figure 7.9: Illustration of sequential analysis of each crack state

Based on the comparison and analysis, it is concluded that the load redistribution caused by the presence of other cracks millimeters away in front of a crack loaded by a pair of point loads is negligible for FMLs. The calculation of $K^*_{pin,bearing}$ and $v_{pin,bearing}(x)$ for each of the multiple cracks therefore can be derived considering each crack as an isolated crack.

It is worth noting that the point load, P, for the MSD scenario should be calculated with the following equation:

$$P = \frac{F_{pin}}{n_{fastener} n_m t_m} \tag{7.20}$$

with $n_{fastener}$ denoting the number of fasteners.

The overall approach for calculating the crack states of MSD cracks in an FML sub-

jected to tension-pin loading is summarized in Fig. 7.9.

7.3. MODEL VALIDATION FOR A JOINT WITHOUT SECONDARY BENDING

One mechanically fastened FML joint was designed and tested to verify the proposed methodology in this work. The configuration of the FML joint is illustrated in Fig. 7.10. The symmetric double shear joint configuration was designed with the intention to exclusively present the loading components in the joint that are accounted for in the proposed methodology. Secondary bending and interference fit fastener, not considered in the model, are not present in the tested joint. As such, the test configuration can provide a more accurate validation of the performance of the model.

7.3.1. TEST PROCEDURE

The symmetric double shear lap joint consisted of two Glare3 3/2-0.4 specimens that were symmetrically jointed to a middle plate which was manufactured by bonding two Glare3 3/2-0.4 panels together with a very thin bond-line. As a consequence the stiffness of the middle plate is equivalent to the total stiffness of the two specimens. Two fastener rows were applied such that each row transfers 50 percent of the applied load from the middle plate to the two specimens.

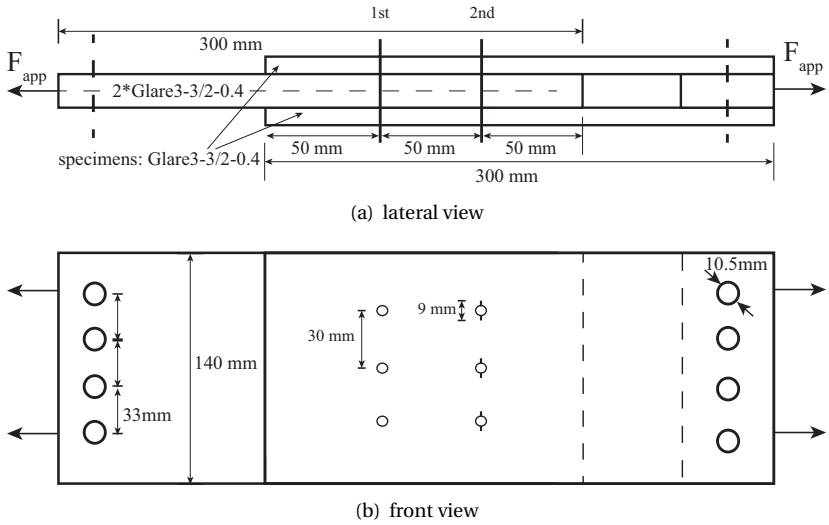

Figure 7.10: Illustration of the double shear lap FML joint

Each fastener row had three evenly spaced fastener holes with the middle hole at the middle of each specimen as shown in Fig. 7.10(b). The fastener pitch was 30 mm. The fastener hole was firstly drilled and later reamed to the diameter of 4.8 mm that is the diameter of used fasteners. Therefore no compressive residual stresses at the fastener holes would present. As shown in Fig. 7.10(b), saw-cuts were applied to the fas-

tener holes in the second fastener row in both specimens. The length of the saw-cut was 2.1 mm. Hi-lok HL12V6 fasteners were used to join the specimens and the middle plate. The Hi-Lok collar was not driven to the maximum protrusion but tightened enough so that the out-of-plan displacement of the specimens were eliminated by the collar and the head of Hi-lok fasteners during fatigue loading.

The fatigue test was conducted on an MTS 810 servo-hydraulic test frame with pin hole clevis and a 250 kN load-cell (model 661. 22D-01). The maximum applied stress was $100MPa$ with a stress ratio of $R = 0.05$ and a frequency of $f = 10Hz$. The fatigue test was paused after a number of fatigue loading cycles, the maximum load was applied to make the crack fully open. Pictures of the surfaces of the two specimens were taken by two high resolution cameras. The corresponding fatigue life was also recorded. The test was resumed then. The crack lengths at different fatigue life were measured from the pictures. Seven-point incremental polynomial method recommended in the ASTM E647-00 [12] was applied to reduce the scatter of the crack growth rate measurement for each crack.

7.3.2. VALIDATION

The test data is used to validate the proposed model. In the tested joint, the bypass load and pin bearing load for the multiple cracks in the second fastener row kept changing as cracks grew. However, this changing due to the load redistribution over the two fastener rows is not simultaneously modelled when calculating the growth of multiple cracks in the proposed model.

A tension-pin loading case is required in the proposed model as input parameters in order to calculate the state of MSD cracks in an FML joint. Five tension-pin loading cases are studied for different initial crack configurations in order to directly illustrate the effects of the load redistribution among the fastener rows on the crack growth behaviour. The studied loading cases for the 2nd fastener row in the tested joint configuration are summarized in Table 7.1. Loading case 1 is based on the fact that the symmetry of the joint permits each fastener row to transfer 50% of the applied load, particularly when the crack length is very small. As the lengths of the cracks in the 2nd fastener row increase, the escalation in the fastener and plate flexibility allows the first row to transfer more and more load. Consequently the bypass load for the 2nd fastener row increases while the pin load decreases. Loading cases 2-4 follows this rule of thumb. Loading case 5 is to demonstrate the impact of a significant increase in the bypass load on the crack growth behaviour with long crack lengths.

Table 7.1: Loading cases for the 2nd fastener row

case	pin load (% of applied load)	bypass load (% of applied load)	initial average crack length (mm)
1	50	50	5.0
2	49	51	6.4
3	45	55	9.1
4	40	60	10.8
5	30	70	10.8

In Fig. 7.11, the measurements and the prediction results of the five loading cases are plotted. The locations of the fastener holes and saw-cuts are indicated in both sub-figures.

The measured and predicted crack growth rates for the symmetric crack tip pairs are compared in Fig. 7.11(a). The test data shows that the crack growth rates are rapid in the vicinity of the fastener hole, become stable after a certain amount of crack increment and soar up when two crack tips approach each other. For the outer crack tips, a_{12} and a_{31}, their crack growth rates increase because they approach the free edge boundaries ahead and the link-up of the inner crack tips results in the two tips being the tips of a lead crack in the laminate.

The predicted crack growth behaviour for loading case 1 in Table 7.1 captures the trend of the growth behaviour of the multiple cracks in the tested joint. The prediction results for the crack tips near the fastener holes correlate very well with the test results. The predicted crack growth rates are very high but decrease dramatically with increasing crack length, which is consistent with the correlation in Fig. 6.7 and can be attributed to the effects of pin loading in the vicinity of a fastener hole. This accurate prediction results for the crack tips in the vicinity of fastener holes is attributed to the fact that the small cracks in the second fastener row hardly altered the portions of the load transferred by the two fastener rows. When the crack lengths are long enough, the prediction results of loading case 1 under estimates the surge in the measured crack growth rate though the predicted crack growth rates of two approaching crack tips soar up. This underestimation is contrary to the over-predicted crack growth rates for FMLs containing multiple cracks subjected to far-field tensile fatigue loading (for example Fig. 5.8(a) in Chapter 5).

Loading case 2 for an initial crack length of 6.4 mm takes the load redistribution over the two fastener rows into consideration, the result shows that a slight rise in the bypass load for the cracks in the 2nd row can significantly enhance the predicted crack growth rates. For even longer crack lengths, the significant rise in the bypass load, however, marginally enhances the predicted crack growth rate (see the prediction results of loading cases 3-5 in Fig. 7.11(a)).

The corresponding predicted a-N curves for the 5 loading cases are compared to the test data in Fig. 7.11(b). As can be seen, the prediction model becomes conservative if the load redistribution over the fastener rows due to the crack growth in the 2nd fastener row is taken into consideration.

7.4. MODEL VALIDATION FOR A JOINT WITH SECONDARY BENDING

This section discusses the difference between the measured crack growth rates of cracks in a single shear lap joint where the secondary bending stresses affect the crack growth behaviour and the predicted results without considering the effects of secondary bending.

The test data is extracted from the experimental study conducted by Müller [3]. Results of test series 4 from the study of fatigue behaviour of Glare3 riveted lap joints are selected for the purpose of this section. The tested joint consisted of two Glare3 3/2-0.3 sheets jointed with three rows of rivets (see the inset in Fig. 7.12) while each row had

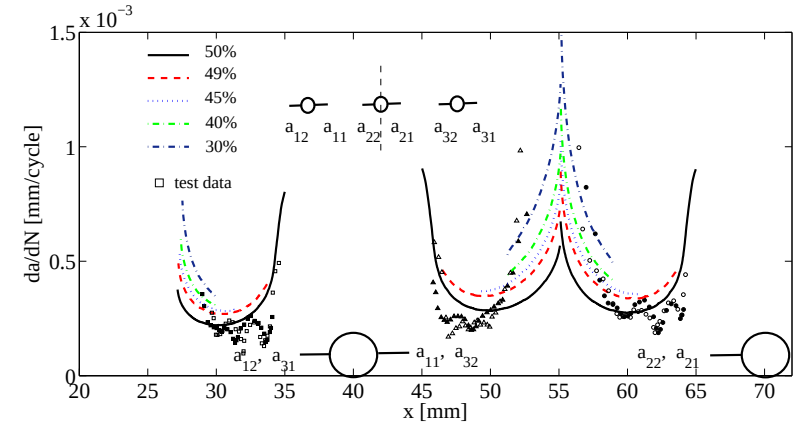

(a) Comparison of measured crack growth rates and prediction results for 5 different loading cases (% denotes the pin load for the 2nd fastener row which is a percentage of applied load)

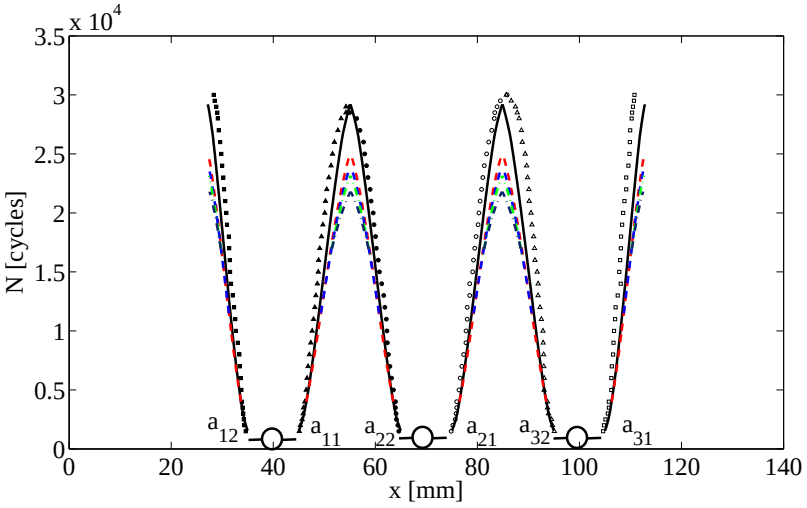

(b) Comparison of measured a-N curves and prediction results for the corresponding loading cases

Figure 7.11: Predictions vs test results

three rivets. The width of the Glare3 sheet was 72 mm. The loading parameters are given in Fig. 7.12.

The compiled crack growth rates in the metal layers of the top sheet in the joint riveted with the squeeze force of 15.6 kN are given in Fig. 7.12. Crack growth were measured only for the central rivet in the critical row with eddy current non-destructive inspection technique [3]. The half crack length was measured from the rivet hole edge to the crack tip. The accuracy of the test data is limited because the inspection method for invisible

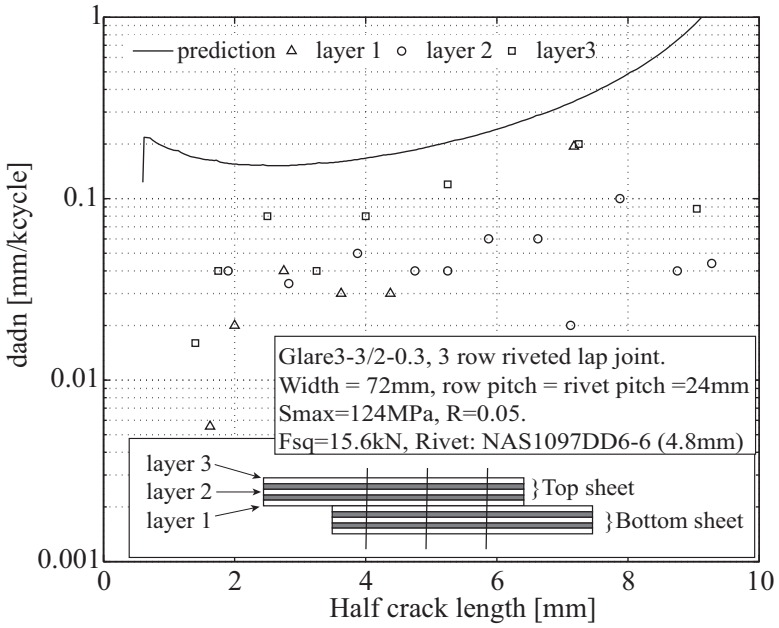

Figure 7.12: Comparison of crack growth rates of 3 layers in the top sheet

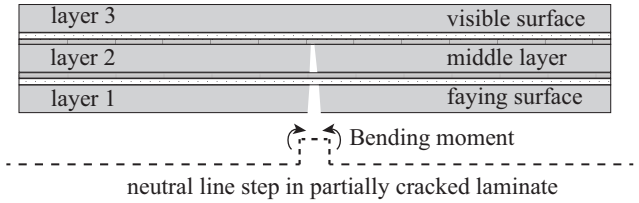

Figure 7.13: Local bending around crack due to neutral line step in partially cracked laminate

cracks is poor [3] and the obtained data points are few. Layer 1 had the highest tensile stress due to the secondary bending stresses (see Fig. 7.3), the crack initiated in layer 1 at first. However the crack growth in this layer in the beginning was very slow as a result of compressive residual stress due to high riveting squeeze force and the bridging mechanism provided by fibre layers and intact layer 2 and layer 3 (larger crack free life due to secondary bending in these two layers). The crack growth rate in layer 2 was higher compared to that in layer 1. Layer 3 had the highest crack growth rate due to the fact that layer 1 had been completely cracked and layer 2 was partially cracked. However, compressive bending stresses resulting both from the eccentric load paths in the joint (see Fig. 7.1) and the neutral line step in the partially cracked laminate (see Fig. 7.13) play a beneficial role in constraining the crack growth rate in layer 3.

The analysis model does not take the effects of squeeze force and the effects of sec-

ondary bending into consideration, it is assumed that cracks initiate in all metal layers simultaneously, i.e. a through thickness crack. The load distribution over the fastener rows can be calculated with the method described in Section 7.1.1 for the tested joint without cracks, i.e. $T1 = 4.366kN$ and $T2 = 4.053kN$. For this given load transfer in the joint, the bypass and pin loads for the multiple cracks can be calculated. The predicted crack growth rate for the middle crack is plotted in Fig. 7.12. Obvious difference can be observed compared to the test data since the prediction model leaves out the influence of bending stresses on the growth behaviour in different layers. It is noteworthy that the greatly simplified prediction model provides conservative prediction results.

This simplified model is very efficient to analyse the crack growth behaviour in an FML joint with MSD cracks. It avoids further discretization of the crack configuration in order to detailedly analyze the bridging mechanism offered by uncracked metal layers and the effects of local secondary bending stresses on the crack growth behaviour. It could be potentially useful for quick screening FML joint design.

7.5. CONCLUSION

The proposed analysis methodology for MSD crack growth prediction in mechanically fastened FML joints is based on LEFM. The analysis methodology does not account for load redistribution over multiple fastener rows as a result of cracks evolution in one fastener row and the effects of secondary bending stresses. For a given load transfer in the joint, the overall stress intensity factor at a crack tip can be calculated using the principle of superposition for different loading cases and the bridging mechanism. And then the crack growth rate can be determined. The crack state needs to be estimated one by one until all the crack states are determined for a MSD configuration.

Neglecting the secondary bending effects is feasible for double-shear lap joints, such as the tested joint in this chapter. The prediction without considering load redistribution over multiple fastener rows captures the feature of rapid crack growth in the vicinity of fastener holes due to pin loading, but starts to underestimate the crack growth rates after several millimetres crack growth. However, the underestimation can be alleviated by adjusting the load transfer in the joint. Since the pin loading effects dramatically fade out with increasing crack length, the bypass load introduced by other fastener rows starts to dominate the crack growth behaviour. The increase in the bypass load therefore can improve the prediction results for MSD cracks with longer crack lengths, resulting in more conservatively predicted fatigue growth life. In order to obtain more accurate prediction results for FML joints containing MSD cracks, the prediction methodology should simultaneously accounts for the load redistribution over multiple fastener rows when analysing the crack growth in the critical fastener row.

The secondary bending effects due to the eccentricities in the load path in single-shear lap joints induce complex crack configuration in FMLs. Even though the secondary bending effects are neglected in the proposed methodology, it provides conservative prediction results for FML single-shear lap joints based on the comparison between prediction and test data from open literature. The slow crack growth in different metal layers compared to the prediction can be attributed to several aspects. The secondary bending results in highest tensile stresses at the faying metal layer and least tensile stress in the outer metal layer (Fig. 7.3). This stress distribution though the laminate

thickness results in the cracks in different layers having different crack lengths. The uncracked metal material in the wake of cracks in other layers could still bridge the crack, alleviating the adverse effects posed by secondary bending on the crack growth in the faying layer in an FML lap joint. For the crack growth in the outer metal layer, the secondary bending stresses resulting from the eccentricities in the load path of the joint and the neutral line step in the partially cracked laminate could play beneficial role in restricting the crack growth in this layer.

REFERENCES

[1] C. D. Rans, *2 - bolted joints in glass reinforced aluminium (glare) and other hybrid fibre metal laminates (fml), in Composite Joints and Connections*, in Composite Joints and Connections (2011).

[2] J. J. M. De Rijck, *Stress analysis of fatigue cracks in mechanically fastened joints: an analytical and experimental investigation*, Ph.D. thesis, Delft University of Technology, Delft, the Netherlands (2005).

[3] R. Müller, *An experimental and analytical investigation on the fatigue behaviour of fuselage riveted lap joints : the significance of the rivet squeeze force, and a comparison of 2024-T3 and glare 3*, Ph.D. thesis, Delft University of Technology, Delft, the Netherlands (1995).

[4] H. Huth, *Influence of fastener flexibility on the prediction of load transfer and fatigue life for multiple-row joints,* (ASTM STP 927, 1986) pp. 221–250.

[5] T. Swift, *Development of the fail-safe design features of the dc-10,* (ASTM STP 486, 1971) pp. 164–214.

[6] R. Kroes, *Description of the Computer Program SLAPJO*, Tech. Rep. (Fokker report SF-63, 1992).

[7] J. Schijve, *Fatigue of structures and materials* (Springer, Dordrecht, The Netherlands, 2008).

[8] J. Schijve, *Some elementary calculations on secondary bending in simple lap joints,* (1977).

[9] G. Wilson, *Fatigue Crack Growth Prediction for generalized fiber metal laminates and hybrid materials*, Ph.D. thesis, Delft University of Technology, Delft, the Netherlands (2013).

[10] W. Wang, C. Rans, R. C. Alderliesten, and R. Benedictus, *Predicting the influence of discretely notched layers on fatigue crack growth in fibre metal laminates,* Engineering Fracture Mechanics **145**, 1 (2015).

[11] H. Tada, P. C. Paris, and G. R. Irwin, *The stress analysis of cracks handbook* (ASME, New York, 2000).

[12] E647-00, ASTM, *Standard test method for measurement of fatigue crack growth rates,* (2011).

8

CONCLUSION

This chapter summarizes the underlying approach adopted for predicting fatigue crack growth in FMLs containing MSD in this thesis. It also provides a critical review of the limiting assumptions made in developing the described prediction models in Chapters 2-7. The effects of the limiting assumptions on the output of the prediction model are discussed to provide potential users with the needed confidence to apply the developed model.

8.1. OVERVIEW

The present research has investigated the crack growth behaviour in FML structures containing MSD scenario. The underlying approach adopted in this research for crack growth prediction employs LEFM: a methodology that has its roots in Hooke's law that associates stress and strain in materials through material stiffness parameters. Normally, the stress or strain distribution in a structure is static indeterminate. Determining the stress or strain requires a thorough analysis of the loads applied to the structure and the stiffness of the structure (including material stiffness and geometric stiffness). Any changes in the stiffness of a structure under the same loading could alter the deformation of the structure, and thus the strain and stress distribution. Macro-damages, such as cracks and fastener holes, in a structure can undermine the geometric stiffness of the structure, the deformation therefore enlarges under the same loading condition, which alters the associated strain and stress states.

The physics of the fatigue damage issue in FMLs is no exemption from Hooke's law. The stress states at areas of interest in FMLs need to be calculated and used to determine whether or not a damage could occur and propagate. In the context of LEFM, the stress states can be related to either K or G to calculate the damage evolution under fatigue loading. Alderliesten has developed an analytical model for predicting the crack growth behaviour of isolated central cracks in FMLs subjected to far-field fatigue loading.

The present research deals with the crack growth behaviour in FMLs containing multiple cracks. Compared to the case of an isolated crack in an FML, multiple cracks further undermine the laminate stiffness, resulting in more deformation of the laminate. Precise analysis and calculation of the associated deformation and stress states for this sophisticated phenomenon is intricate. To simplify the problem, other adjacent cracks are idealized as "negative stiffeners" so that the reductions in the geometric stiffness due to the cracks can be modelled in a simplified way when calculating the stress states of a single crack (Chapter 2, Chapter 5). However, the assumption of "negative stiffeners" artificially introduces more stiffness reduction in the FML in comparison with that caused by real cracks accompanied with small scale delamination shapes, resulting in more load redistribution from the adjacent cracks to the single crack. As a consequence the described prediction model overestimates the stress states at the tips of a single crack and its COD due to applied loads. The bridging stress distribution therefore is also overestimated by the prediction model due to the overepredicted COD, which can partially offset the overestimation in calculated K_{total}. Yet the prediction model provides conservative results.

An overview of the structure of this thesis in Chapter 1 is represented in Fig. 8.1. In order to develop models to predict MSD crack growth behaviour in flat FML panel (Chapter 5) and in FML joint (Chapter 7), the load redistribution mechanism due to stiffness reductions was first validated in Chapter 2, followed by the extensions of the capability to calculate the stress states for generic eccentric cracks in metals (Chapter 3) and in FMLs (Chapter 4). Meanwhile, the pin loading effects on the crack growth behaviour in FMLs was analysed (Chapter 6) in order to implement the approach for fastened FML joints containing MSD cracks (Chapter 7).

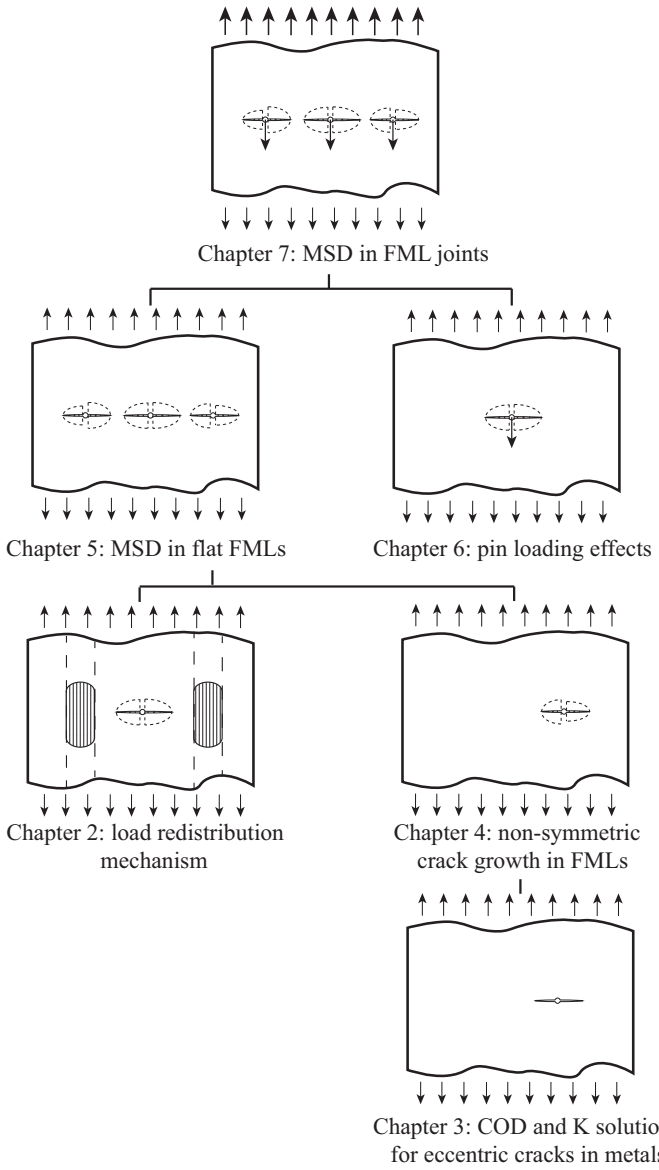

Figure 8.1: Structure of this research

8.2. ASSUMPTIONS AND CONSEQUENCES

Any predictive model is only useful with a thorough understanding of any limiting assumptions and their consequences on the model output. In order to provide potential users with the needed confidence in the developed model to apply it, its key assumptions and their consequences are discussed here.

LEFM assumption The approach in this work is based on LEFM with a lack of plasticity at crack tips. A small plastic zone develops in front of a crack tip in the metal layers in an FML, which is not characterized by the LEFM approach. It should be less of an issue for FMLs since the bridging mechanism significantly reduces the plastic zone size in the metal layers. When one crack tip is in the vicinity of a notch or another crack tip, the plasticity interaction can occur over a very small portion of crack length and result in dramatic increase in the crack growth rate, the model underestimates the results (Figs. 2.9, 2.10 and Figs. 5.9, 5.10).

Negative stiffeners assumption The influence of other cracks on a single crack is evaluated by considering the cracks as removals of metal strips. In comparison with an actual crack with small scale delamination shapes in an FML, the non-physical representation of the crack exaggerates the damage status, i.e. more materials are assumed not to bear the applied load and lager delamination shapes. The load redistribution from the exaggerated damages therefore is higher than that from actual cracks. This assumption leads to the prediction model providing conservative prediction results (Figs. 2.9, 2.10 and Figs. 5.9, 5.10).

Application of Westergaard stress distributions The stress distributions in front of crack tips of an asymmetric crack in a metal panel are assumed to be characterized with two different Westergaard stress distributions. In Fig. 3.10, the two Westergaard stress distributions for the analysed eccentric crack in the metal panel correlate with the FEM results very well. The application of two Westergaard stress distributions allows the asymmetric crack opening displacement of an eccentric crack to be derived (Fig. 3.9); however, leads to underestimation of the stress intensity factor of the crack tip that is relatively away from the free edge boundaries. This error is only obvious for an eccentric crack with a normalized crack length longer than 0.7, see Fig. 3.7.

Simplification of pin bearing loads In Chapter 6, the bearing load applied by a fastener to the hole edge in an FML is modelled as a concentrated load and assumed to be borne by the metal layers only. This simplification and assumption is analogous to the pin bearing transfer in fibre reinforced polymer composites where the matrix bears the pin loading and then transfers the load to stiffer fibres. This simplification may lead to some error when the crack tip is in the vicinity of the fastener hole (Fig. 6.7). In addition, the damage caused by the bearing load in the fibre layers cannot be analysed with this assumption.

Application of the principle of superposition for splitting asymmetric loading cases An asymmetric tension-pin loading case is regarded as a half of the superposition of a pair of pin loads and symmetric far-field tension in Chapter 6. The asymmetric tension-pin fatigue loading acting on FMLs results in non-symmetric delamination shapes and Mixed Mode crack growth in the metal layers (Fig. 6.8(a)). This superposition enables a simple prediction of the crack growth under pin bearing. On the other hand, the predicted crack configuration is a Mode I crack, which cannot capture the crack path deviation from the transverse direction. In FMLs, the loading case leads to asymmetric delamination shapes with respect to the transverse section, which cannot be captured by the prediction model either.

Neglecting the load redistribution among fastener rows Load redistribution among fastener rows is not simultaneously accounted for when calculating the growth behaviour

of multiple cracks in an FML joint. As cracks grow in the joint, the changes in fastener and plate flexibility alter the portion of load transferred by each fastener row. This load redistribution among fastener rows is still indeterminate. Yet the study of 5 loading cases summarized in Table 7.1 shows that the increase in the bypass load for the cracks can increase the conservativeness of the prediction model (Fig. 7.11). Nevertheless, neglecting load redistribution among fastener rows leaves out the real-time influence of variation in bypass and pin loads on the MSD crack growth behaviour.

Neglecting secondary bending stresses The effects of secondary bending are not taken into consideration in the analysis for single-shear lap joints. The eccentricities in the load path of such joints lead to out-of plane displacement and bending stresses. The bending stress could result in different crack lengths through thickness in the metal layers. By neglecting the secondary bending stresses, the prediction model can not capture the complex crack configuration through thickness (Fig. 7.12). A detailed analysis of the crack problem can not be obtained.

8.3. PERFORMANCE OF THE MODEL

With the limiting assumptions of the model discussed, the overall performance can be thoroughly critiqued.

- The prediction model can accurately predict the crack growth rate in a cracked FML containing discretely notched layers, see Figs. 2.9, 2.10. The model captures the crack acceleration when the crack tip approaches the notch edge. This accurate prediction is attributed to the fact that the idealization does not exaggerate the reduction in geometric stiffness compared to the reduction caused by the actual notches in the metal layers.

- The model for MSD crack growth prediction consistently over-predicts the crack growth rates over the major portion of the crack length for multiple collinear cracks in FMLs, which results in a conservatively predicted fatigue growth life. However, without considering the load redistribution caused by the stiffness reduction resulting from the cracked metal layers leads to very non-conservative predictions (Figs. 5.8, 5.9 and 5.10). The over-predicted crack growth rate is due to the consequences of the non-physical representations of cracks. From Table 5.2, it is observed that the analysis method performs better for FMLs with lower MVF in terms of predicting fatigue growth life.

  Over approximate 1 to 2 mm crack length just before two crack tips link-up, the predicted crack growth rate is lower than test data since the effects of plasticity interaction is not considered. Due to the rapid crack growth before two crack tips coalesce, the error resulting from neglecting plasticity interaction effects in predicted fatigue growth life is negligible.

  The model provides very accurate MSD damage configuration prediction compared to the measurements, see Fig. 5.11.

- The prediction model for eccentric cracks in FMLs successfully captures the effects of the delamination shape asymmetry and crack tip asymmetry. The predicted crack configuration, including the delamination shapes for two crack tips,

correlates very well with test data (Fig. 4.11 and Fig. 4.12). The assumption made for calculating non-symmetric crack state in metals results in an over-predicted crack growth rate for the critical crack tip that is very close to the free edge and an under-predicted crack growth rate for another tip that is relatively away from any free edges in FMLs (Fig. 4.13). However, this error is pronounced only when the normalized crack length is larger than 0.7, which means the ligament between the critical crack tip and the free edge ahead is much smaller than the crack size.

In practical aircraft structures, panels are usually very wide and the edges are jointed to supporting structures such as frames, stringers and straps. Load redistribution between a cracked panel and supporting structures occurs when a crack tip in the panel approaches the jointed edge. The boundary conditions in this case for the prediction model do not valid anymore. It is therefore appropriate to use the non-symmetric crack growth prediction model for a non-symmetric crack with normalized crack length smaller than 0.7 in a practical wide panel so that the boundary conditions can still be considered valid.

- The model for predicting the effects of pin loading on crack growth behaviour in FMLs accurately determines the crack growth rate (Fig. 6.7). However, the model fails to predict the crack path and non-symmetric delamination shapes with respect to the crack path. The important aspect is that the symmetric delamination shape determined with the prediction model has equivalent delaminated lengths in comparison with the delamination shape in the tested specimen (Fig. 6.8).

- The implementation of the models developed in Chapter 5 and Chapter 6 for predicting crack growth in FML joints captures the rapid crack growth behaviour in the vicinity of fastener holes and surge in crack growth rates before link-up of cracks (Fig. 7.11). However, the methodology losses the conservativeness for FML joints containing MSD cracks without considering the load redistribution over multiple fastener rows.

  The loading case study (Table 7.1) proves that the methodology presented in this theses should provide conservative predictions for double-shear lap joints containing multiple cracks if the real-time bypass load and pin loads for the cracks in the joint are known.

- The methodology for FML single-shear lap joints does not take secondary bending effects into consideration, which cannot predict complex crack configurations in the metal layers through laminate thickness. It is noteworthy that the predictions derived from the methodology are conservative compared to the different crack growth rates in different metal layers in the Glare riveted lap joint tested by Müller (Fig. 7.12).

8.4. FINAL CONCLUSION

The nature of slow and stable crack growth in FMLs, thanks to the bridging mechanism offered by the fatigue resistant fibres, leads modelling load redistribution to be the key

factor when analysing MSD crack growth behaviour. In this work, models have been developed to analyse the load redistribution mechanism and non-symmetric growth behaviour in FMLs containing MSD scenarios, the effects of pin loading on crack growth behaviour in FML joints.

Further research is necessary to lead the present work to a more realistic analysis for FML joints where load redistribution over multiple fastener rows and secondary bending effects are present.

A

INTEGRALS

The typical integrals in Chapter 3 are given here for $x > a > 0$

$$\int \frac{1}{\sqrt{1-(a/x)^2}} dx = \sqrt{x^2 - a^2} + C_1 \tag{A.1}$$

where C_1 is a constant.

$$\int \frac{x}{\sqrt{1-(a/x)^2}} dx = \frac{a^2 ln(x + \sqrt{x^2 - a^2}) + x\sqrt{x^2 - a^2}}{2} + C_2 \tag{A.2}$$

where C_2 is a constant.

B

WESTERGAARD STRESS FUNCTIONS

The Westergaard stress functions for cracked body under two-point loads (see Fig. 4.8) are given by:

$$Z_I = \frac{P}{2\pi\sqrt{z^2-a^2}}(Part1 - i\cdot\alpha y_0 Part2) \tag{B.1}$$

where

$$Part1 = \frac{\sqrt{a^2-z_0^2}}{z-z_0} + \frac{\sqrt{a^2-\bar{z}_0^2}}{z-\bar{z}_0} \tag{B.2}$$

$$Part2 = \frac{\sqrt{a^2-z_0^2}}{(z-z_0)^2} - \frac{\sqrt{a^2-\bar{z}_0^2}}{(z-\bar{z}_0)^2} - \frac{z_0}{\sqrt{a^2-z_0^2}(z-z_0)} + \frac{\bar{z}_0}{\sqrt{a^2-\bar{z}_0^2}(z-\bar{z}_0)} \tag{B.3}$$

$$\alpha = \frac{1}{2}(1+\upsilon) \tag{B.4}$$

and

$$\bar{Z}_I = \frac{P}{\pi}(Part3 - \alpha y_0 Part4) \tag{B.5}$$

where

$$Part3 = tan^{-1}\left(\sqrt{\frac{a+z_0}{a-z_0}}\sqrt{\frac{z-a}{z+a}}\right) + tan^{-1}\left(\sqrt{\frac{a+\bar{z}_0}{a-\bar{z}_0}}\sqrt{\frac{z-a}{z+a}}\right) \tag{B.6}$$

$$\begin{aligned} Part4 = &\frac{1}{1+\dfrac{a+z_0}{a-z_0}\dfrac{z-a}{z+a}}\sqrt{\frac{z-a}{z+a}}\sqrt{\frac{a-z_0}{a+z_0}}\frac{i\cdot a}{(a-z_0)^2} - \\ &\frac{1}{1+\dfrac{a+\bar{z}_0}{a-\bar{z}_0}\dfrac{z-a}{z+a}}\sqrt{\frac{z-a}{z+a}}\sqrt{\frac{a-\bar{z}_0}{a+\bar{z}_0}}\frac{i\cdot a}{(a-\bar{z}_0)^2} \end{aligned} \tag{B.7}$$

In these functions, P represents the point load per unit thickness, and the complex numbers z_0 $(x_0 + i \cdot y_0)$, $\bar{z}_0$ $(x_0 - i \cdot y_0)$ indicate the locations of the applied point loads in a xy-coordinates; z $(x + i \cdot y)$ indicates the location of interest in the same coordinates (Fig. 4.8).

For the application in this paper, the following substitutions are needed:

$$z = x + i \cdot 0 \tag{B.8}$$

$$z_0 = x_i + i \cdot b(x_i) \tag{B.9}$$

$$\bar{z}_0 = x_i - i \cdot b(x_i) \tag{B.10}$$

ACKNOWLEDGEMENTS

A PhD dissertation is normally deemed an achievement accomplished independently by the author whose name appears on the cover. However, to me it would feel like a lonely person sailing in an enormous ocean without the contribution and support from many people during my PhD life. I would like to express my sincerest gratitude to them.

First of all, I would like to acknowledge my supervisor Dr. Calvin Rans. You are always supportive and encouraging, inspiring me to explore more while being critical. You taught me more than just how to do research, our conversations extend to which beer is the best in Munich, how to prepare a nice presentation, the feelings one can experience when taking care of kids, and so on. Without your support and guidance, I would not have been able to complete this milestone in my academic life. Thank you Calvin!

I would also like to acknowledge my promotor Prof. Rinze Benedictus. Thank you for giving me the chance to be in this active and inspiring Structural Integrity and Composite group to expose myself to extensive knowledge created and disseminated here. Thank you for placing trust in me and for the advices to my personal development. Dr. René Alderliesten, my supervisor in the first year of my PhD, thank you for opening the door of knowledge about FML for me. Your supervision and guidance was valuable.

I am very grateful to Gemma who took care of all kinds of paperwork, including my visa application, employment contract, hospitality form etc. Thank you Gemma! Your enthusiastic help simplifies a lot of things for me. Without your help I would have gotten lost in other stuff instead of focusing on my research.

There was a substantial amount of experimental work involved in my PhD research, the completion of the testing could not be possible without help and support from lab secretary and technicians working in the lab. I want to thank Marianne, Berthil, Cees, Bob, Ed, Gertjan, Misja, Johan, Lijing, Frans and Fred for your contribution.

All wonderful colleagues and friends I meet in Delft make living and working here very much enjoyable and comfortable for me. Special thanks to Huajie, Lu Zhang, Lei, Ping, Chongxin, Hao who provided very useful tips to diminish scary surprises in the first couple of months. As you all know, it is not easy for a person to move from one continent to another and live there. The support and help from you were very much valuable. Thank you guys also for the fun we had together. Thank you Tian for all the help whenever I need you. I also want to thank Big Adrian, Small Adrian, Andrei, Arianna, Bernhard, Chirag, Cornelis, Chunsen, Davide, Derek, Dimitrios, Eirini, Fabricio, Genevieve, Changzhang, Chenguang, Chuang, Hongzhi, Hans, Ilias, Ilhan, Irene, John-Alan, Jos, Konstantin, Leila, Liaojun, Lucas, Lu Peng, Marcello, Marcias, Maria, Maria Pia, Maro, Mayank, Megan, Michiel, Morteza, Nat, Niels, Nikas, Otto, Paola, Rob, Roger, Romina, Sofia, Sotiris, Vincent, Vincentius, Weiling, Wenfeng, Xuezhou, Yan Ni, Yaolong, Ye, Yibole, Yuan, Zahid, Zaoxu, Zhinan, Zhaolong and everyone I have forgotten to mention (sorry!). Thank you for all the nice talks, cakes and parties. All of you have made my PhD life very colorful in Delft.

Thank you my dear office-mates Freddy, Daniel, Nikos, Pedro, Freek and Hongwei for the harmonious environment in the office. The exchange of ideas, jokes, debates and games will never be forgotten. I also want to express my appreciation to you since you have made your own contribution to improving my English, as a result of all kinds of activities that happened in and out of our office.

Special thanks goes to John-Alan, Megan, Nikos for useful comments after proofreading one or several chapters of this thesis. I also want to acknowledge Freek for translating the Summary and Propositions from English to Dutch.

Last, but certainly not least, I would like to express my gratitude to my family members. Thank you my parents for your enduring love and support. You have been trying your best to provide a better life for me. I feel so lucky to be your son! Thank you my younger sister, you are a wonderful companion to me, it is so sweet to have you as my sister. I am very grateful to my parents-in-law and my brother-in-law. You all are so nice to me. Especially when I was busy with finishing this thesis and at the same time we were preparing for the wedding ceremony, you were very supportive and patient with me. I am very thankful to my mother-in-law for putting her life aside temporarily to come over and take care of my newborn daughter in Delft. I want to thank my wife Tingting. Your endless and selfless love have made my life so enjoyable. You gave-up your career in Germany to join me in Delft and gave birth to our daughter Lan Xin here. Without all the support you have provided, I would not have finished my PhD work and this thesis so smoothly.

CURRICULUM VITÆ

Wandong WANG

The author was born in Xingren, Ningxia, China, on the 8^{th} of May 1989. He graduated from Ningxia Liupanshan High School in 2006. In the same year he moved to Xi'an, where he obtained his Bachelor in Aerospace Engineering at Northwestern Polytechnical University in 2010. Later he enrolled in Beihang University in Beijing to pursue his MSc degree in Engineering in the School of Aeronautic Science and Engineering. He worked on numerically modelling fatigue crack turning in integrally machined metallic panels under supervision of Prof Dr Y. Xu. He defended his master's thesis, entitled: 'Investigation on Life Prediction of Fatigue Crack Growth in Integrally Stiffened Panels' , in December 2012 and obtained his MSc degree. Three months before he graduated from Beihang University, he started his research at TU Delft as a CSC-sponsored PhD student under the supervision of Prof Dr Ir R. Benedictus as promotor and Dr C. Rans as co-promotor and daily supervisor.

List of Publications

Journal Papers

5. **W. Wang**, C. Rans, Z. Zhang, R. Benedictus, *Prediction methodology for fatigue crack growth behaviour in fibre metal laminates subjected to tension and pin loading*, Under review at the Composite Structures.

4. **W. Wang**, C. Rans, R. Benedictus, *Analytical prediction model for fatigue crack growth in fibre metal laminates with MSD scenario*, to be submitted to International Journal of Fatigue.

3. **W. Wang**, C. Rans, R. Benedictus, *Analytical prediction model for non-symmetric fatigue crack growth in fibre metal laminates*, to be submitted to International Journal of Fatigue.

2. **W. Wang**, C. Rans, R. Benedictus, *Towards the analysis of built-up structures containing eccentric cracks: Analytical solutions for crack opening displacements of eccentric cracks,*, to be submitted to European Journal of Mechanics - A/Solids.

1. **W. Wang**, C. Rans, R. C. Alderliesten, R. Benedictus, *Predicting the influence of discretely notched layers on fatigue crack growth in fibre metal laminates*, Engineering Fracture Mechanics **145**, 1-14 (2015).

Conference Papers

4. **W. Wang**, C. Rans, R. Benedictus, *Analysis of MSD crack growth in mechanically fastened fibre metal laminate joints*, in: Proceedings of the 17th European Conference on Composite Materials (2016).

3. Z. Zhang, **W. Wang**, C. Rans, R. Benedictus, *An experimental investigation into pin loading effects on fatigue crack growth in Fibre Metal Laminates*, Procedia Structural Integrity (21st European Conference on Fracture) **2**, 3361–3368 (2016).

2. **W. Wang**, C. Rans, R. C. Alderliesten, R. Benedictus, *Philosophy of multiple-site damage analysis for fibre metal laminate structures*, in: Proceedings of the 28th Symposium of the International Committee on Aeronautical Fatigue (ICAF 2015), (2015).

1. **W. Wang**, R. C. Alderliesten, R. Benedictus, *On the development of a prediction methodology for crack growth in Fibre Metal Laminates with MSD scenario*, Advanced Materials Research (11th International Fatigue Congress) **891-892**, 1651-1656, (2014).